JAERI-M
91-173

EVALUATION REPORT ON CCTF CORE-II REFLOOD TEST C2-1 (RUN 55)

— EFFECT OF PRESSURE ON REFLOOD PHENOMENA —

October 1991

Tadashi IGUCHI, Jun SUGIMOTO, Hajime AKIMOTO
Tsutomu OKUBO and Yoshio MURAO

日本原子力研究所
Japan Atomic Energy Research Institute

JAERI-Mレポートは，日本原子力研究所が不定期に公刊している研究報告書です。
入手の問合わせは，日本原子力研究所技術情報部情報資料課（〒319-11茨城県那珂郡東海村）あて，お申しこしください。なお，このほかに財団法人原子力弘済会資料センター（〒319-11 茨城県那珂郡東海村日本原子力研究所内）で複写による実費頒布をおこなっております。

JAERI-M reports are issued irregularly.
Inquiries about availability of the reports should be addressed to Information Division Department of Technical Information, Japan Atomic Energy Research Institute, Tokai-mura, Naka-gun, Ibaraki-ken 319-11, Japan.

編集兼発行　日本原子力研究所
印　　刷　いばらき印刷㈱

Evaluation Report on CCTF Core-II Reflood Test C2-1 (Run 55)
- Effect of Pressure on Reflood Phenomena -

Tadashi IGUCHI, Jun SUGIMOTO+, Hajime AKIMOTO
Tsutomu OKUBO and Yoshio MURAO

Department of Reactor Engineering
Tokai Research Establishment
Japan Atomic Energy Research Institute
Tokai-mura, Naka-gun, Ibaraki-ken

(Received October 1, 1991)

A high pressure test (0.42 MPa) on the reflood phenomena was performed with the CCTF. The result of the test was compared with the experimental result of the base case test (0.2 MPa).

(1) The overall flow characteristics in the high pressure test were qualitatively similar to that of the base case test. Any qualitatively different phenomena were not recognized during reflood phase. This indicates that it is reasonable to utilize the physical reflood model developed from the result of the base case test to the high pressure condition at least up to 0.42 MPa for prediction of reflood behavior of PWRs.

(2) On the other hand, following quantitative influence of high pressure on reflood phenomena was observed. The core cooling was better, and the mass flow rate of the steam generated in the core was larger. However, the steam velocity was smaller due to higher density of the steam. Therefore, the steam discharge through loops was easier and hence the so-called steam binding effect was weaker. And, the water accumulation rate in the core was larger. Consequently the core flooding mass flow rate was larger. Since the core cooling was better, the maximum core temperature was lower and the

---

+ Department of Fuel Safety Research

last quenching was earlier. This result was the same as that previously observed in CCTF tests in the scope of the pressure upto 0.3 MPa.

(3) The higher pressure leads to the better core cooling, and hence the safety margin increases with the increase in the pressure.

Keywords: Reactor Safety, ECCS, Steam Binding, PWR, Reflood, Two-phase Flow, CCTF, Core Cooling, Pressure Effect, LOCA

JAERI－M 91－173

大型再冠水円筒第二次炉心試験C2－1（Run 55）の評価
－再冠水現象に及ぼす圧力の影響－

日本原子力研究所東海研究所原子炉工学部
井口　正・杉本　純[+]・秋本　肇
大久保　努・村尾　良夫

（1991年10月1日受理）

CCTFにより高圧条件（0.42MPa）の再冠水試験を行った。本試験の結果を，基準試験（圧力0.2MPa）の結果と比較した。

(1) 高圧試験での再冠水現象は基準試験での再冠水現象と定性的に殆ど等しかった。このことは，PWR の再冠水現象予測を行うに際し，基準試験結果を基礎にして開発した再冠水物理モデルを少なくとも圧力0.42MPaの条件まで拡張して使用することに問題はないことを示す。

(2) 一方，定量的には次のような高圧力の影響が見られた。即ち，炉心冷却はよく炉心内での蒸気発生量は大きい。しかし，蒸気密度が大きいため蒸気流速は逆に小さい。このため，蒸気のループを通っての排出は容易でいわゆる蒸気閉塞効果は小さく，また，炉心内の蓄水量は多い。従って，炉心冠水速度は大きい。炉心冷却がよいため，最高炉心温度は低く，最終クエンチは早い。この結果は，従来0.3MPaまでの圧力範囲で見いだされていた結果と等しい。

(3) 高圧ほど炉心冷却はよく，従って炉心安全性は高まる。

東海研究所：〒319-11　茨城県那珂郡東海村白方字白根2-4
＋燃料安全工学部

Contents

目　　次

Table List

Figure List

1. Introduction

CCTF program

A reflood test program[1] using large scale test facilities has been conducted at Japan Atomic Energy Research Institute (JAERI). The facilities are the Cylindrical Core Test Facility (CCTF)[2] and the Slab Core Test Facility (SCTF)[3]. This report describes the evaluated result of the CCTF test C2−1 (Run 55), which is a high pressure test for investigating the high pressure effect on reflood behavior in the primary coolant system of a PWR.

The CCTF is an experimental facility designed to model a full−height core section, four primary loops and their components of pressurized water reactors (PWRs). This facility is used to provide information of the refill−reflood behaviors in pressure vessel (core, downcomer, upper and lower plena) and in primary loops (including steam generators and pumps) at a hypothetical loss−of−coolant accident (LOCA) of a PWR. The central part of the test facility is a non−nuclear core which consists of 1,824 electrically heated rods and 224 non−heated rods arranged in a cylindrical array. The core is housed in a pressure vessel which includes a downcomer, lower plenum and upper plenum in addition to the core. The core design is based on 8 x 8 rod assemblies which model typical 15 x 15 fuel assemblies of a PWR. Volumetric scaling ratio to a 1,100 MWe four−loop PWR is 1/21 based on core flow area scaling.

The objectives of the test program using the CCTF are:

a. Demonstration of capability of emergency core cooling system (ECCS) during refill and reflood periods
b. Verification of reflood analysis codes
c. Collection of information on the reflood phenomena to improve the thermo−hydrodynamic models in the analysis codes.

As the first series of the CCTF tests, twenty−seven CCTF Core−I tests were conducted. This series of tests presented a lot of information[4],[5] on the system thermo−hydrodynamic behavior as well as the core behavior during the refill and reflood phases of a LOCA in a PWR. The CCTF Core−I test series was initiated in March 1979 and completed in April 1981. Subsequently, as the second series of the CCTF tests, the CCTF Core−II test series was initiated in March 1982 and completed in 1985.

Test discussed in this report

The test discussed in this report is a high pressure test C2−1 (Run 55). The objective of the test is to study the effect of the pressure on the reflood phenomena. The test was conducted at the system pressure of 0.42 MPa as a counterpart test of the

base case test C2-SH1 (Run 53; system pressure 0.2 MPa). Other initial and boundary conditions were set to be identical between the high pressure test and the base case test. The ECC flow conditions were same as those of the Evaluation Model test[6] in CCTF Core-I.

In Core-I test series, the parametric tests on the pressure were performed in the range of 0.15 MP-0.3 MPa, and the effect of the pressure on the reflood behavior was studied.[7] However, in these parametric tests, the ECC flow rates were relatively small, comparing with the ECC flow rates expected during the reflood phase of the actual reactors. Therefore, the present tests, C2-1 (Run 55) and C2-SH1 (Run 53), have been performed under more practical ECC flow condition.

In Core-II test series, another test to investigate the pressure effect on the reflood phenomena, C2-8 (Run 67), has been perforemd at the system pressure of 0.15 MPa in addition to tests C2-1 and C2-SH1. The evaluated result has been presented in the references (8) and (9). This report is a supplemental of those references, and focused on the reflood phenomena under the high pressure.

2. Test facility

CCTF was designed to be a full−height, 1/21 scale model of the primary coolant system of a 1,100 MWe four−loop PWR in order to study the overall primary system response as well as the in−core behavior during the refill and reflood phases of a large cold leg break LOCA. Figure 2.1 depicts the major components in the facility. They included a pressure vessel, four primary piping loops (three intact and one broken), two steam generators, four pump simulators, and two tanks attached to the ends of the broken loop to simulate containment. Vertical dimensions and locations of system components were as close as practicable to the corresponding dimensions and locations in the reference reactor.

The schematic diagram of the CCTF is shown in Fig.2.2 and Fig.2.3. The scaled dimensions of the components are given in Tables 2.1 and 2.2.

2.1 Pressure vessel and internals

Figures 2.4 and 2.5 show the CCTF pressure vessel. The full−height pressure vessel housed a downcomer, lower plenum, core, and upper plenum. Pressure vessel flow area was scaled at a ratio of 1/21.4 as compared to a 1,100 MWe PWR, except that the downcomer annulus was somewhat larger to avoid excessive hot wall effects which would lead to an unrealistically low effective downcomer driving head. To simulate the effective downcomer driving head more realistically, the baffle area of PWR was included in the downcomer. Resultantly, the gap size of the downcomer was 61.5 mm, which was larger than the scaled gap. The design pressure of the pressure vessel and the entire primary system was 0.6 MPa. The pressure vessel wall was constructed of carbon steel which was cladded with stainless steel lining. The wall was 90 mm thick and simulated the stored energy as reasonably as possible during a test. Electrical resistance heaters on the wall of the pressure vessel were used to preheat the wall before a test, to accurately simulate the release of latent heat which would occur during a LOCA in PWR. The CCTF−II pressure vessel was the same as that used in CCTF−I, except for the addition of an upper ring containing an upper plenum emergency core coolant (ECC) injection header and additional instrumentation nozzles.

The design of upper plenum internals was based on that of the new Westing−house 17 x 17 type fuel assemblies instead of the old type simulated in CCTF−I. The internals consisted of ten control rod guide tubes, ten support columns and twelve open holes as shown in Fig.2.5. The radius of each internals was scaled down by factor of 8/15 from that of an reference reactor. They are illustrated in Fig.2.6. Flow resistance baffles were inserted into the guide tubes. The baffles consisted of kinds of baffle

plates and a shaft, simulating real ones. The baffle plates are shown in Fig.2.7.

The end box and the upper core support plate (UCSP) were installed between the core and the upper plenum, as in PWRs. The structure for one heater rod bundle is shownin Fig.2.8. The tie plate was a 10 mm thick perforated plate with round flow holes. Plugging devices were installed on the tie plate as shown in Figs.2.8 and 2.9 to simulate the flow resistance more correctly. The UCSP was a 60 mm thick perforated plate. The geometry of the perforation was analogous to that of an reference reactor.

2.2 Heater rod assembly

The heater rod assembly simulating the fuel assembly consisted of thirty−two 8 x 8 array rod bundles. Each bundle consisted of fifty−seven electrically heated rods and seven non−heated rods as shown in Fig.2.10. The core was usually subdivided into three regions to achieve a desired radial power distribution. This is shown in Fig.2.5. The high, medium and low power regions were named as A, B and C regions, respectively. The local peaking factor of heated rods in a bundle was unity, that is, all heated rods in a bundle had the same power density.

A heater rod consisted of a nichrome heating element, magnesium oxide (MgO) and boron nitride (BN) insulators, and inconel−600 sheath. BN was used for only central part of the heated region and MgO for the other part as shown in Fig.2.11. The heated length and the outer diameter of the heater rods were 3.66 m and 10.7 mm, respectively, which are identical to the corresponding dimensions of reference PWR fuel rods. The sheath wall thickness was 1.0 mm and was thicker than the reference fuel cladding, because of the requirements for thermocouple installation to measure the clad temperature. The heating element was a helical coil with a varying pitch to generate a 17 steps chopped cosine axial power profile as shown in Fig.2.12. The axial peaking factor was 1.40.

Non−heated rods were either stainless steel pipes or solid bars of 13.8 mm O.D. All the pipes were utilized for installation of instruments such as steam superheat probes and thermocouples. All the bars were used for carrying the assembly loads.

The heater rods and non−heated rods were held in radial position by grid spacers which were located at six elevations along the axial length as shown in Fig.2.12. A grid spacer was a lattice structure composed of stainless steel plates of 0.4 mm and 0.8 mm thick and 40 mm high. The top and the bottom edges of the stainless steel plates were sharpened. The rod pitch was 14.3 mm, which was the same as that of the reference PWR.

The heater rods penetrated through the bottom plate of the pressure vessel to facilitate lead out of the power cables. The outer diameter of the rods in the lower

plenum was reduced to 8.6 mm. Three phase electric current was used for heating the heater rods and the electrical neutral point was at the top of the rods, where they were inter−connected to each other.

2.3 Primary loops

The primary loop arrangement is shown in Figs.2.13 and 2.14. Primary loop consisted of three intact loops and a broken loop. Each loop consisted of hot leg and cold leg pipings (including cross over legs), a steam generator simulator and a pump simulator. Each intact loop connected the upper plenum to the upper portion of the downcomer, as a reference PWR. A broken loop simulated 200% cold leg break about 2 m from the pressure vessel wall, and consisted of two parts. One of them connected the upper plenum to a containment tank simulator (Containment tank 2) through a steam generator simulator. This part was called a broken loop SG side in CCTF. The other connected the upper portion of the downcomer to a containment tank simulator (Containment tank 1). This part was called a broken loop PV side in CCTF.

The inner diameter of the hot leg and cold leg pipings (0.155 m) was scaled down in proportion to the core flow area scaling. The length of each piping section was almost the same as the corresponding sections of the reference PWR.

The steam generator simulators were of U−tube and shell type heat exchangers as shown in Fig.2.15. The tube length was about 5 m shorter than the reference PWR. The vertical height of the steam generator simulators was also about 5 m lower than the reference PWR. During a test, the steam generator secondary sides contained high pressure saturated water at 540 K and 5.3 MPa. These conditions corresponded to those in the secondary side of the steam generators in a PWR during the reflood portion of a LOCA. The primary coolant passed through the tube side and the secondary coolant was stagnant in the shell side during the tests. The steam generator simulators of two loops were housed in a single shell assembly which had two sets of separated inlet and outlet headers for two loops. The wall thickness of the U−tube was 2.9 mm instead of 1.27 mm of the reference PWR, because of a higher pressure difference between the primary and secondary sides in the steam generator simulator.

The pump simulator consisted of the casing and vane simulators and an orifice plate as shown in Fig.2.16. The each loop flow resistance was simulated with the orifice plate. Each orifice plate had one hole with diameter and thickness of 95 mm and 10 mm, respectively.

The 200% cold leg break was simulated with two fast−open break valves (Blowdown valves) located at the two ends of the cold leg break, as shown in Figs.2.1, 2.2 and 2.13.

Two interconnected tanks (Containment tank 1 and containment tank 2), one

attached to each of the two ends of the cold leg break, simulated the PWR containment (Figs.2.1 and 2.2). On the Containment tank 2 connected to the hot leg side of the break, a pressure regulation system maintained the pressure at a preselected value by venting steam, as needed, to the atmosphere.

2.4 ECC injection system

ECC water could be injected into each cold leg and lower plenum, as shown in Figs.2.2 and 2.13. The ECC water stored two water supply tanks (Fig.2.3): the "Acc" tank, capable of providing water at a high flow rate for a short duration, and the "LPCI" tank, capable of providing water at a lower flow rate for a longer duration. Each tank could supply water to either the lower plenum or to the four cold legs through the feeding lines and the ECC nozzles (ECC ports).

The ECC water in the Acc tank was supplied to the primary loop with the pressurization by nitrogen, as in the reference PWR. The water flow rate was adjusted with the pressure in the Acc tank and the flow resistance of the feeding lines. The ECC water in the LPCI tank was supplid to the primary loop with the LPCI pumps, as in the reference PWR. The water flow rate was adjusted with the control valves located in the feeding lines.

The cold leg feeding lines were connected to the top of the cold leg pipings with 45 degree (Fig.2.14), as in the reference PWR. To simulate the linear velocity of the ECC water, the flow area of the exit of the feeding lines was adjusted by inserting a throtling devices.

2.5 Instrumentation

The instrumentation is divided into two groups. One of them is JAERI−supplied instruments measuring the temperatures, absolute pressures, differential pressures, water levels and flow rates. Thermocouples measured the temperatures of the rod surface, fluid and structure. The absolute pressures were measured in the upper and lower plena, steam generator plena and containment tanks. The differential pressure measurements were carried out at many locations covering the whole system almost completely. In the ECC water supply tanks and the containment tank 1, the liquid levels were measured. The flow meters measured the ECC water flow rate. Furthermore, flow rates in the downcomer, cross over leg pipings and vent line from the containment tank 2 to the atmosphere were measured with the drag disk flow meter, pitot tubes and ventulli tube, respectively. The total number of the JAERI−supplied instruments were 1316 channels and the signals from these instruments were recorded on magnetic tapes.

The other group of the instrumentation is the USNRC−supplied instruments.

They are the advanced instrumentation for the two-phase flow measurement. The names and quantities of those are tabulated in Table 2.3. The total number was 536 channels.

3. Test procedure and test conditions

3.1 Test procedure

The test procedure of the present tests, C2−1 (Run 55) and C2−SH1 (Run 53), was as follows (Fig.3.1):

i) Set−up of facility; Blowdown valves were set open. Pressure regulation valves on the containment tank−2 were controlled to keep pressure in the tank at a specified value (0.42 MPa) upto the end of the test.

ii) Setting of initial conditions; The primary system was preheated with external heaters to its specified temperature (Downcomer wall: 491 K, Core internals: 425 K, Primary loop pipings: 425 K) (During the test, the external heaters were turned off.). The pressure vessel and primary loops was pressurized to a specified pressure (0.42 MPa) with saturated steam. Temperature of water for ECC injection was set to a specified values (Water in Acc tank: 308 K; Water in LPCI tank: 310 K). ECC feeding lines was heated by circulating water in LPCI tank through circulation lines (During the test, this lines were closed.). The water in the secondary side of steam generator simulators was heated and pressurized (538 K and 5.3 MPa). The water level in lower plenum was set to a specified level (0.86 m in depth) with a suturated water. Core, upper plenum, loops and downcomer had no water for pretest conditioning phase.

iii) Supply of electric power to the heated rods in the core; Electric power was supplied to heat the heated rods after initial conditions had stabilized. Since steam around the heated rods was stagnant, the temperature of the heated rods increased adiabatically and reached a specified clad temperature (995 K) for initiation of ECC water injection. Figure 3.2 shows the initial set−up for C2−1 (Run 55).

iv) ECC water injection into lower plenum; When the temperature of the heated rods reached a specified clad temperature, ECC water injection into lower plenum was initiated (Note 1) for simulation of ECC water injection from Acc and LPCI tanks and accordingly the water level in lower plenum rose. ECC water injection rate was 0.103 m^3/s.

v) Initiation of decaying of electric power; When the water level in lower plenum reached the bottom of the core (This is called the reflood initiation or BOCREC.), the decay of electric power was initiated to

simulate the decay of heat of nuclear fuels at a LOCA.

vi) Termination of ECC water injection into lower plenum and starting of ECC water injection into cold legs; Few seconds after the reflood initiation, ECC water injection was switched from lower plenum to intact cold legs. ECC water injection rate was reduced to 0.089 m^3/s for simulation of ECC water injection from Acc and LPCI tanks. At a specified time (26.5 s) after initiation of ECC water injection to lower plenum, injection from Acc tank was terminated. As the result, ECC water injection rate decreased (0.011 m^3/s) for simulation of ECC water injection only from LPCI tank. The ECC water injection rate was maintained constantly until the end of the test.

vii) Termination of test: Clad temperature of heated rods was monitored during the test. When all thermocouples on the clad of heated rods indicated quenching of the heated rods, it was judged that the test was terminated. Several tens seconds after the termination of the test, electric power supplied to the heated rods was turned off. Then ECC water injection was stopped.

(Note 1)

In PWR, ECC water was injected only to cold legs. Therefore, ECC water injection into lower plenum in the tests was not real simulation to PWR case. However, since the violent condensation at ECC ports in cold legs may atypically affect the reflood behavior in CCTF tests, ECC water was injected first into lower plenum. After sufficient steam flow was established through intact cold legs, ECC water was injected into intact cold legs. Atypicality of this ECC injection method was investigated through the result of other CCTF tests called refill simulation tests.
The conclusion of the tests is that the atypical ECC injection procedure has no major influence on the test result and it is considered that the present ECC injection procedure is valid for simulation of PWR reflood behavior.

3.2 Test condition

Table 3.1 lists the initial test conditions of the present high pressure test C2-1 (Run 55). The test conditions were selected to simulate the reflood behavior under evaluation model (EM) condition of PWR 200% cold-leg break LOCA. Therefore, the test conditions were the same as those in the CCTF base case test C2-SH1 (Run 53), simulating EM conditions, except for the pressure. In C2-1 (Run 55) the pressure in containment tank-2 was controlled at 0.42 MPa, while in C2-SH1 (Run 53) it was controlled at 0.2 MPa. Figure 3.3 shows the comparison of the pressure between C2-1

(Run 55) and C2-SH1 (Run 53).

Basic phylosophy to determine the test conditions is summarized in the following.

(1) Pressure

Typical reactor safety evaluation result indicated that the pressure in the containment tank was 0.2–0.26 MPa during the reflood phase. This pressure depends on steam discharge rate from the primary system to the containment, condensation characteristics in the containment, and volume of the containment. Accordingly, the pressure depends on the type of containment. For the most probable case, the pressure is considered to be higher than the pressure indicated in the reactor safety evaluation (eg. 0.4 MPa). In addition, CCTF had small containment simulators (Containment tank 1 and containment tank 2) comparing with the containment of reference PWRs and the pressure in the CCTF containment simulators was controlled by discharging the excessive steam from the containment tank 2 to the atmosphere. Therefore, the pressure was not simulated exactly and then it was necessary to study the pressure effect on the reflood behavior in scope of the pressure of 0.2–0.4 MPa.

Based on the discussion mentioned above, the pressure in the present test was set at 0.42 MPa, while it was set at 0.2 MPa in the base case test.

(2) Power profile

Axial peaking factor for each heated rods was 1.4.

Radial power profile was convex, which meant that the power density was high in the central zone of the core and low in the peripheral zone of the core. The power ratios for the central, intermediate and peripheral zones were set at 1.37, 1.20, and 0.76, respectively. Radial power profile of the reference PWR was somewhat different profile. The power ratio was the highest in the intermediate zone of the core, which was between the central and the peripheral zones. It was the lowest in the peripheral zone of the core. Averaged power ratio of each zone for the beginning life was 1.09, 1.13 and 0.9 in the reference PWR. Therefore, the radial power profile of the present test is steeper than PWR case.

(3) Total power to heated rods and power decay

Total power was determined to simulate the EM condition with the following equation.

$$P_{CCTF} = 1.02 \times P_{0PWR} \times F_S \times F_M \times (\text{Old ANS} \times 1.2 + \text{Act.} \times 1.1)$$

P_{0PWR} = steady state power of reference PWR = 3411 MW

F_S = CCTF scaling factor = 1/21.2
F_M = CCTF experimental margine = 1.07
Old ANS x 1.2 + Act. x 1.1 = 0.0532 (Assuming 30 seconds after scram)

Factor 1.02 in the above equation is to account for the instrument error required for the licensing calculation. CCTF scale factor can be obtained in two ways as follows.

F_S = 1824/39372 = 1/21.59 based on number of heated rods
F_S = 0.26/5.5 = 1/21.2 based on core flow area

Since the difference between the two scaling factors above was less than 2%, F_S=1/21.2 was used. CCTF experimental margine was taken to account for the in strument error in the experiment and the contribution of the delayed neutron fission which is neglected in the licensing calculation. This margine also gives the margine for the highest power density of heated rods as shown in (4) below.

As the result,
P_{CCTF} = 9.35 MW

(4) Highest power density of heated rods

In reference PWR, the highest power density can be obtained as follows:

q_{PWR}= 1.02 x P_{0PWR} x 0.95 x F_r x F_a x (Old ANS x 1.2 + Act. x 1.1)/(NL)
F_r = Radial peaking factor for hot rod = 1.552
F_a = Axial peaking factor = 1.495
N = Number of fuel rods = 39372 for 15 x 15 bundle array and
50952 for 17 x 17 bundle array
L = Heated length of fuel rods = 3.66 m

Factor 0.95 in the above equation was introduced to account for gamma heating. Resultantly,

q_{PWR}= 2.83 kW/m for 15 x 15 bundle array and
2.19 kW/m for 17 x 17 bundle array

On the other hand, in CCTF it can be obtained as follows:

q_{CCTF} = P_{CCTF} x F_r x F_a x F_t /(NL)

F_r = Radial peaking factor for hot rod = 1.37 as shown in (2) above

F_a = Axial peaking factor = 1.4 as shown in (2) above

F_t = Power decay factor defined as follows

$$= \frac{\text{(Old ANS x 1.2 + Act.x 1.1) at time = t seconds after scram}}{\text{(Old ANS x 1.2 + Act.x 1.1) at time = 30 seconds after scram}}$$

N = Number of fuel rods = 1824

L = Heated length of fuel rods = 3.66 m

Resultantly,

q_{CCTF} = 2.69 kW/m

This power density is 5% less and 23% more for 15 x 15 and 17 x 17 bundle arrays of reference PWRs, respectively.

(5) Initial clad temperature

The highest initial clad temperature (1073 K; = Temperature at midplane of the heated rods in the highest power zone) at the reflood initiation was determined to simulate the clad temperature (1140 K) calculated in the representative reactor safety evaluation.

(6) Mode of ECC injection

In the licensing calculation followings were assumed for single failure of ECC injection system.

(1) ECC water injected into the broken loop is not effective.

(2) One LPCI pump out of two is not working.

Resultantly, three Acc systems out of four, two HCPI pumps and one LPCI pump out of two work. In CCTF tests the above injection mode was simulated as EM condition.

3.3 Chronology of events

The sequence of events that occurred during the test is listed in Table 3.2.

The data recording was initiated at the same time when the power supply to the heater rods in the core was initiated. This time was defined as 0 s. The Acc injection into the lower plenum was initiated at 81.0 s, the power decay was initiated at 90.0 s which was the bottom of core recovery time and the ECC injection location was changed from the lower plenum to the cold legs at 95.0 s. The ECC injection mode

was changed from Acc injection to LPCI at 107.5 s. All the heater rods were quenched by 417 s. The power was turned off at 708 s. LPCI was terminated at 828 s and the data recording was ended at 1029 s.

4. Results and discussion

4.1 Overall flow characteristics in high pressure test

The overall flow characteristics in high pressure test, C2-1, was similar to that of CCTF base case test, C2-SH1. Any qualitatively different phenomena were not recognized during reflood phase (Until whole core quenching). This indicates that it is reasonable to utilize the physical reflood model introduced from the result of the base case test to the high pressure condition. The following characteristics were commonly ovserved in C2-1 and C2-SH1 tests.

(1) The differential pressure in the downcomer indicated the maximum value at the end of Acc injection period. Then, it slightly decreased and kept nearly constant value due to the voiding in the downcomer and the entrainment phenomena at the top downcomer.

(2) The overflow of the water from the downcomer to the containment tank 1 initiated approximately at the end of Acc injection period and continued through the rest of the whole transient.

(3) Flooding mass flow rate into core was high (73 $kg/m^2/s$) in Acc injection period. It followed a stepwise decrease at the end of Acc injection period and was low (23 kg/m^2s) in LPCI injection period. Flooding mass flow rate was almost constant in LPCI injection period.

(4) The mass flow rate through each intact loop was identical each other. No parallel oscillation occurred among the intact loops.

(5) Mass flow rate through the broken loop was nearly 150% of that through each intact loop. This is due to an additional differential pressure at the broken cold leg nozzle from the downcomer to the break. The additional differential pressure increased the steam flow through the broken loop.

(6) The fluid temperature upstream the steam generator showed a saturation temperature. On the contrary, the fluid temperature downstream the steam generator showed a fair amount of superheat. This indicates that the flow can be regarded as almost single-phase vapor downstream the steam generator, and that the flowing water droplets evaporate in the steam generator completely by the heat exchange with water in the steam generator secondary side.

(7) In Acc injection period, the fluid temperature at the cold leg ECC ports was subcooled, and the flowing steam from the upper plenum to the downcomer was completely condensed. Resultantly water plug was formed in the cold leg and moved oscillatorily. In LPCI injection period, the fluid temperature at the cold leg ECC ports was at saturation. Flowing steam was not condensed completely

and the steam flow remained at exit of cold leg to the downcomer. Almost thermal equilibrium was established in cold legs.

(8) The broken cold leg nozzle pressure difference indicated a fairly large value comparing to the broken hot leg pressure difference. This indicates the effect of the broken cold leg nozzle pressure loss on the suppression of the steam flow through the intact loops is not negligible in order to estimate the core flooding coolant velocity.

(9) The water accumulation in the upper plenum and the steam generator inlet plenum was recognized, and then steam binding effect is considered to be reduced.

(10) The cooling of the heater rods began just after the reflood initiation at the entire elevation of the core due to the early water spreading from the bottom to the top of the core.

(11) Both bottom quenching and top quenching occurred.

(12) The maximum turnaround temperature (1116 K) was observed at the midplane (1.83 m elevation) and in the central high power zone, which was in the region of the bottom quenching.

(13) The bottom quench front propagation was roughly one−dimensional in each power zone. The bottom quench front advanced more slowly in the higher power zone.

(14) The top quench time was very variant depending on the radial location.

(15) The water accumulations in the downcomer, core, and upper plenum were azimuthally nearly uniform.

(16) The void fraction rapidly decreased after reflood initiation. The void fraction became almost constant at about 20 s after reflood initiation.

4.2 Comparison of high pressure test result with CCTF Core−II base case test results and Core−I test results

Referred tests

In order to investigate the effect of pressure on reflood behavior, the result of the high pressure test C2−1 (Run 55) is compared quantitatively with the result of the CCTF Core−II base case test C2−SH1 (Run 53). In Core−I test series, the parametric effect tests on the pressure were performed under three different pressures (0.15 MPa, 0.2 MPa and 0.3 MPa). By comparing the experimental results of Core−II series with those of Core−I series, the further understanding on the pressure effect can be obtained. The major difference of the test conditions between Core−I series and Core−II series is in the ECC condition.

The ECC flow rates in Core−II series are nearly identical to the expected ECC flow rates in the actual reactor under single failure condition. Whereas, the ECC flow rates in Core−I series were relatively small and more conservative compared to single failure conditions. The comparison of the ECC flow rates is listed below.

	Core−II test series		Core−I test series		
	C2−SH1	C2−2	C1−10	C1−5	C1−12
Pressure (MPa)	0.2	0.42	0.15	0.2	0.3
Acc injection rate (m^3/s)	1.1×10^{-1}	1.0×10^{-1}	7.5×10^{-2}	7.7×10^{-2}	8.8×10^{-2}
LPCI injection rate (m^3/s)	1.1×10^{-2}	1.1×10^{-2}	8.4×10^{-3}	8.4×10^{-3}	8.5×10^{-3}

Note In Core−II test series, low pressure test C2−8 (Run 67)[8],[9] was performed under the pressure of 0.15 MPa. Also Run 104 was performed under the pressure of 0.1 MPa.[10] Results have been written in JAERI open report and unclassified report, respectively.

Summary of comparison

Comparison indicated the following characteristics.

(1) The higher pressure resulted in the higher steam generation rate in the core due to the better core cooling. However, the higher pressure resulted in the lower steam velocity and the lower momentum flux because of the smaller specific volume of the steam. This led to the weaker steam binding effect through primary system although the steam mass flow rate was higher in the higher pressure test.

(2) The core differential pressure and the upper plenum differential pressure were higher at the high pressure due to the lower steam velocity resulting from the smaller specific volume of the steam. This fact suggests more water accumulation.

(3) The intact and broken loop differential pressures were lower at the higher pressure due to the lower momentum flux.

(4) With the pressure, the broken cold leg differential pressure decreased. This indicates that the improvement of the core cooling due to the pressurization

caused by the broken cold leg differential pressure becomes smaller with the pressure.

(5) The core flooding mass flow rate was higher at the higher pressure. The roughly one third of the increased core flooding mass flow rate was due to the higher water accumulation rate in the core and the roughly two thirds due to the higher steam flow rate through primary loops arising from weaker steam binding effect.

(6) The better core cooling with the pressure resulted in the lower turnaround temperature, the shorter turnaround and quench times.

These results, mentioned above, are consistent with the result of Core−I test series, which is described in the reference (7). These results are also consistent with the result of Core−II low pressure test C2−8 (Run 67) and Run 104. Detail comparison is shown in the following sections 4.2.1 and 4.2.2.

4.2.1 Comparison of system behavior

Steam generation in core

Figure 4.1(a) shows the transient of the evaluated mass flux of the steam generated in the core. The steam generation rate was evaluated by the heat balance calculation in the core using the measured clad temperature transients of the heater rods. The mass flux of the generated steam is higher (20%) in the high pressure test before the whole core quench (300 s) than in the Core−II base case test. This suggests a better core cooling with the pressure. After the time, the mass flux in the high pressure test is lower. This is because in the high pressure test the stored energy has already released and only the heat input is released during the period. Figure 4.1(b) shows the evaluated steam velocity at core outlet. Although the mass flux is higher in the high pressure test, the steam velocity is lower (−25%) because of the smaller specific volume of the steam. The momentum flux is also lower (−10%) in the high pressure test, as shown in Fig.4.1(c).

Core and upper plenum differential pressure

Figures 4.2 and 4.3 show the core and upper plenum differential pressures, respectively. Both differential pressures increase with the pressure. This indicates more water accumulation with the pressure. This is due to the lower void fraction and the lower carryover rate from the upper plenum to hot legs caused by the lower steam velocity with the pressure. The more water accumulation in the core and the upper plenum with the pressure is also observed in CCTF Core−I test results[7] and FLECHT−SET data[11].

Loop differential pressure

Figure 4.4 shows the differential pressures across the intact loop and the broken loop. The differential pressure across the intact loop is lower (−10% at 250 s) in the high pressure test than in the Core−II base case test. This is due to the lower momentum flux with the pressure.

The differential pressure across the broken loop is lower (−30% or −15 kPa at 250 s) in the high pressure test than in the base case test. This is mainly due to the lower differential pressure across the broken cold leg with the pressure because the differential pressure across the broken loop ΔP_B can be described as follows.

$$\Delta P_B = \Delta P_I + \Delta P_{BCL}$$

where ΔP_I and ΔP_{BCL} are the differential pressures across the intact loop and across the broken cold leg, respectively. The lower ΔP_{BCL} with the pressure is shown in Fig.4.5.

Downcomer differential pressure

In Core−I test results[7], the downcomer differential pressure was higher with the higher pressure during the early stage of the reflood (<60 s), and it was lower with the higher pressure during the later stage of the reflood (>80 s). The higher downcomer differential pressure with the higher pressure during the early stage of the reflood was explained by the higher Acc injection rate with the pressure. The lower downcomer differential pressure with the pressure during the later stage of the reflood was explained by the lower saturated water density with the pressure.

Figure 4.6 shows the downcomer differential pressure obtained in Core−II tests. The downcomer differential pressure tends to be lower with the pressure. This tendency is consistent with the tendency of Core−I test result during the later stage of the reflood. However, the tendency observed in Core−I tests during the early stage of the reflood is not recognized in Core−II tests. This is because of the higher Acc flow rate in Core−II tests than in Core−I tests. Since in Core−II tests the Acc flow rate is high, simulating PWR case, the downcomer differential pressure observed in Core−II tests is considered to be PWR typical. In Core−II tests the downcomer is completely filled with water very soon after reflood initiation. The water accumulation in the downcomer is mainly controlled by the Acc flow rate in this period until the downcomer water filling, almost independently of the pressure. After the downcomer water filling, when the ECC injection rate decreased by switching from Acc injection to LPCI, the pressure rather than the ECC injection rate influenced the downcomer differential pressure. The downcomer differential pressure can be described by the core differential pressure ΔP_C, the intact differential pressure ΔP_I and the lower and

upper plenum differential pressures ΔP_L and ΔP_U, as follows.

$$\Delta P_D = \Delta P_C + \Delta P_U + \Delta P_I + \Delta P_L$$

The lower ΔP_D in the high pressure test can be attributed mainly to the lower ΔP_I.

Loop mass flow

Figure 4.7 shows the effluent mass from the upper plenum to the hot legs, i.e. the integrated loop mass flow rate. Although the loop differential pressure is lower with the pressure, the loop mass flow rate is higher. It is approximately 20% higher in the high pressure test than that in the base case test. The higher loop mass flow rate with the pressure is due to the more steam generation caused by the better core cooling at the higher pressure.

Figure 4.8 shows the integrated overflowing mass from the downcomer to containment tank 1. The higher pressure gives the less overflowing mass. This tendency is consistent with Core−I test results. This tendency is due to the higher flooding rate in the higher pressure test, as shown later.

Core flooding mass flow

Figure 4.9 shows the core flooding flow rate and the integrated flooding water mass into the core. The integrated flooding mass with the higher pressure is higher, as same in Core−I test results. It is approximately 30% higher in the high pressure test than that in the base case test. Figure 4.10 shows the mass balance characteristics in the core. The higher flooding rate into the core with the higher pressure is contributed about two thirds by the higher loop mass flow rate and about one third by the higher water accumulation at 250 s.

Fluid temperature at core inlet

Figure 4.11 shows the subcooling at the core inlet. The subcooling is about 10 K smaller in the high pressure test than in Core−II base case test. In Core−I test, the subcooling was almost identical among three tests, C1−10 (P=0.15 MPa), C1−5 (P=0.20 MPa) and C1−12 (P=0.3 MPa). The history of the subcooling in Core−I test is almost identical with that of the high pressure test. The particularly different tendency of the subcooling in Core−II base case test is probably due to the different setting procedure of the fluid temperature in the lower plenum prior to the initiation of the test. In Core−II base case test, the fluid temperature in the lower plenum was set at the lower value in comparison with other tests.

Through the above result, fluid temperature at core inlet of PWRs during reflood

phase is considered to be nearly the same in different pressure condition.

4.2.2 Comparison of core cooling behavior

Clad temperature

Figure 4.12 show the clad temperatures measured in the lower and upper elevations of the core. The lower turnaround temperature and the earlier turnaround time with the pressure are noticed from the figure. This is due to the higher heat transfer coefficient with the pressure, as shown in Fig.4.13. Figure 4.14 shows the effect of the pressure on the axial distribution of the turnaround and the quench times of the heater rods in the medium power region. The turnaround time is almost identical in the lower elevation of the core. This is because the clad temperature in the lower elevation of the core turns around very soon after the reflood initiation and the effect of the pressure on the turnaround time in the lower elevation of the core is not recognized. The turnaround time in the upper elevation of the core is smaller with the pressure. This is because of the better core cooling with the pressure. The quench time is smaller with the pressure. This is also because of the better core cooling with the pressure. From the inclination of the quench time in Fig.4.14, the faster quench front velocity with the pressure is noticed.

Figure 4.15 shows the effect of the pressure on the axial distribution of the turnaround temperature, the quench temperature and the temperature rise in the medium power region. The quench temperature at a given elevation is almost similar with each other regardless the different pressure. However, it is slightly higher with the pressure. The relationship of the quench front velocity and the quench temperature is incosistent with the previous quench front velocity correlation, which describes the faster quench front velocity with the lower quench temperature. The turnaround temperature at a given elevation is almost similar with each other in the lower elevation of the core and it is lower with the pressure in the upper elevation of the core. The temperature rise shows the same trend as the turnaround temperature. The lower turnaround temperature and the lower temperature rise with the pressure in the upper elevation of the core is due to the better core cooling with the pressure.

Figure 4.16 and 4.17 show the effect of the pressure on the maximum temperature rise and the maximum turnaround time of the midelevation in the high power region. It is clearly seen that the higher pressure gives the smaller maximum temperature rise and the earlier maximum turnaround time. The temperature rise at the midelevation is 32 K lower under 0.42 MPa than under 0.2 MPa. The discrepancy between symbols and in Core-I data is due to the different ECC injection rate. Data was obtained under the lower ECC injection rate than EM condition, while data was obtained under EM condition. Then, the ECC injection rate of the test

shown by was identical with that of Core-II tests.

Figure 4.18 shows the effect of the pressure on the quench time of the midelevation in the high power region. The higher pressure gives the earlier quench. The last quenching at the midelevation was about 120 s earlier under 0.42 MPa than under 0.2 MPa.

Sectional differential pressure in core

Figure 4.19 and 4.20 show the sectional differential pressures in the lower and the upper elevations of the core, respectively. In Fig.4.20, data which were obtained before the time indicated by arrows were not correct due to instrumentation error. The higher differential pressure, i.e. the more water accumulation, with the pressure is observed at every elevation except for the lowest elevation, as in Core-I tests. The opposite tendency in the lowest elevation is due to the lower boiling initiation point caused by the lower subcooling in the high pressure test, as shown in Fig.4.11.

4.3 Effect of pressure on system behavior

Figure 4.21(a) shows the effect of the pressure on the core differential pressure ΔP_C, the upper plenum differential pressure ΔP_U, the intact loop differential pressure ΔP_I and the downcomer differential pressure ΔP_D. ΔP_C and ΔP_U increase with the increase ΔP_I in the pressure, while ΔP_I and ΔP_D decrease with the increase in the pressure. The cause of these trends is basically the higher steam generation rate in the core due to the better core cooling and the smaller specific volume of the steam with the pressure. In order to get the more understanding on the effect of the pressure, a quantitative investigation has been performed. The differential pressure through each intact loop ΔP_I can be roughly described by the momentum flux (m_{gI}^2 / ρ_{gI}) as follows.

$$\Delta P_I = K_I (m_{gI}^2 / \rho_{gI})$$

Approximately, the steam density ρ_{gI} and the steam mass flux m_{gI} are proportional to the pressure P and the total steam mass flux m_T, respectively. Consequently,

$$\rho_{gI} = K_1 P$$

$$a\ m_{gI} = m_T$$

where, K_1 and a are constants. Finally,

$$\Delta P_I = (\frac{K_I}{a^2 K_1})(\frac{m_T^2}{P}) \quad (1)$$

The pressures in the upper plenum were 0.45 MPa in the high pressure test and 0.26 MPa in the Core−II base case test, respectively. This means P is 70% higher in the high pressure test. The m_T is 20% higher in the high pressure test, as described in 4.2.1. Since the term (K_I/a^2K_1) is insensitive to the pressure, the 70% higher P and the 20% higher m_T leads nearly 15% decrease in ΔP_I by Eq.(1). This is nearly equal to the measured decrease in ΔP_I (20%). In the above evaluation, the steam mass flow rate generated in the steam generator is neglected, since it is below 10% of that generated in the core.

Figure 4.21(b) shows the effect of the pressure on the broken loop differential pressure ΔP_B and the broken cold leg differential pressure ΔP_{BCL}. Both ΔP_B and ΔP_{BCL} decrease with the increase in the pressure. The ΔP_{BCL} can be described as follows[12].

$$\Delta P_{BCL} = K_{BCL}(\frac{1}{2})\rho_m u_m^2 \quad (2)$$

The evaluated steam and water mass flow rates in the high pressure test and the Core−II base case test are as follows.

- Steam mass flow rate
  - 0.8 kg/s in the high pressure test
  - 0.65 kg/s in the Core−II base case test
- Water mass flow rate
  - 5 kg/s in the high pressure test
  - 6.5 kg/s in the Core−II base case test

Since ρ_m is proportional to 1/x (x=quality) at the low quality flow (14% in the high pressure test and 9% in the Core−II base case test), ρ_m is 35% lower in the high pressure test. In addition, since the u_m is roughly proportional to m_g/ρ_g or m_g/P, the 20% higher m_g and the 70% higher P lead the 30% lower u_m in the high pressure test. The above values result in the 70% decrease in ΔP_{BCL} by Eq.(2). This is nearly equal to the measured decrease in ΔP_{BCL}. Thus, the effect of the pressure on ΔP_I, ΔP_{BCL} and ΔP_B can be explained quantitatively with the pressurization and the enhancement of the core cooling with the increase in the pressure.

Figure 4.22 shows the mass flow rate distribution in the primary system. The upper number in each location is the mass flow rate evaluated in the high pressure test. The lower number is that evaluated in the Core−II base case test. The noticeable points from the figure are as follows.

(1) The core flooding mass flow rate is higher in the high pressure test.
This is partly due to the higher water accumulation rate in the core and the higher steam flow rate through primary loops arising from weaker steam binding.

(2) The intact loop mass flow rate is higher in the high pressure test. This means the flow rate ratio between the intact loop and the broken loop increase with the increase in the pressure. This is due to the lower ΔP_{BCL} with the pressure.

5. Conclusion

A high pressure test C2−1 (Run 55) was performed using the Cylindrical Core Test Facility (CCTF). In the test, the containment pressure was set at 0.42 MPa, which is maximum pressure expected during reflood phase of PWR LOCAs. Through the comparison of the test result with the experimental result of CCTF Core−II base case test C2−SH1 (Run 53) (The containment pressure was 0.2 MPa), the following conclusions were obtained.

(1) The overall flow characteristics in the high pressure test were qualitatively similar to that of Core−II base case test and Core−I tests. Any qualitatively different phenomena were not recognized during reflood phase. This indicates that it is reasonable to utilize the physical reflood model developed from the result of the base case test to the high pressure condition at least up to 0.42 MPa for prediction of reflood phenomena of PWRs.

(2) On the other hand, following quantitative influence of high pressure on reflood phenomena was observed. These results were the same as that previously observed in CCTF tests in the scope of the pressure up to 0.3 MPa.

(i) The higher pressure resulted in the higher steam generation rate in the core due to the better core cooling. However, the higher pressure resulted in the lower steam velocity and the lower momentum flux due to the smaller specific volume of the steam.

(ii) The core differential pressure and the upper plenum differential pressure were higher in the high pressure due to the lower steam velocity. The intact and broken loop differential pressures were lower in the high pressure due to the lower momentum flux and due to the lower broken cold leg differential pressure, respectively. Hence, so−called steam binding effect was weaker in the higher pressure test.

(iii) With the pressure, the broken cold leg differential pressure decreased. This indicates that the improvement of the core cooling due to the pressurization with the broken cold leg differential pressure becomes smaller with the pressure.

(iv) The core flooding mass flow rate increased with the pressure. It was about 30 % higher under 0.42 MPa than under 0.2 MPa. The roughly one third of the increased core flooding mass flow rate was due to the higher water accumulation rate in the core and the roughly two thirds due to the higher steam flow rate through primary loops arising from weaker steam binding effect.

(v) The better core cooling with the pressure resulted in the lower turnaround

temperature and the shorter turnaround and quench times in the high pressure test than in the base case test. This tendency was significant in the upper elevation of the core.

The maximum turnaround temperature at the midplane was 32 K lower under 0.42 MPa than under 0.2 MPa. The last quenching at the midplane was about 120 s earlier under 0.42 MPa than under 0.2 MPa.

(3) The higher pressure leads to the better core cooling, and hence the safety margin increases with the pressure.

Acknowledgements

The authors are much indebted to Drs. Y. Kaneko and T. Hiraoka for their guidance and encouragement for this program. The authors wish to express their appreciation to the members of their analysis group for valuable discussions. They also would like to express their thanks to the 2D/3D project members of the USA and FRG for valuable discussions.

temperature and the shorter turnaround and quench times in the high pressure test than in the base case test. This tendency was significant in the upper elevation of the core.

The maximum turnaround temperature at the midplane was 32 K lower under 0.42 MPa than under 0.2 MPa. The last quenching at the midplane was about 120 s earlier under 0.42 MPa than under 0.2 MPa.

(3) The higher pressure leads to the better core cooling, and hence the safety margin increases with the pressure.

Acknowledgements

The authors are much indebted to Drs. Y. Kaneko and T. Hiraoka for their guidance and encouragement for this program. The authors wish to express their appreciation to the members of their analysis group for valuable discussions. They also would like to express their thanks to the 2D/3D project members of the USA and FRG for valuable discussions.

References

(1) Hirano, K. and Murao, Y.: 'Large Scale Reflood Test', Nihon−Genshiryoku−Gakkai Shi (J. At. Energy Soc. Jpn.)[in Japanese], 2(10),681(1980)

(2) Iguchi, T. et al.: 'Analysis report on CCTF reflood tests' [in Japanese], to be published as a JAERI−M report

(3) Adachi, H. et al.: 'Design of Slab Core Test Facility (SCTF) in Large Scale Reflood Test Program, Part I: Core−I', JAERI−M 83−080, (1983)

(4) Murao, Y., et al., "Analysis Report on CCTF Core−I Reflood Tests", to be published as a JAERI−M report.

(5) Murao, Y., et al., "Evaluation Report on CCTF Core−I Reflood Test C1−5 (Run 014) − Over−all System Thermo−hydrodynamic Behaviors observed in the Base Case Test", JAERI−M 83−027, February (1983).

(6) Murao, Y., et al., "Evaluation Report on CCTF Core−I Reflood Test C1−19 (Run 38) − Experimental Assessment of the Evaluation Model for the Safety Analysis on the Reflood Phase of a PWR−LOCA", JAERI−M 83−029, February (1983).

(7) Akimoto, H., et al., "Evaluation Report on CCTF Core−I Reflood Tests C1−5 (Run 14), C1−10 (Run 19) and C1−12 (Run 21) − Effect of Containment Pressure −", JAERI−M 83−091, June (1983).

(8) Akimoto, H., et al., "Evaluation Report on CCTF Core−II Reflood Test C2−8 (Run 67) − Effect of system pressure −", JAERI−M 87−001, January (1987).

(9) Akimoto, H., et al., "System pressure effect on system and core cooling behavior during reflood phase of PWR LOCA", J. Nucl. Sci. Technol., 24(4), PP.276−288, April (1987).

(10) Iguchi, T., et al., "Effect of low pressure in containment tank on reflood behavior", to be published as a JAERI−M report

(11) Waring, J.P., et al., "PWR FLECHT−SET Phase B1 Evaluation Report", WCAP−8583, August (1975).

(12) Akimoto, H., et al., " Pressure drop through broken cold leg during reflood phase of loss−of−coolant accident of pressurized water reactor", J. Nucl. Sci. Technol., 21(6), PP.450−465, June (1984).

Table 2.1 Scaled dimensions of CCTF components

(Scaling of components)

Component		PWR	CCTF	Ratio
Pressure vessel				
Vessel inside diameter	(mm)	4394 (173″)	1084	
Vessel thickness	(mm)	216 (8 1/2″)	90	
Core barrel outside diameter	(mm)	3874	961	
Core barrel inside diameter	(mm)	3760	929	
Thermal shield outside diameter	(mm)	4170		
Thermal shield inside diameter	(mm)	4030		
Downcomer length	(mm)	4849	4849	1/1
Downcomer gap	(mm)	114.3	61.5	
Downcomer flow area	(m^2)	4.23	0.197	1/21.44
Lower plenum volume	(m^3)	29.6	1.38	1/21.44
Upper plenum volume	(m^3)	43.6	2.76	1/15.8
Fuel (heater rod) assembly				
Number of bundles	(--)	193	32	
Rod array per bundle	(--)	15x15	8x8	
Rod heated length	(mm)	3660	3660	1/1
Rod pitch	(mm)	14.3	14.3	1/1
Fuel rod outside diameter	(mm)	10.72	10.7	1/1
Thimble tude diameter	(mm)	13.87	13.8	1/1
Instrument tude diameter	(mm)	13.87	13.8	1/1
Number of heater rods	(--)	39372	1824	1/21.58
Number of non-heated rods	(--)	4053	244	1/18.09
Core flow area	(m^2)	5.29	0.25	1/21.2
Core fluid volume	(m^3)	17.95	0.915	1/19.6
Primary loop				
Hot leg inside diameter	(mm)	736.6 (29″)	155.2	1/4.75
Hot leg flow area	(m^2)	0.426	0.019	1/22.54
Hot leg length	(mm)	3940	3940	1/1
Pump suction inside diameter	(mm)	787.4 (31″)	155.2	1/5.07
Pump suction flow area	(m^2)	0.487	0.019	1/25.77
Pump suction length	(mm)	9750	7950	1/1
Cold leg inside diameter	(mm)	698.5 (27.5″)	155.2	1/4.50
Cold leg flow area	(m^2)	0.383	0.019	1/20.26
Cold leg length	(mm)	5600	5600	1/1

Table 2.1 (Cont.)

Component		PWR	CCTF	Ratio
Steam generator simulator				
Number of tubes/loop	(--)	3388	158	1/21.44
Tube length (average)	(m)	20.5	15.2	1/1.35
Tube outside diameter	(mm)	22.225 (0.875″)	25.4	
Tube inside diameter	(mm)	19.7 (0.05″)	19.6	1/1
Tube wall thickness	(mm)	1.27	2.9	
Heat transfer area/loop	(m^2)	4784 (51500 ft^2)	192	1/24.92
Tube flow area/loop	(m^2)	1.03	0.048	1/21.44
Inlet plenum volume/loop	(m^3)	4.25	0.198	1/21.44
Outlet plenum volume/loop	(m^3)	4.25	0.198	1/21.44
Primary side volume/loop	(m^3)	30.50 (1077 ft^3)	1.2	1/25.4
Secondary side volume/loop	(m^3)	157.33 (5556 ft^3)	2.5	1/62.9
Others				
Containment tank 1	(m^3)		30	
Containment tank 2	(m^3)		50	
Storage tank	(m^3)		25	
Acc. tank	(m^3)		5	
Saturated water tank	(m^3)		3.5	

Table 2.2 Elevations of CCTF components

(Elevation of components)

Component		PWR	CCTF	Discrepancy
Bottom of heated region in core	(mm)	0	0	0
Top of heated region in core	(mm)	3660	3660	0
Top of downcomer	(mm)	4849	4849	0
Bottom of downcomer	(mm)	0	0	0
Centerline of cold leg	(mm)	5198	4927	-271
Bottom of cold leg (inside)	(mm)	4849	4849	0
Centerline of loop seal lower end	(mm)	2056	2047	-9
Bottom of loop seal lower end	(mm)	1662	1959	+297
Center of hot leg	(mm)	5198	4927	-271
Bottom of hot leg (inside)	(mm)	4830	4849	+19
Bottom of upper core plate	(mm)	3957	3957	0
Top of lower core plate	(mm)	-108	-50	+58
Bottom of tube sheet of steam generator	(mm)	7308	7307	-1
Lower end of steam generator plenum	(mm)	5713	5712	-1
Top of tubes of steam generator (avg)	(mm)	17952.7	14820	-3132.7

(Number of upper plenum internals)

Component	PWR (New type)	CCTF-Ⅱ	
	Quantity	Desired quantity	Selected quantity
Control rod guide tubes	57	9.45	10
Support columns without mixers	50	8.29	10
Orifice plates	16	2.65	--
Open holes	70	11.61	12
Total	193	32	32

Table 2.3 Instruments provided by USNRC

Instrument	Number of sets	Number of sensors
DC FDG	18	162
DC VOP	1	1
DC drag disk	4	4
Core velocimeter	4	4
Core impedance probe	12	24
Core LLD	6	96
LP LLD	3	15
End box turbine meter	8	8
UP turbine meter	4	4
UP FDG	11	110
UP film probe	2	4
UP prong probe	2	4
UP VOP	1	1
VV turbine meter	2	2
VV string probe	2	2
HL film probe	2	4
HL VOP	1	1
Reference probe	1	1
Spool piece	8	89
Total	92	536

Note:

DC : Downcomer, FDG: Fluid distribution grid,
VOP: Video optical probe, LLD: Liquid level detector,
LP : Lower plenum, UP : Upper plenum,
VV : Vent valve HL : Hot leg

Table 3.1 Summary of measured test conditions for test C2-1 (Run 55)

		Measured	
Power			
Total (MW)	:	9.35	(Initial)
Linear (kW/m)	:	1.4	(Initial, Average)
Radial Power Distribution	:	1.36:1.20:0.76	
Decay Type: ANSx1.2 + Actinidex1.1 (30 sec after Scram)			
Pressure (MPa)			
System	:	0.42	
Steam Generator Secondary	:	5.3	
Temperature (K)			
Downcomer Wall	:	491	(Initial)
Primary Piping Wall	:	425	(Initial)
Steam Generator Secondary	:	538	(Initial)
Peak Clad at ECC Initiation	:	995	
Peak Clad at BOCREC	:	1073	
Lower Plenum Filled Liquid	:	421	(Initial)
ECC Liquid	:	309	
Water Level (m)			
Lower Plenum	:	0.86	(Initial)
Steam Generator Secondary	:	7.4	(Initial)
Injection Rate (m^3/s)			
Accumulator : into lower plenum		0.103	
into cold leg		0.089	
LPCI	:	0.011	
ECC Injection Duration Time (s)			
Accumulator (After BOCREC)	:	17.5	

Table 3.2 Chronology of events for test C2-1 (Run 55)

EVENT	TIME (sec)
Test Initiated (Heater Rods Power on) (Data Recording Initiated)	0
Accumulator Injection Initiated	81.0
Power Decay Initiated (Bottom of Core Recovery)	90.0
Accumulator Injection Switched from Lower Plemum to Cold Leg	95.0
Accumulator Injection Ended and LPCI Injection Initiated	107.5
All Heater Rod Quenched	417.0
Power Turned off	708.0
LPCI Injection Ended	828.0
Test Ended (Data Recording Ended)	1029.0

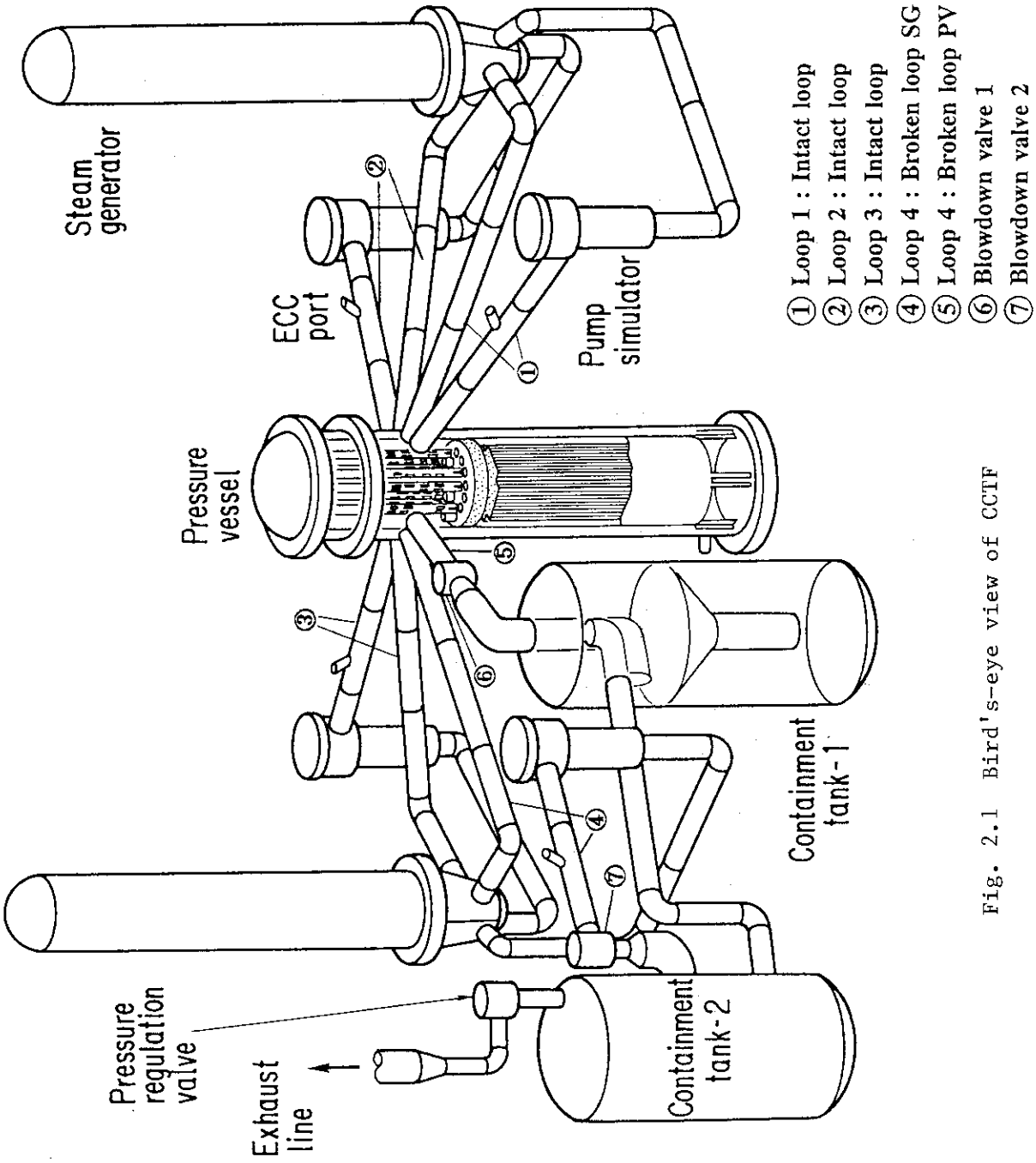

Fig. 2.1 Bird's-eye view of CCTF

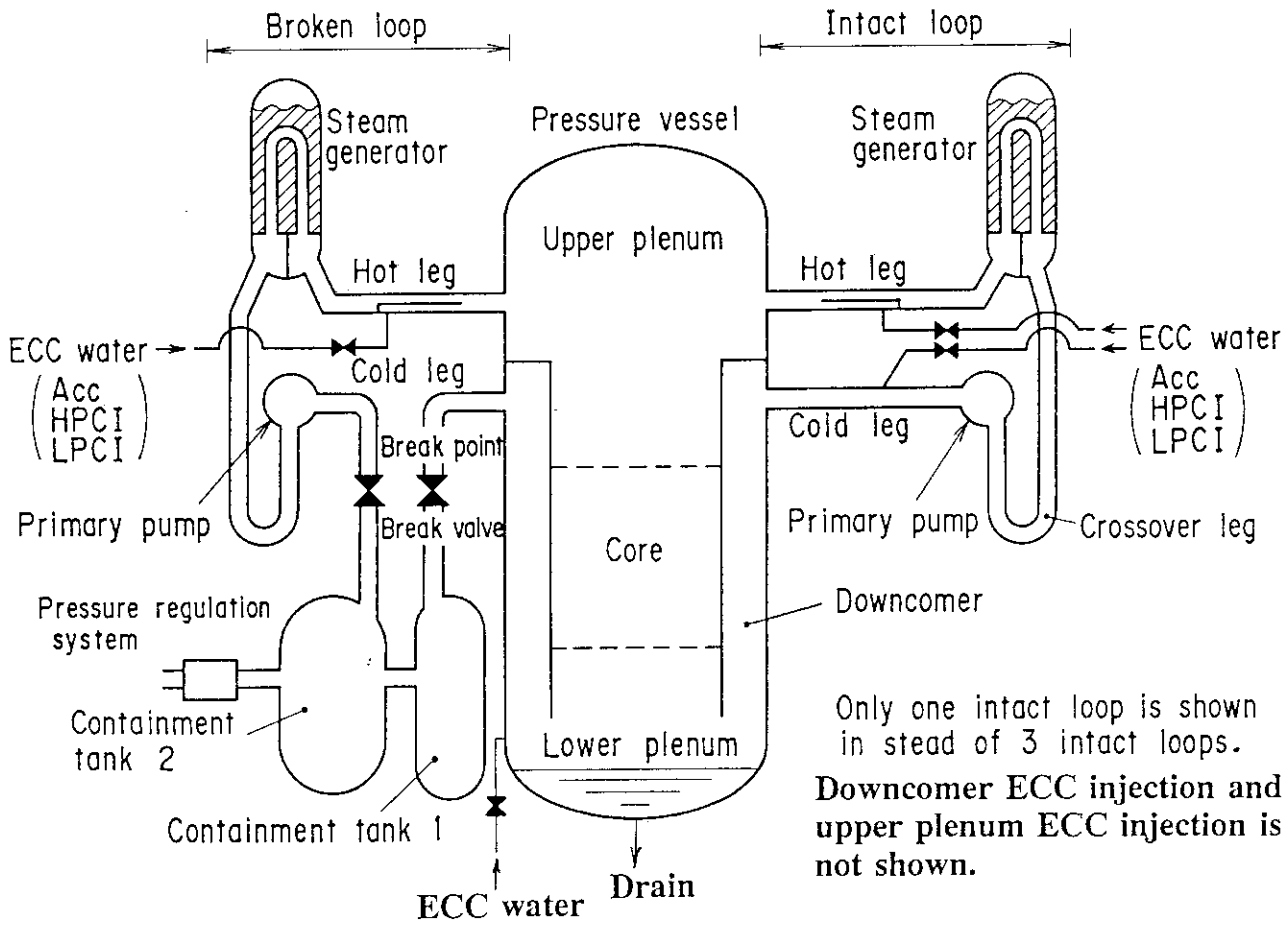

Fig. 2.2 Schematic diagram of CCTF main parts

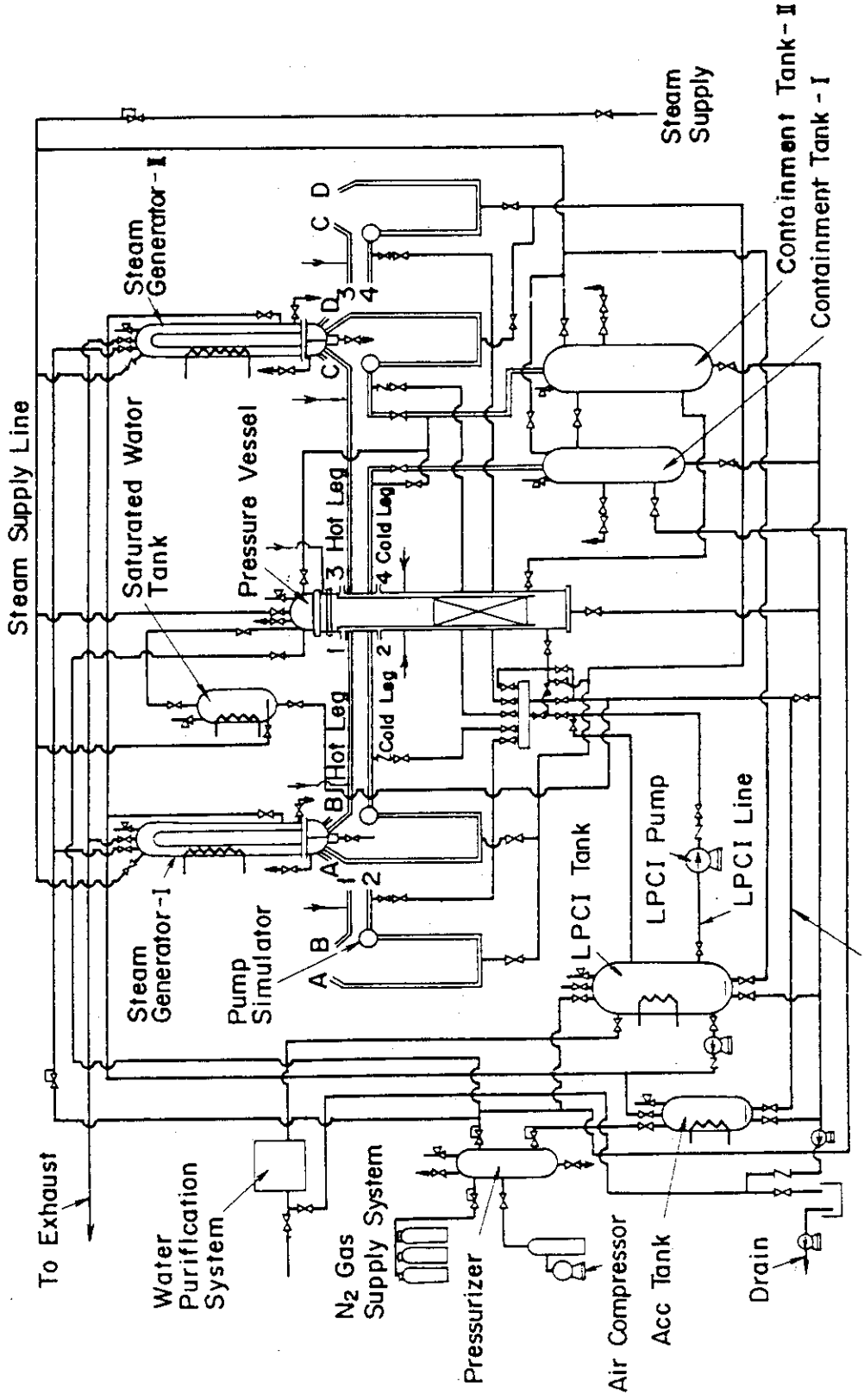

Fig. 2.3 Flow diagram of CCTF

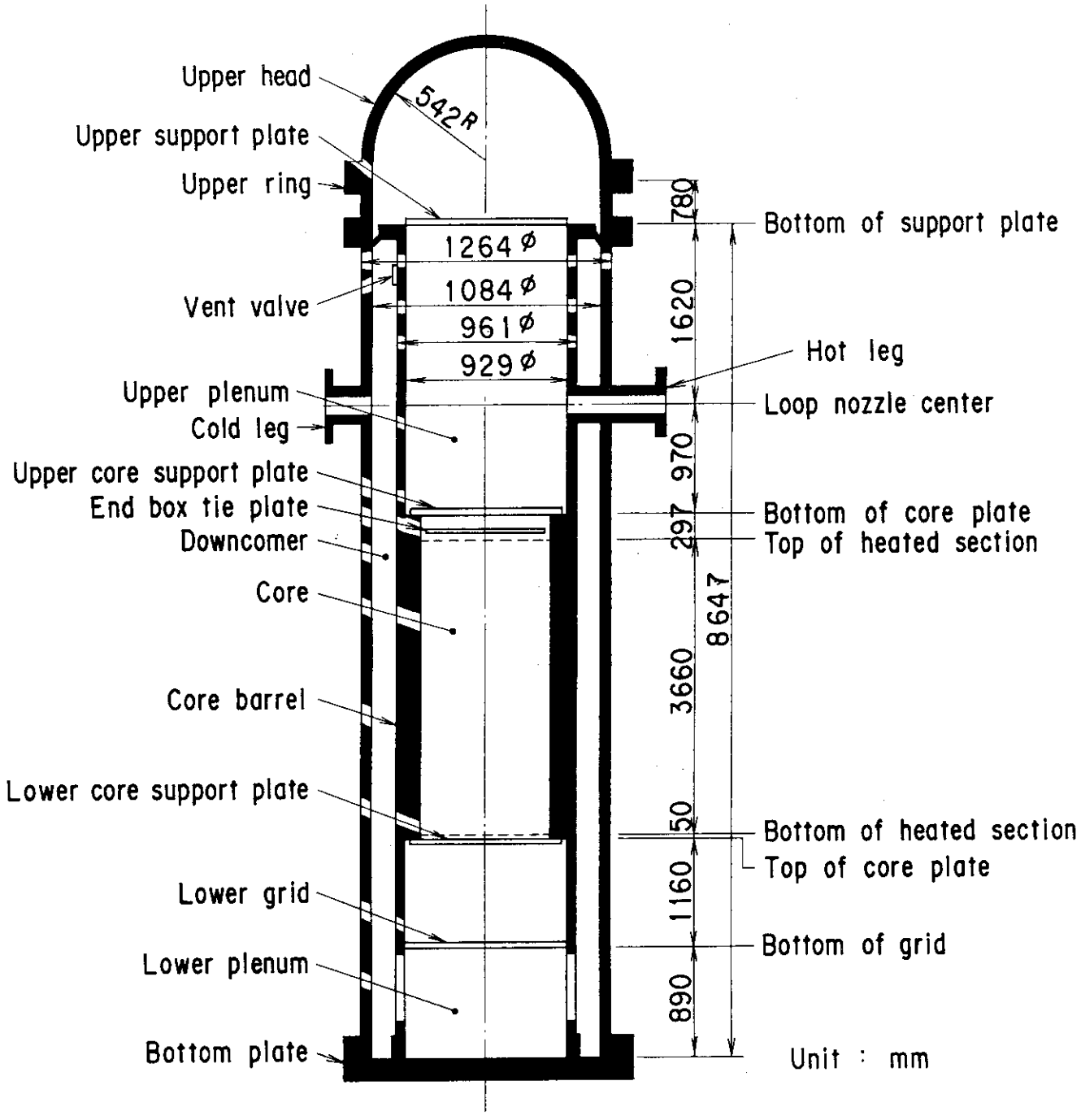

Fig. 2.4 CCTF Core-II pressure vessel

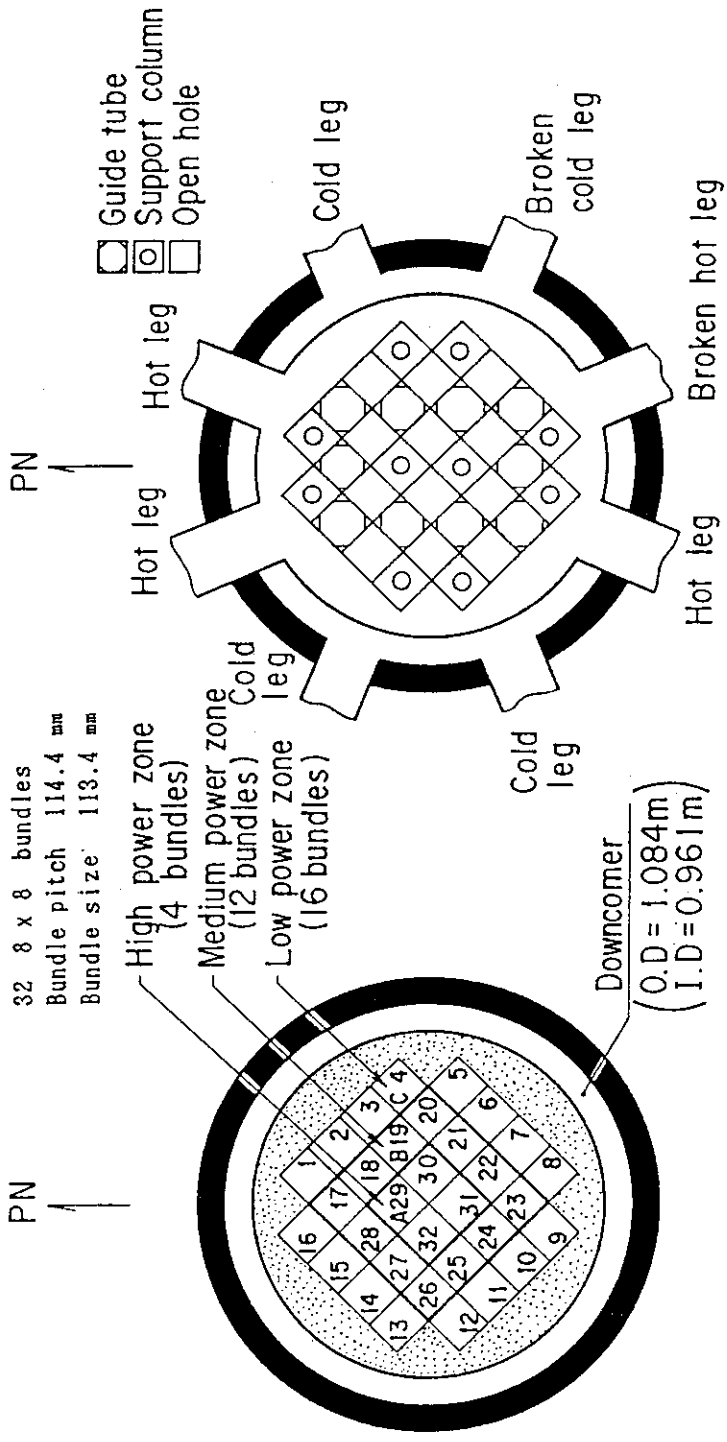

Fig. 2.5 Cross section of CCTF Core-II pressure vessel

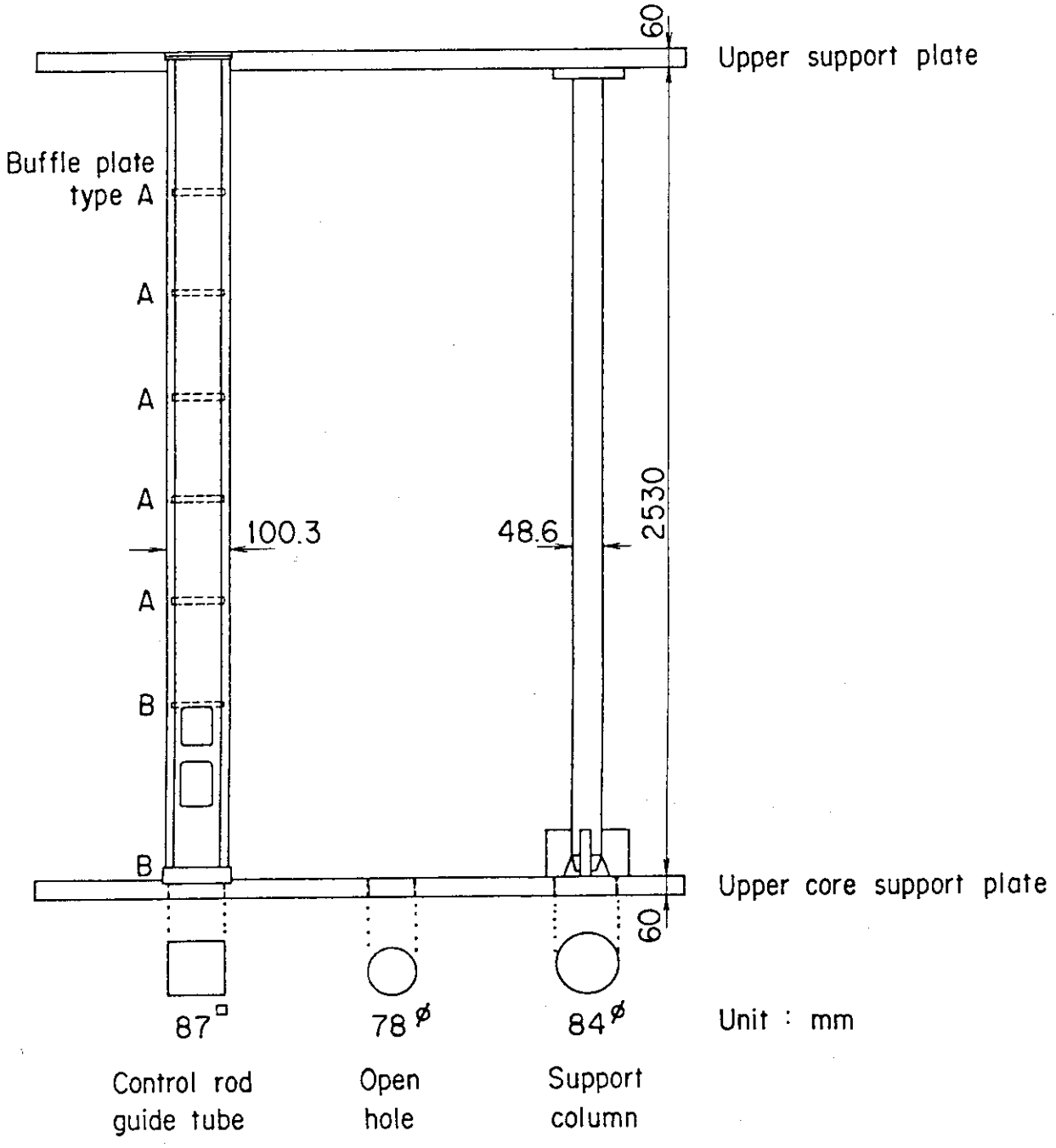

Fig. 2.6 Upper plenum internals

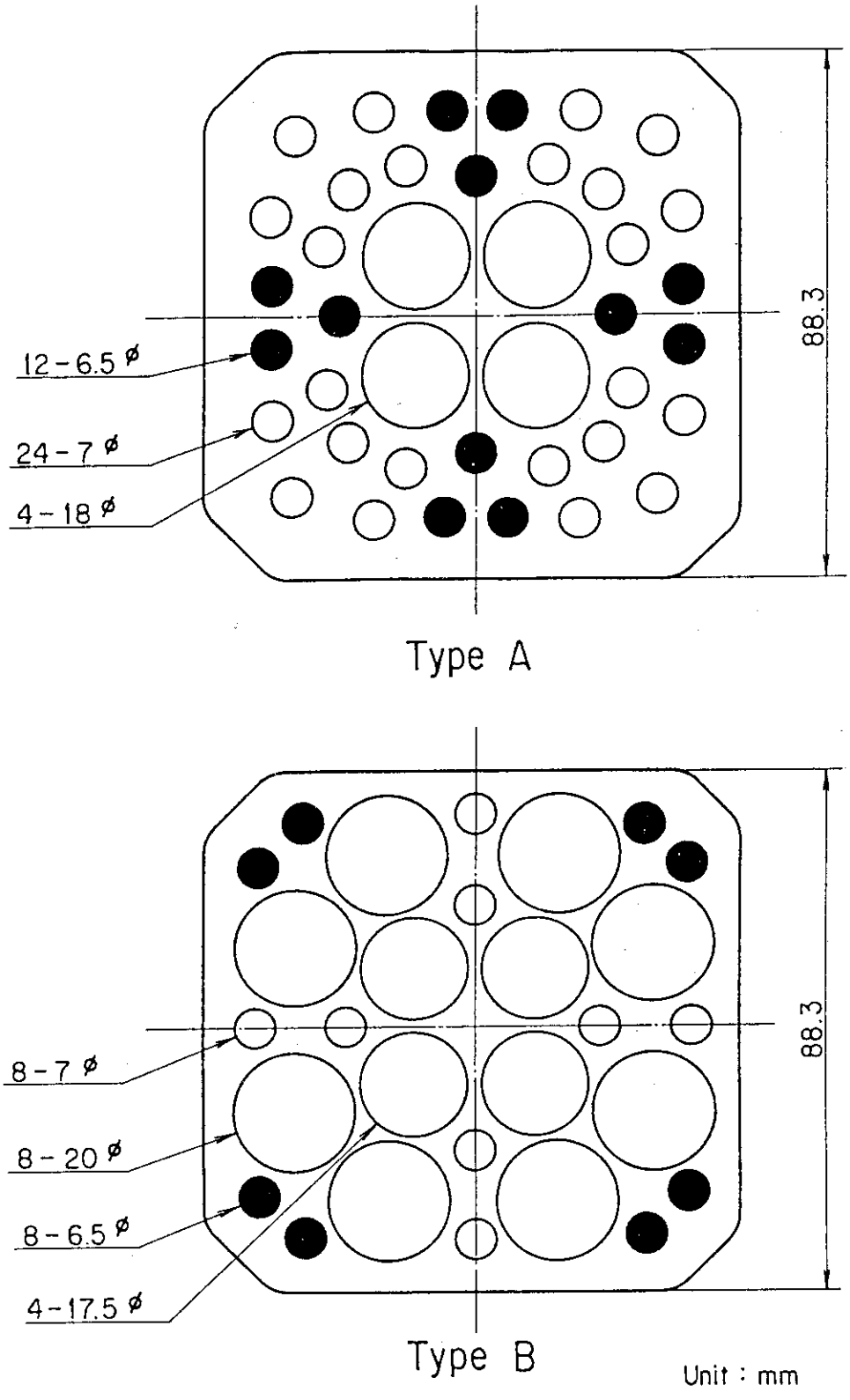

Fig. 2.7 Buffle plates in control rod guide tube

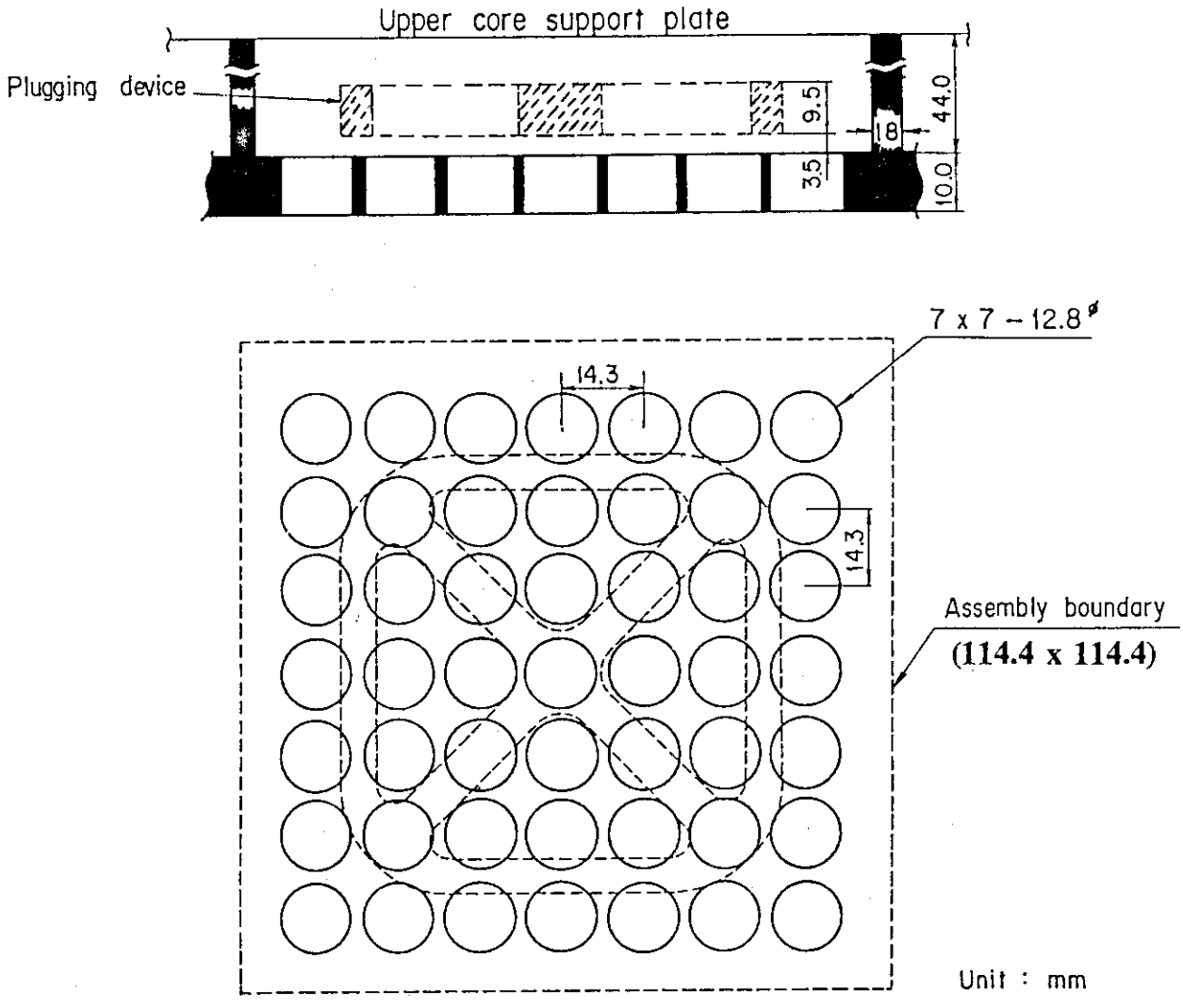

Fig. 2.8 Dimensions of holes of end box tie plate

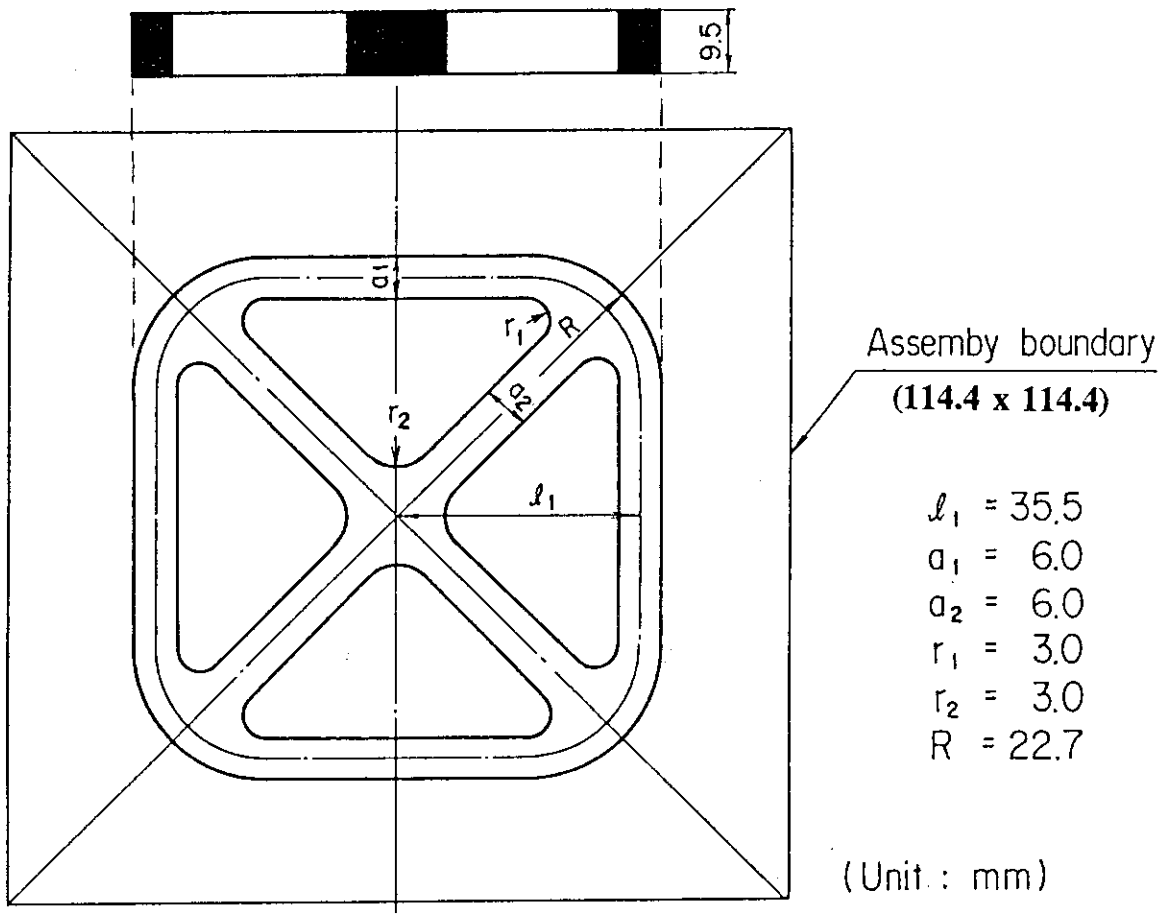

Fig. 2.9 Dimensions of plugging device

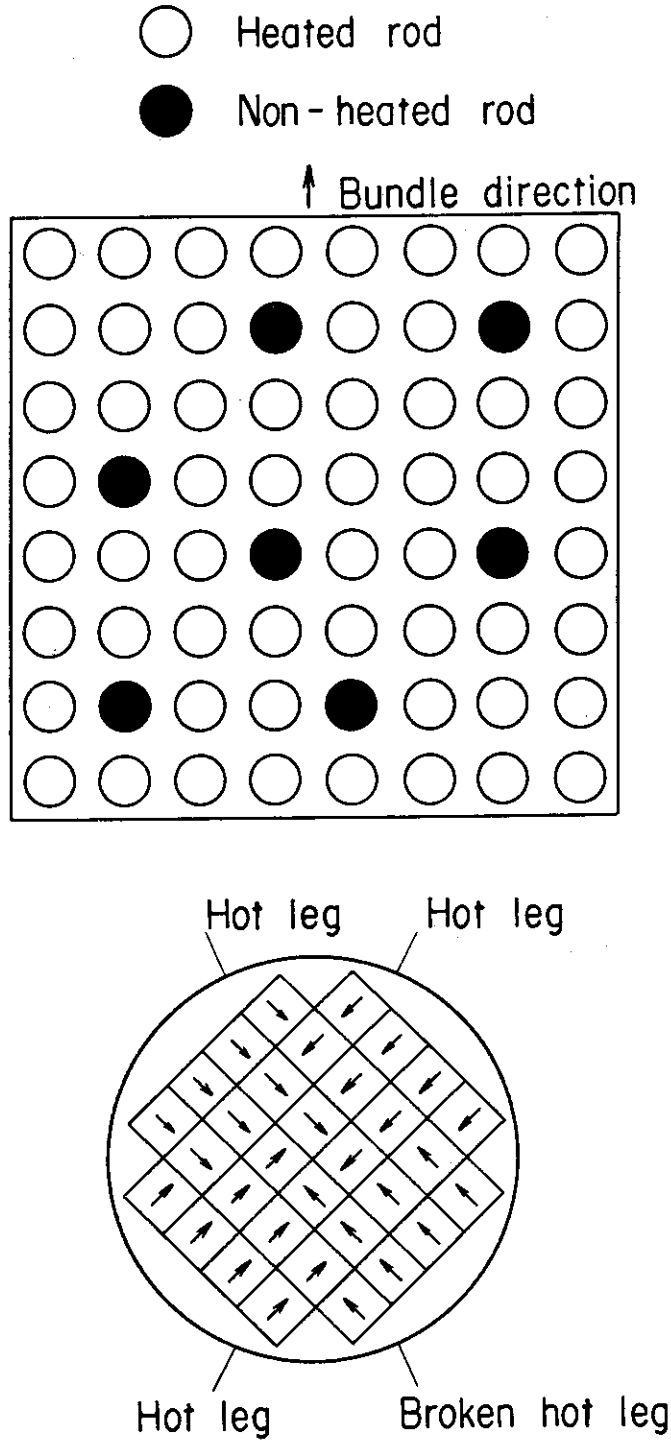

Fig. 2.10 Arrangement of non-heated rods

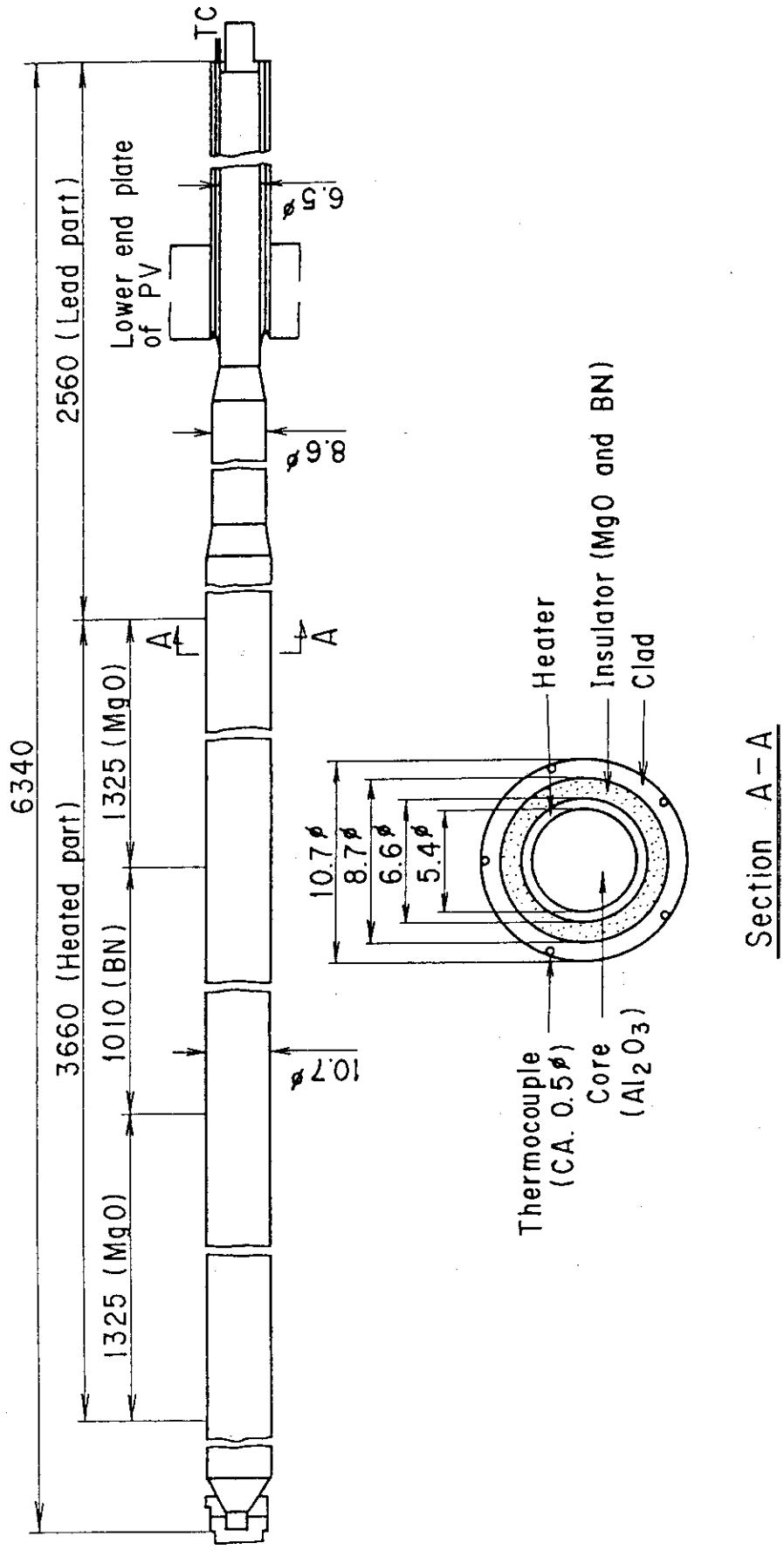

Fig. 2.11 Heater rod

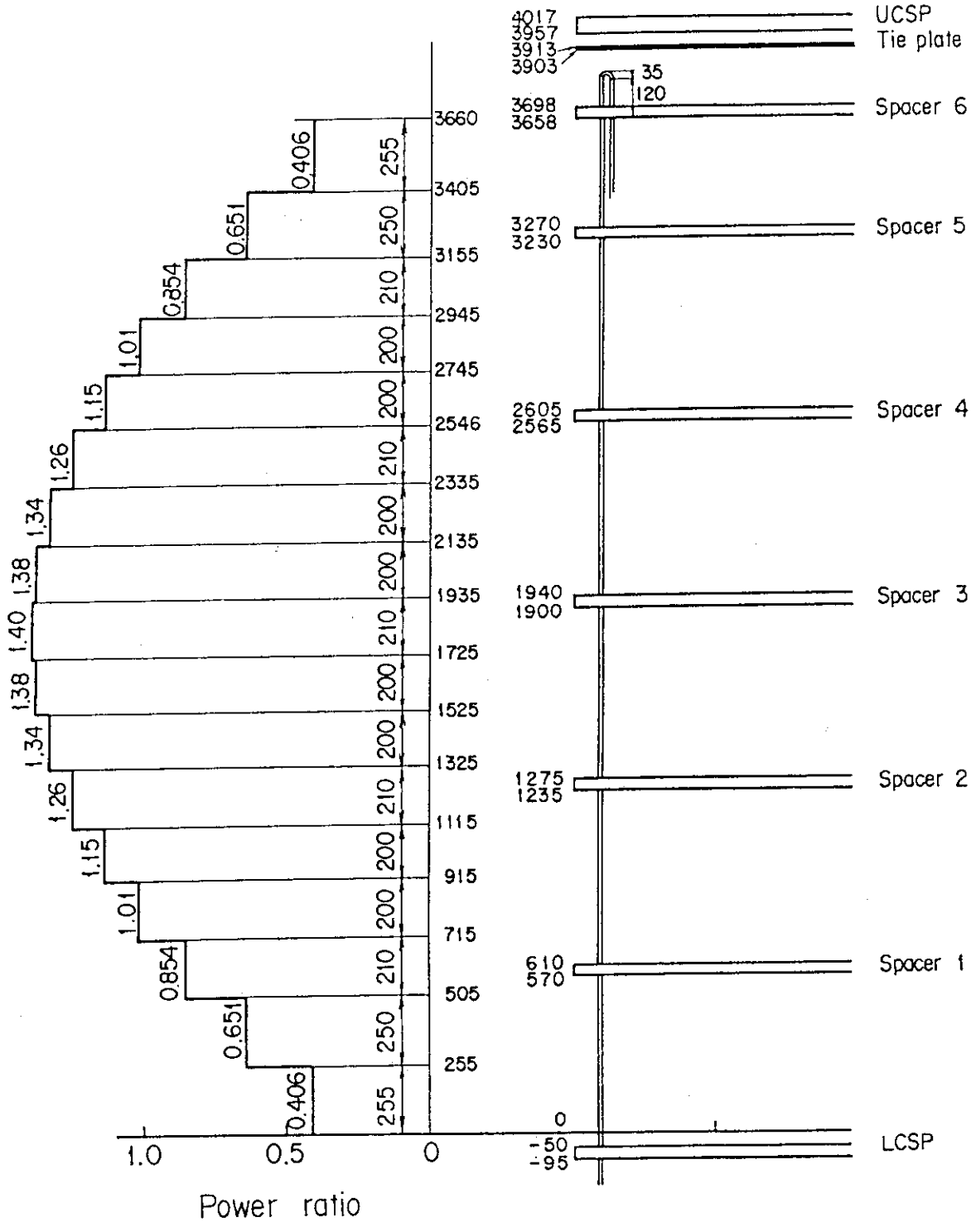

Fig. 2.12 Axial power profile of CCTF Core-II heater rod

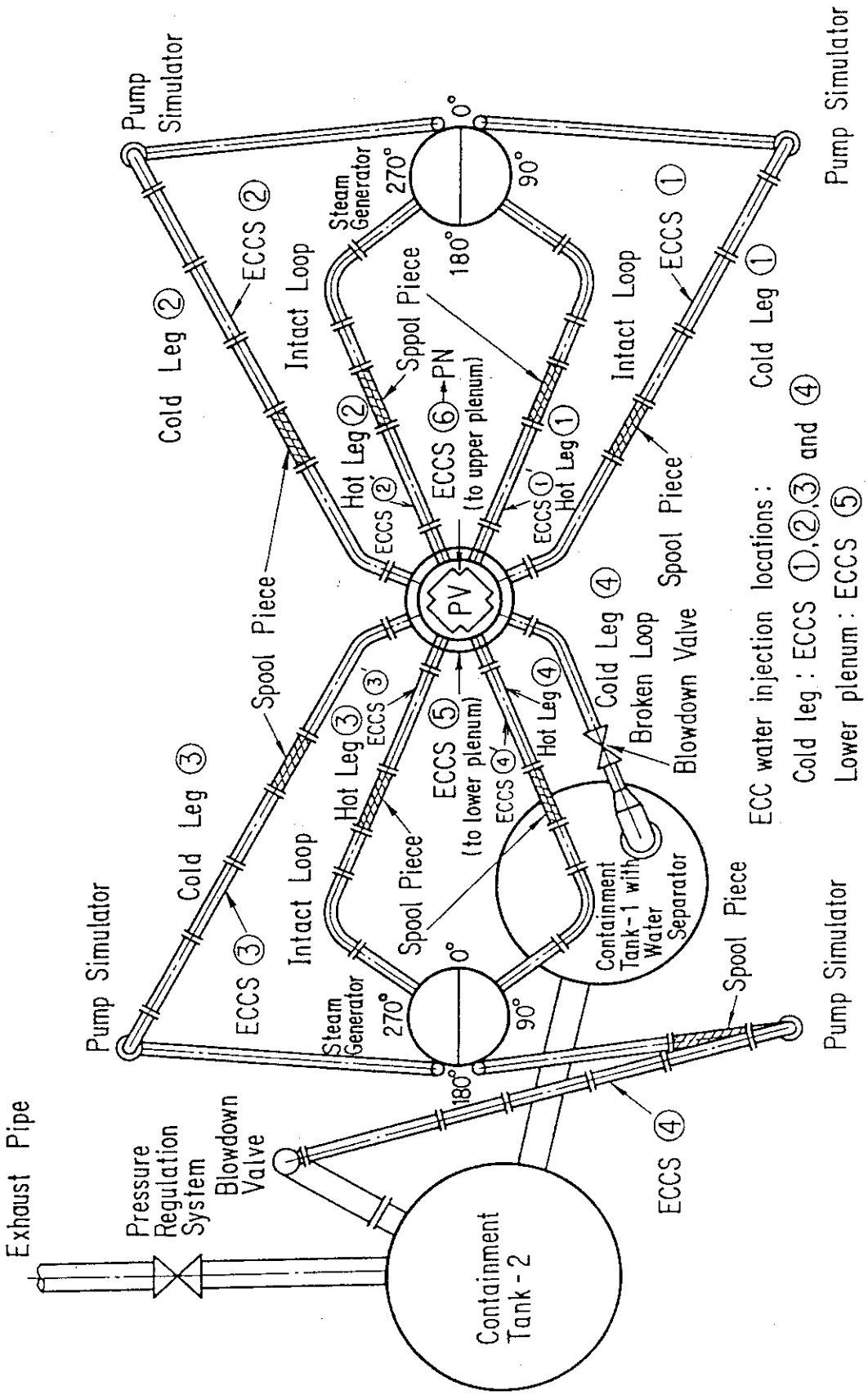

Fig. 2.13 Top view of primary loop pipings

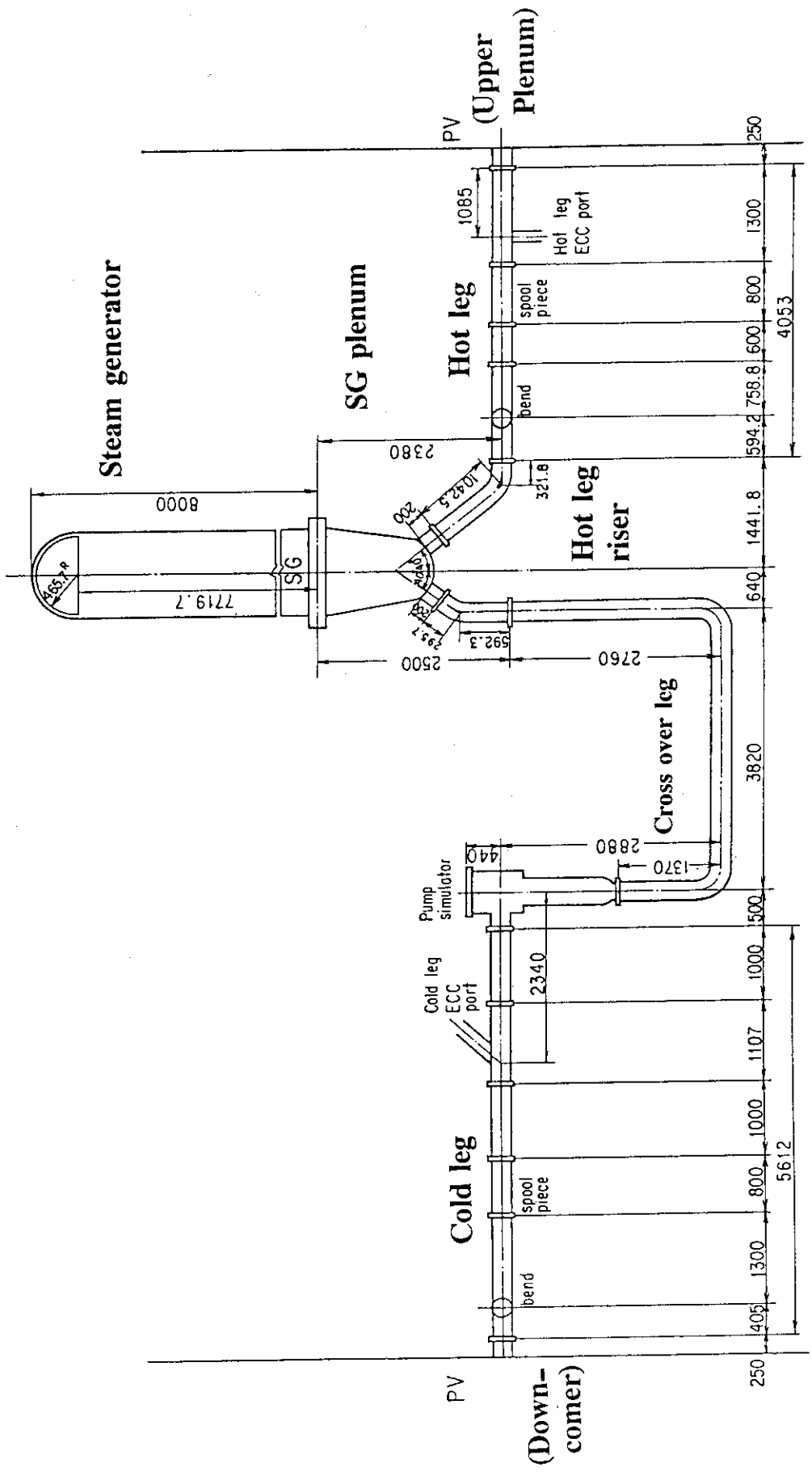

Fig. 2.14 Dimensions of intact loop

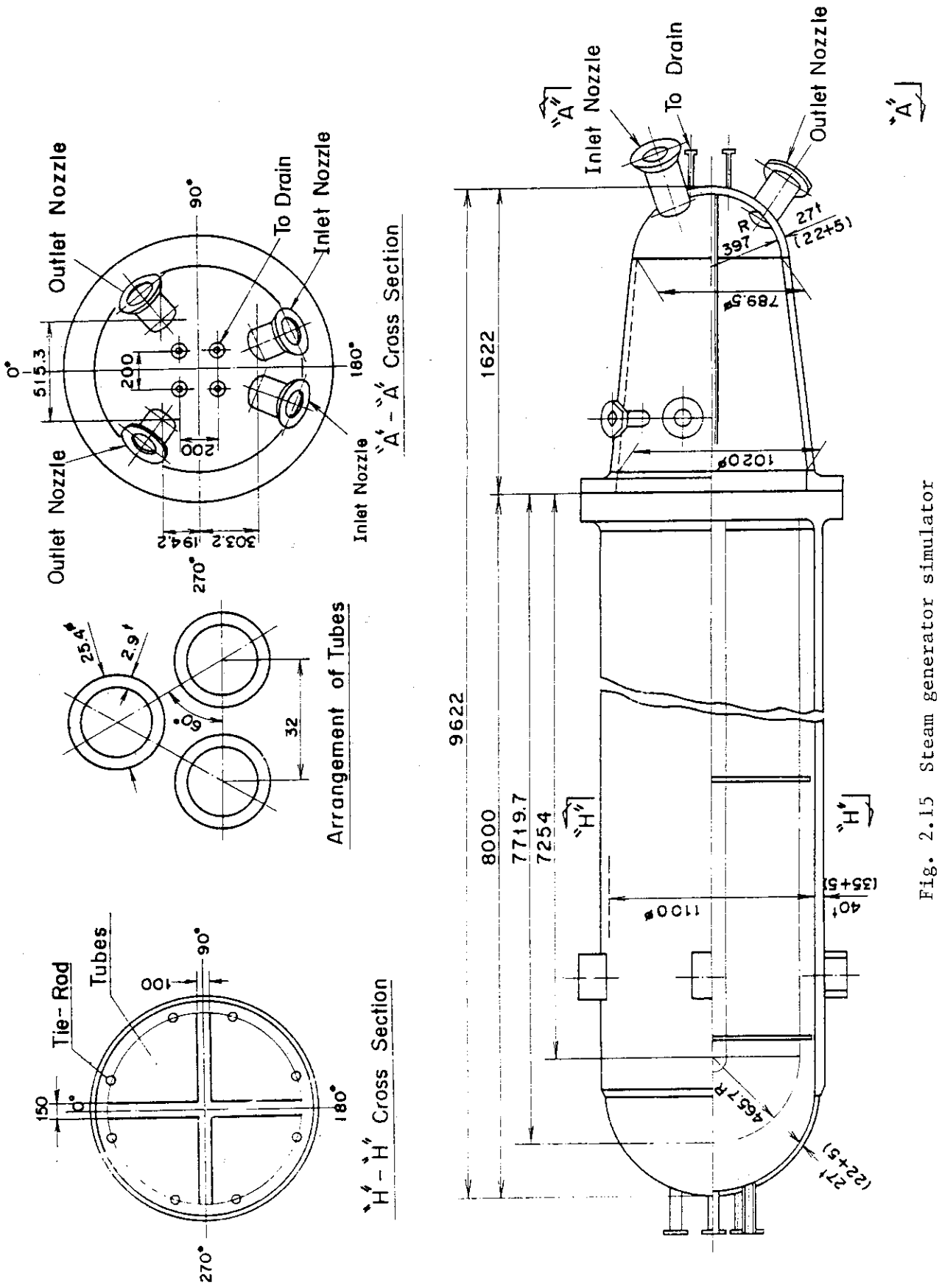

Fig. 2.15 Steam generator simulator

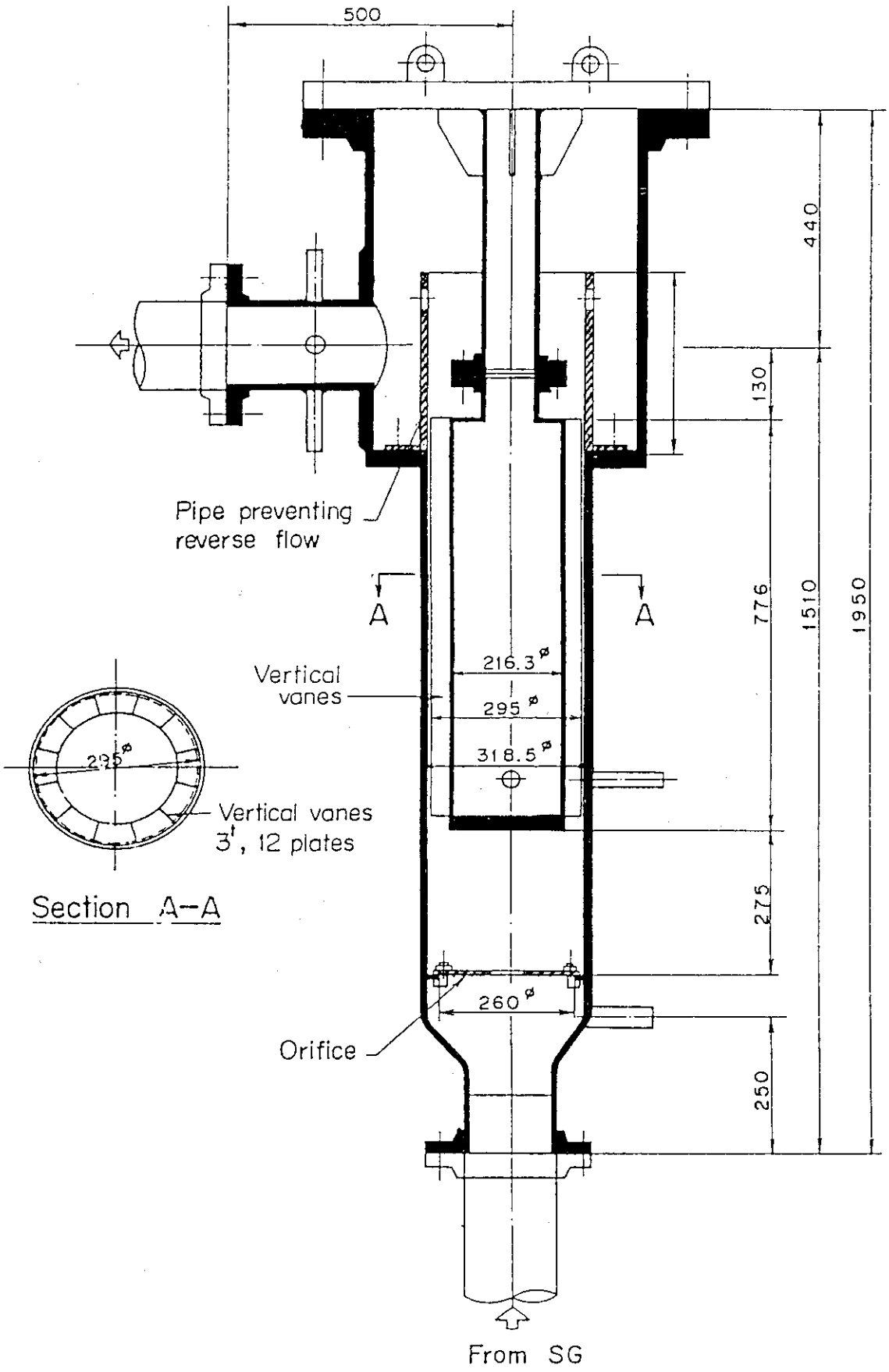

Fig. 2.16 Pump simulator

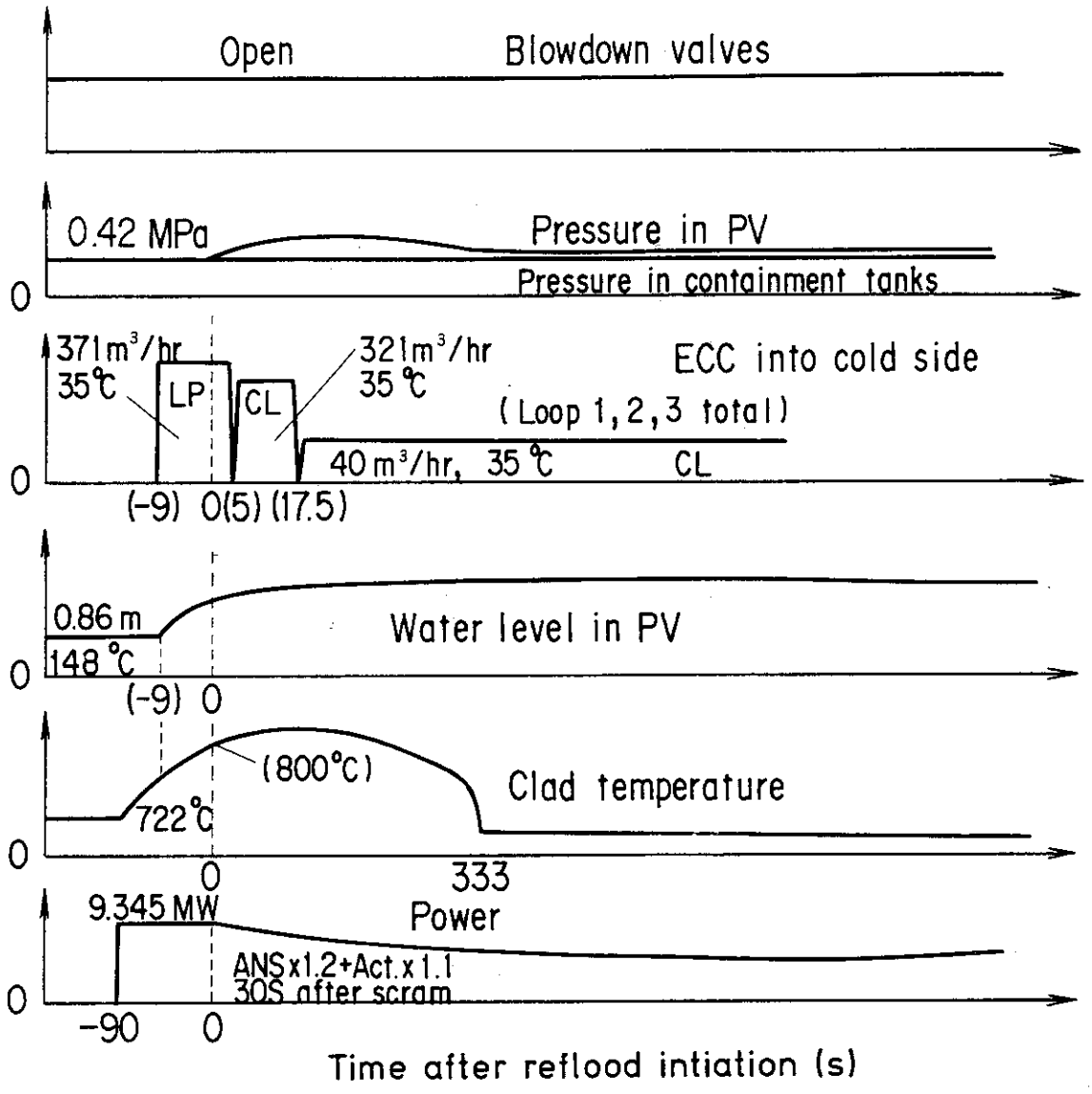

Note : ( ) means predicted value.

Fig. 3.1 Test sequence of test C2-1 (Run 55)

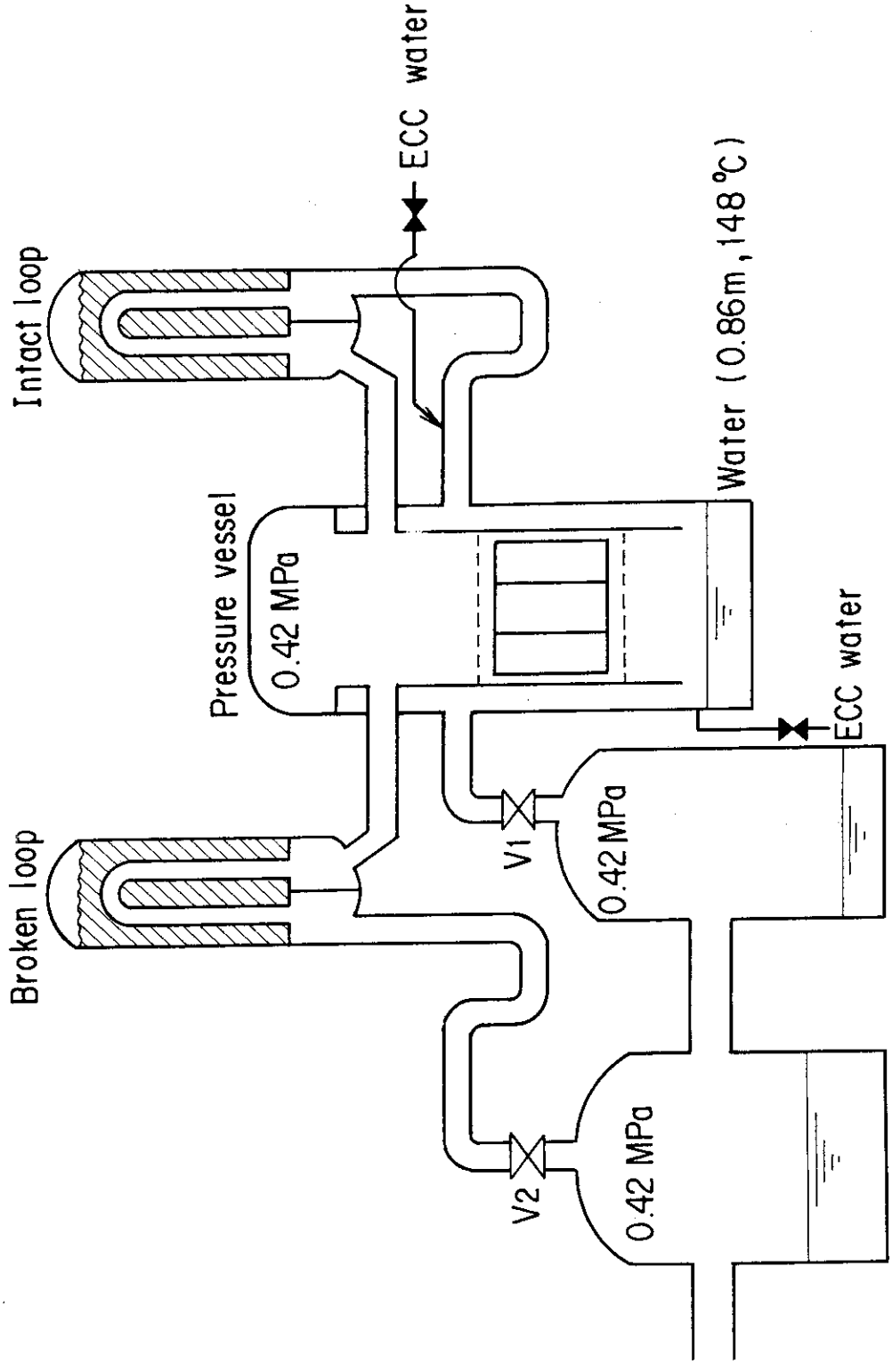

Fig. 3.2 Initial set-up of test C2-1 (Run 55)

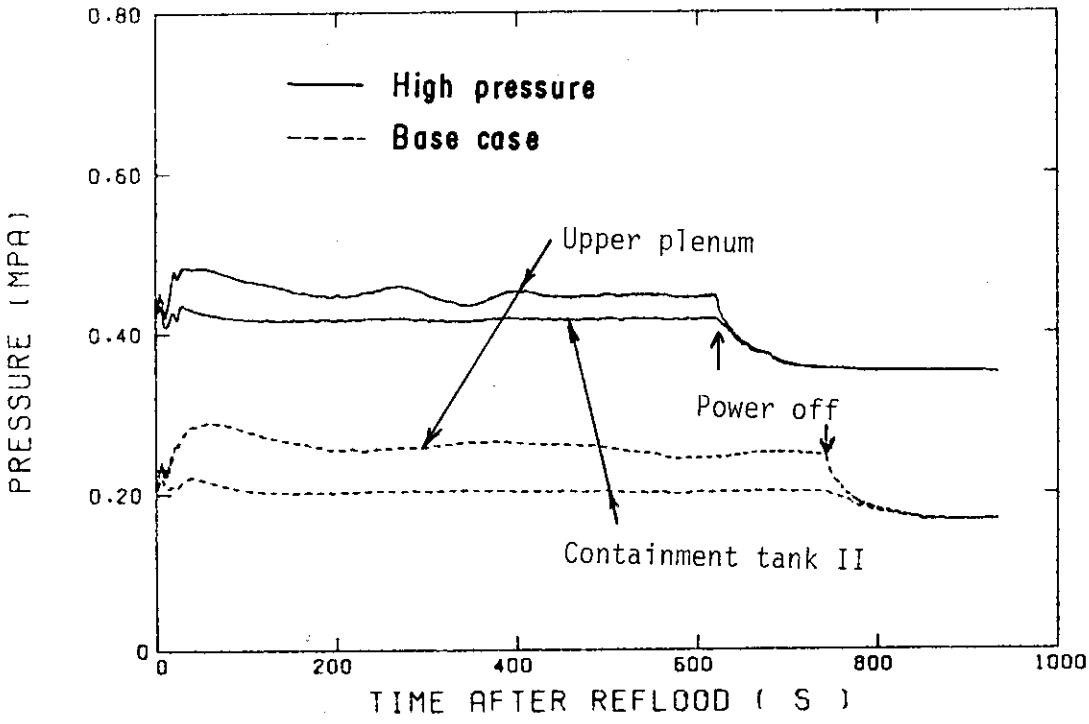

Fig. 3.3 Pressure in the Containment tank 2 and the upper plenum in the high pressure test and the base case test

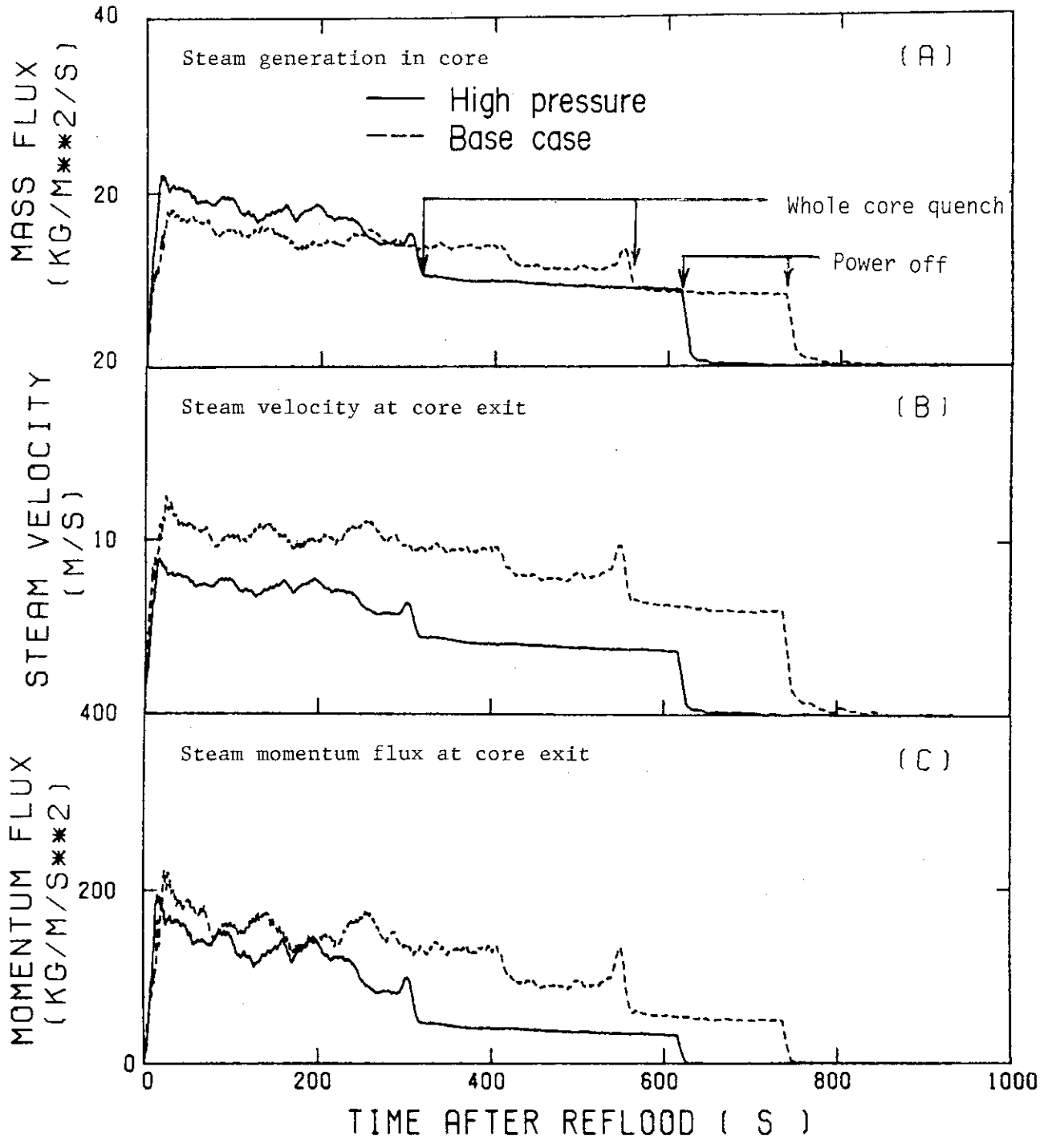

Fig. 4.1 Comparison of the mass flux of the steam generated in the core, the steam velocity of the core outlet and the momentum flux of the steam between the high pressure test and the base case test

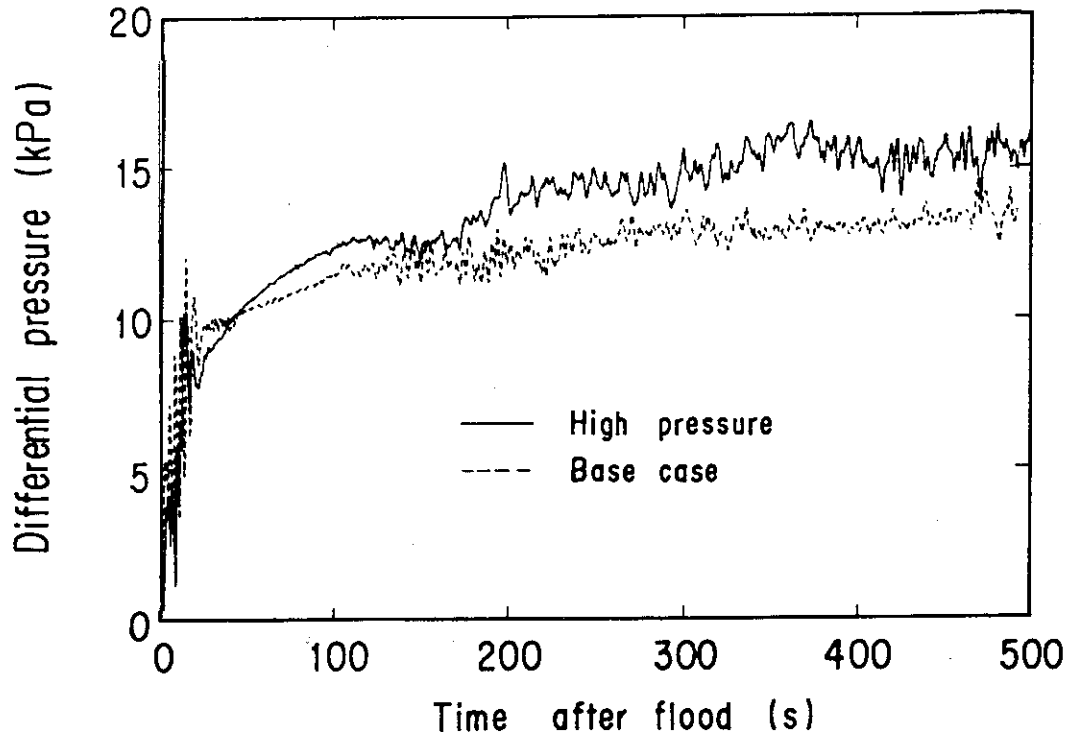

Fig. 4.2 Differential pressure in core

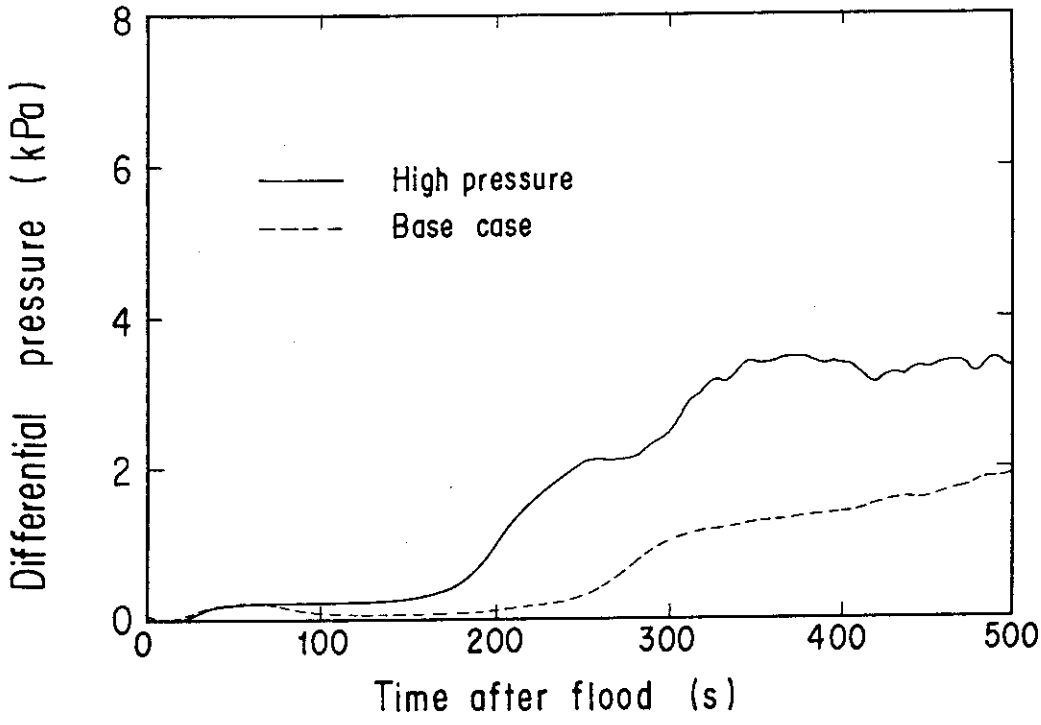

Fig. 4.3 Differential pressure in upper plenum

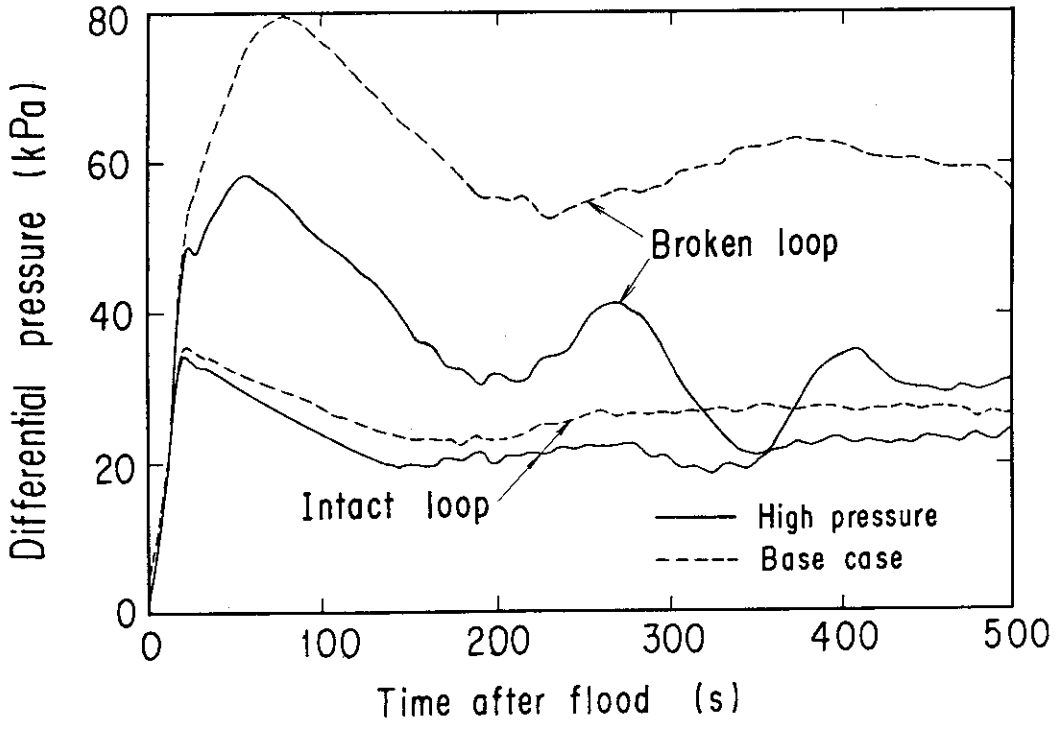

Fig. 4.4 Differential pressure across loops

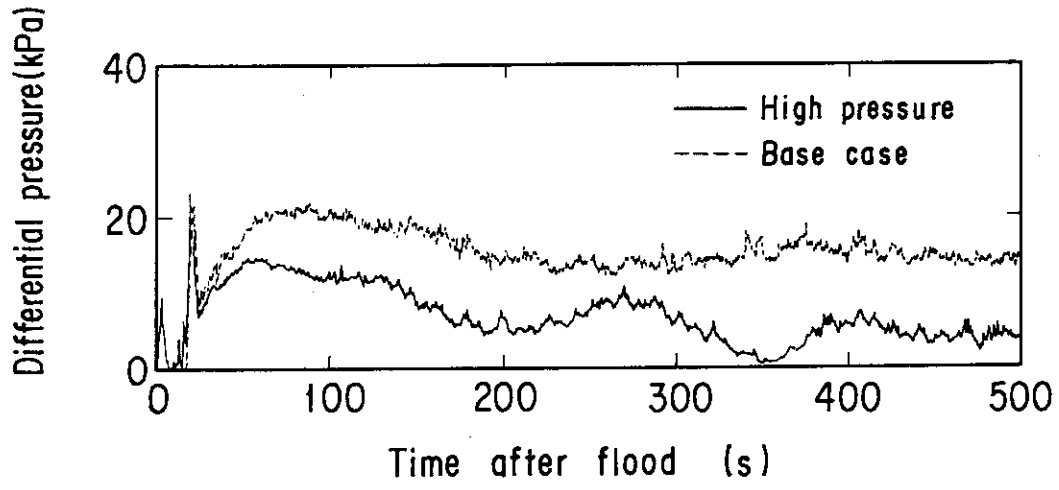

Fig. 4.5 Differential pressure across broken cold leg nozzle

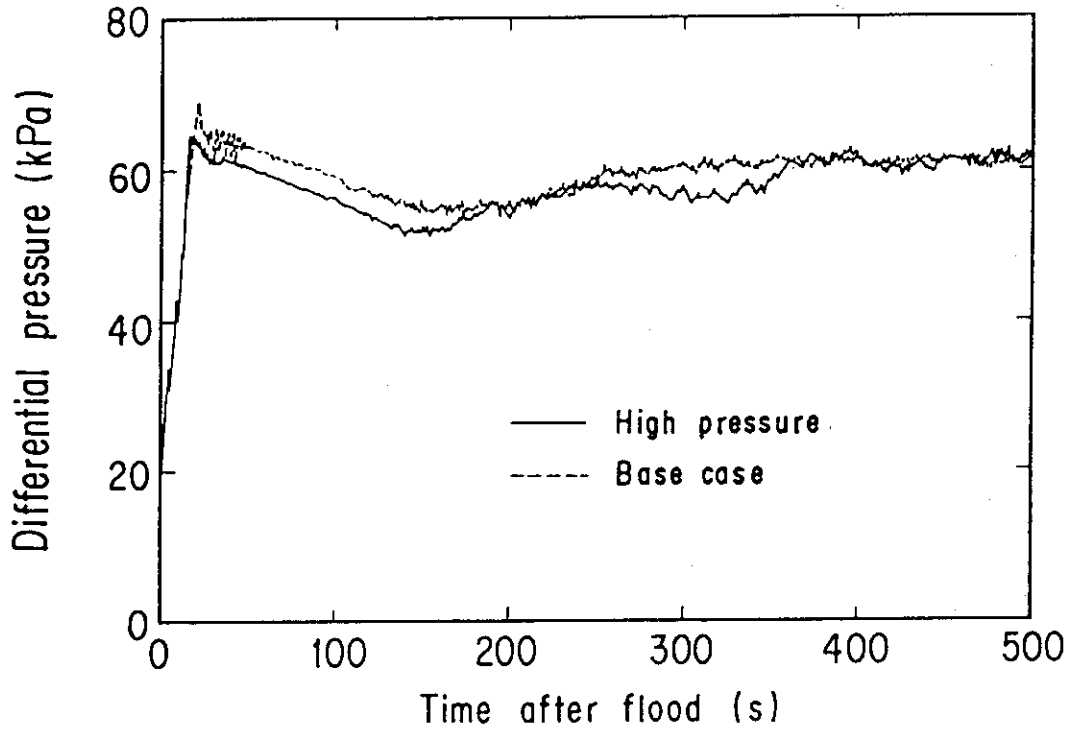

Fig. 4.6 Differential pressure in downcomer

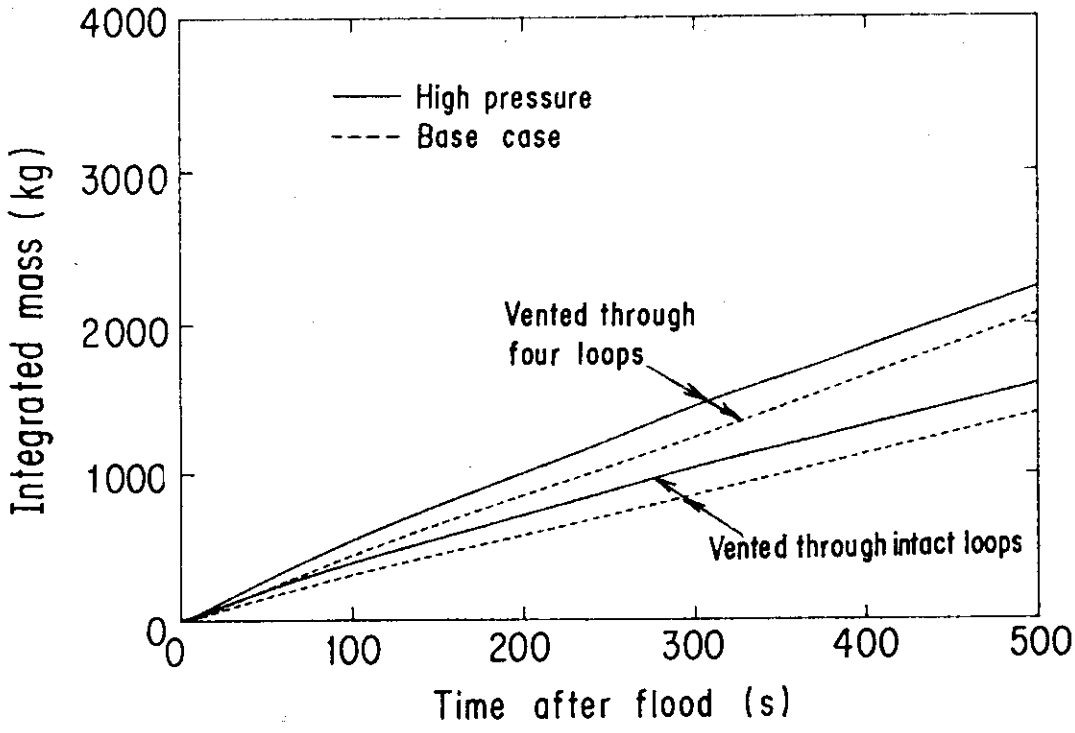

Fig. 4.7 Effluent mass from upper plenum through four loops and three intact loops

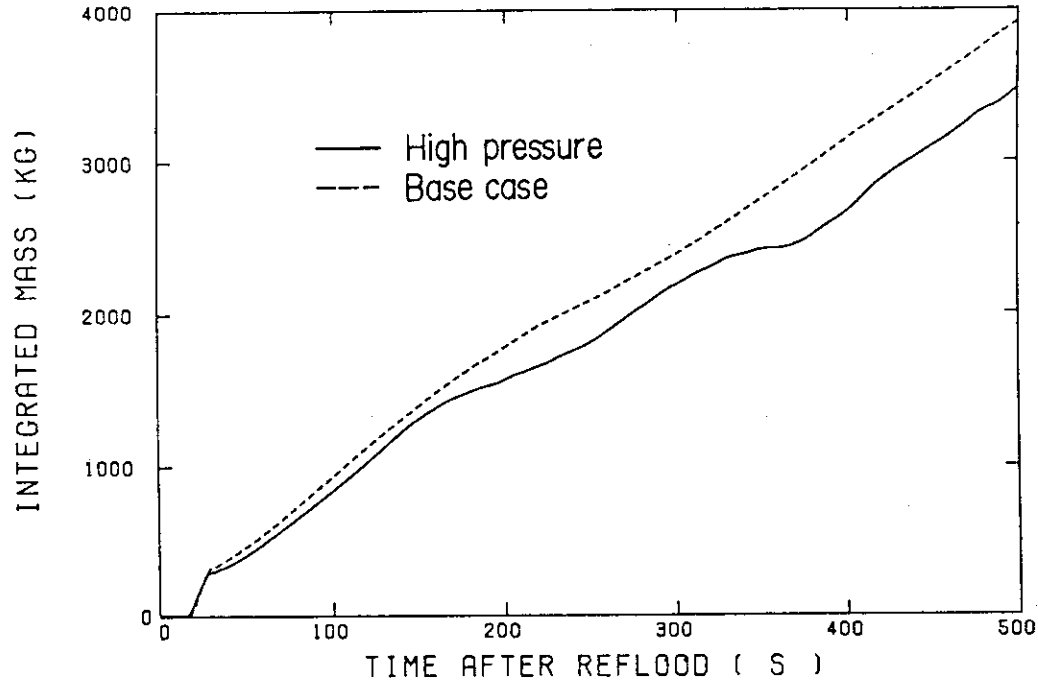

Fig. 4.8 Effluent water mass from downcomer through broken cold leg

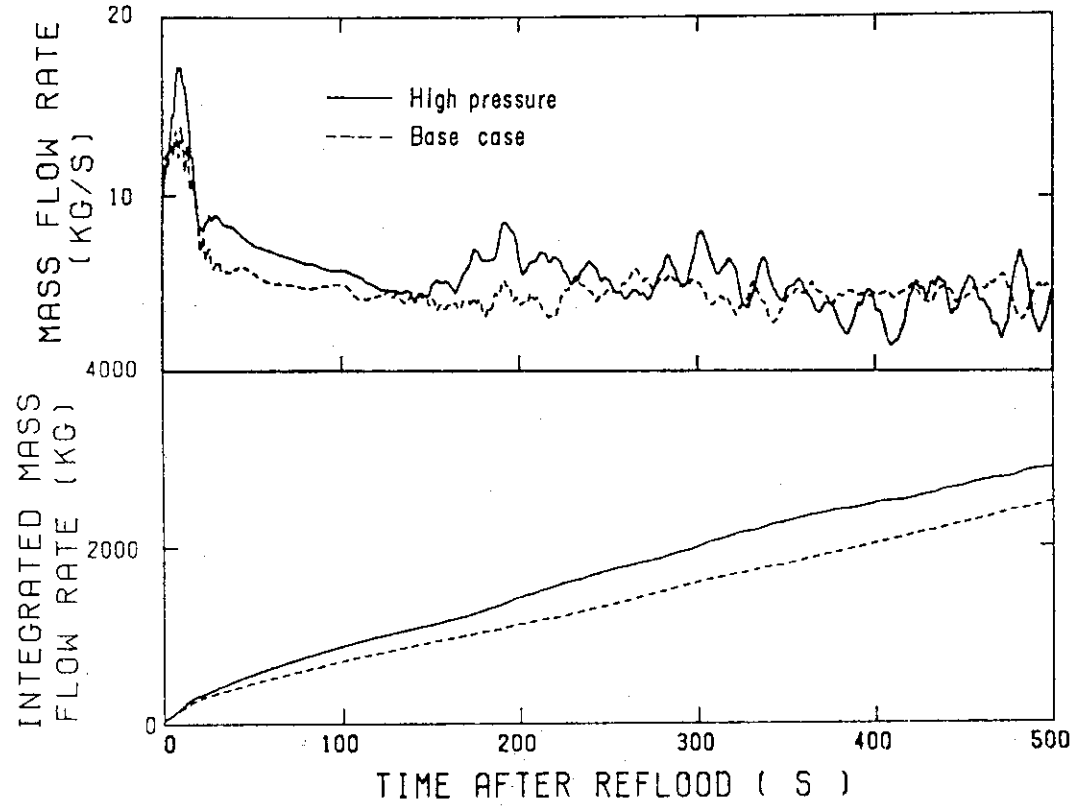

Fig. 4.9 Water mass flow rate into core and the time integration

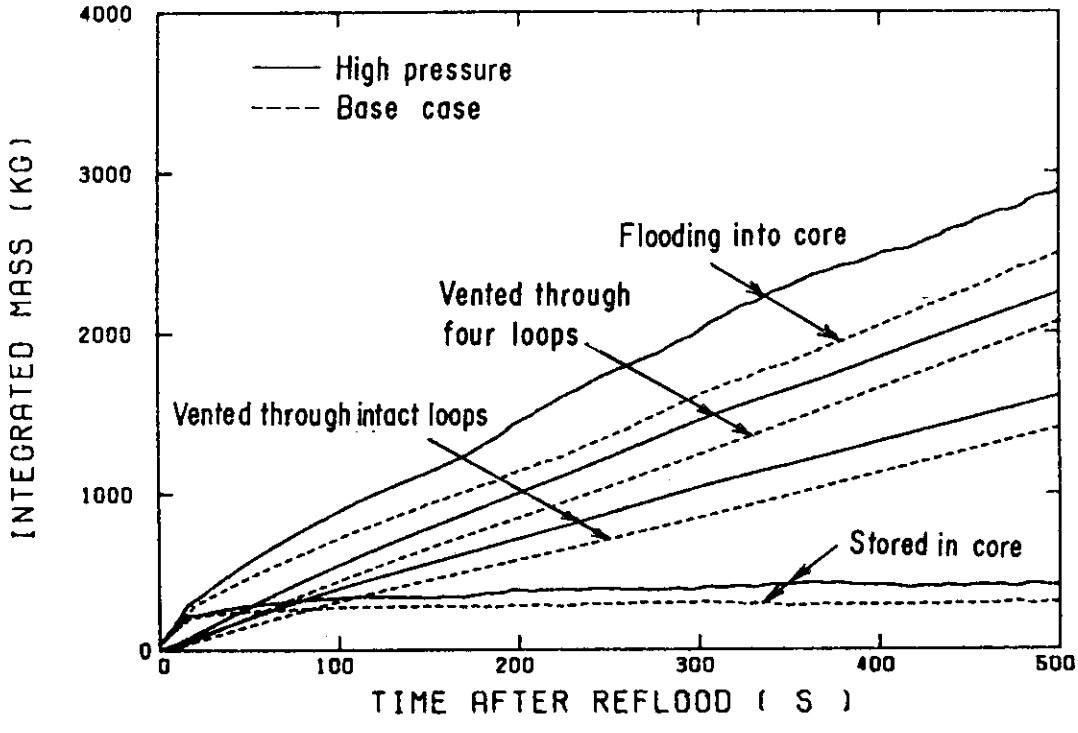

Fig. 4.10 Mass balance characteristics in core

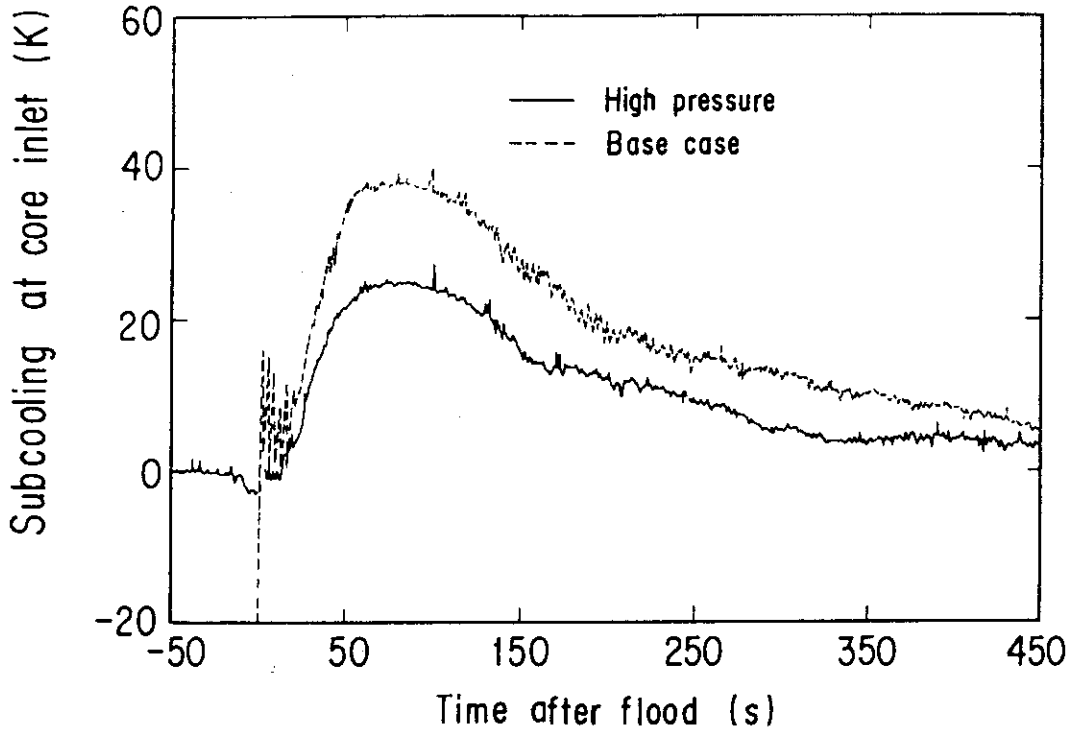

Fig. 4.11 Subcooling of the water at core inlet

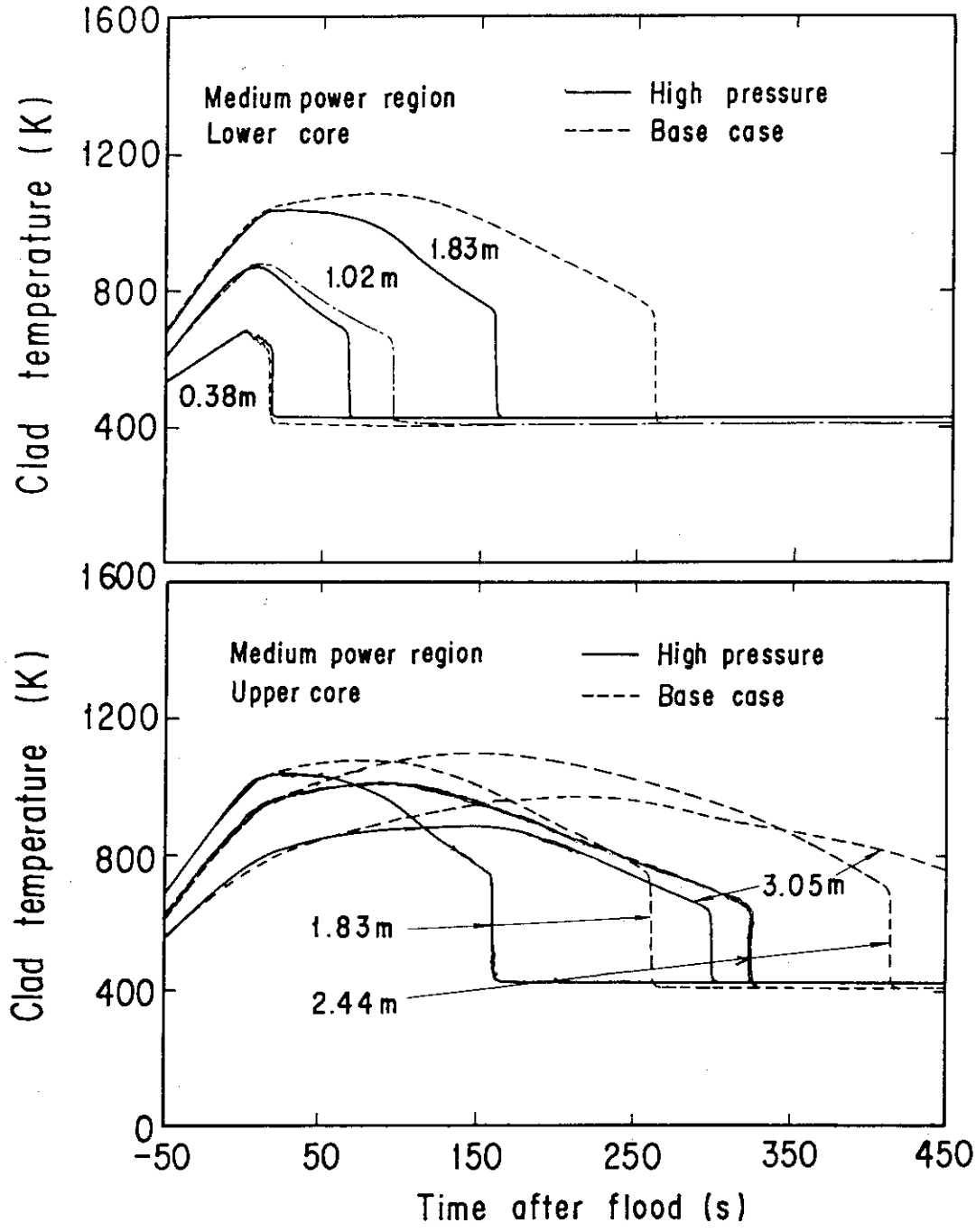

Fig. 4.12 Comparison of clad temperature between the high pressure test and the base case test

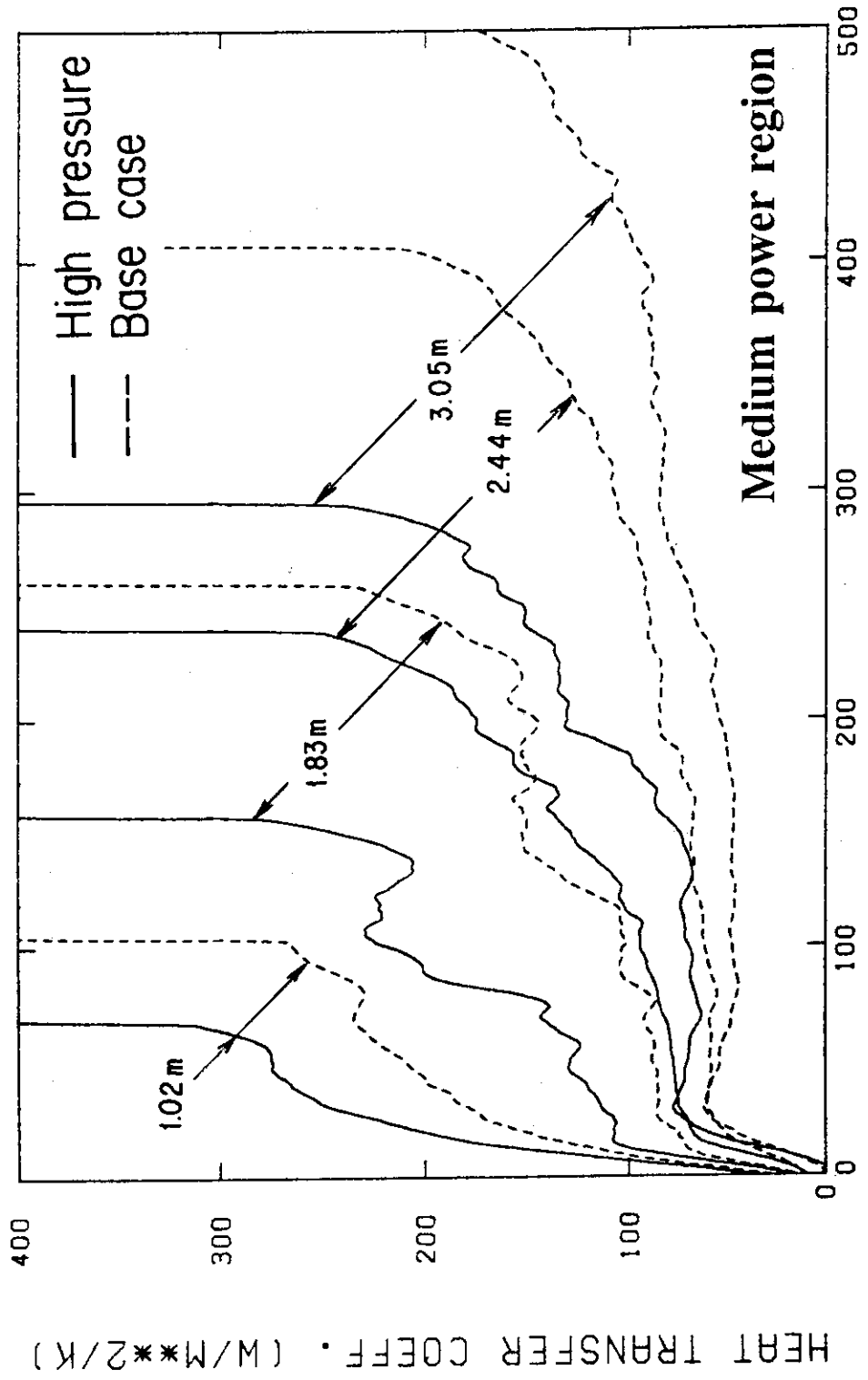

Fig. 4.13 Comparison of heat transfer coefficient between the high pressure test and the base case test

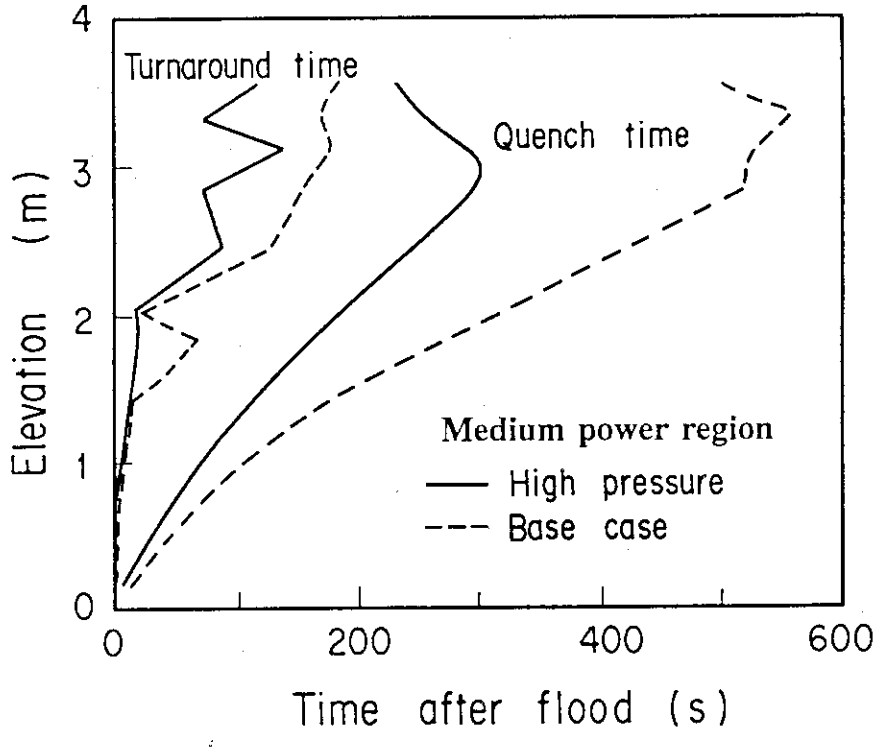

Fig. 4.14 Comparison of turnaround and quench times between the high pressure test and the base case test

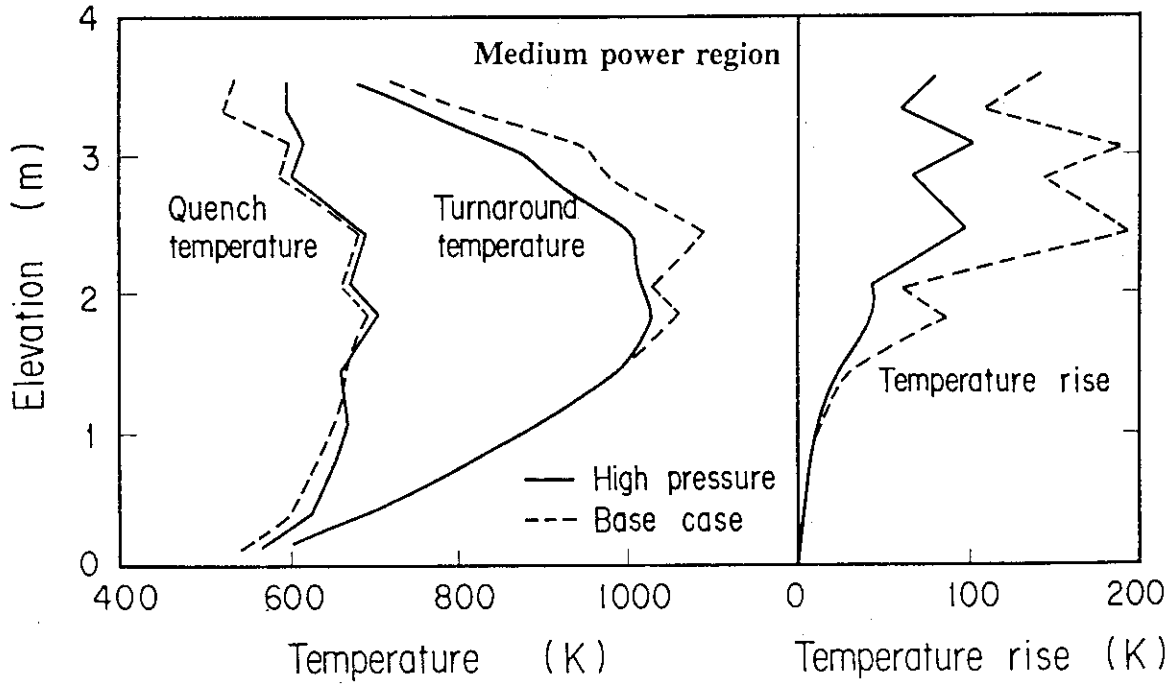

Fig. 4.15 Comparison of turnaround temperature, quench temperature and temperature rise between the high pessure test and the base case test

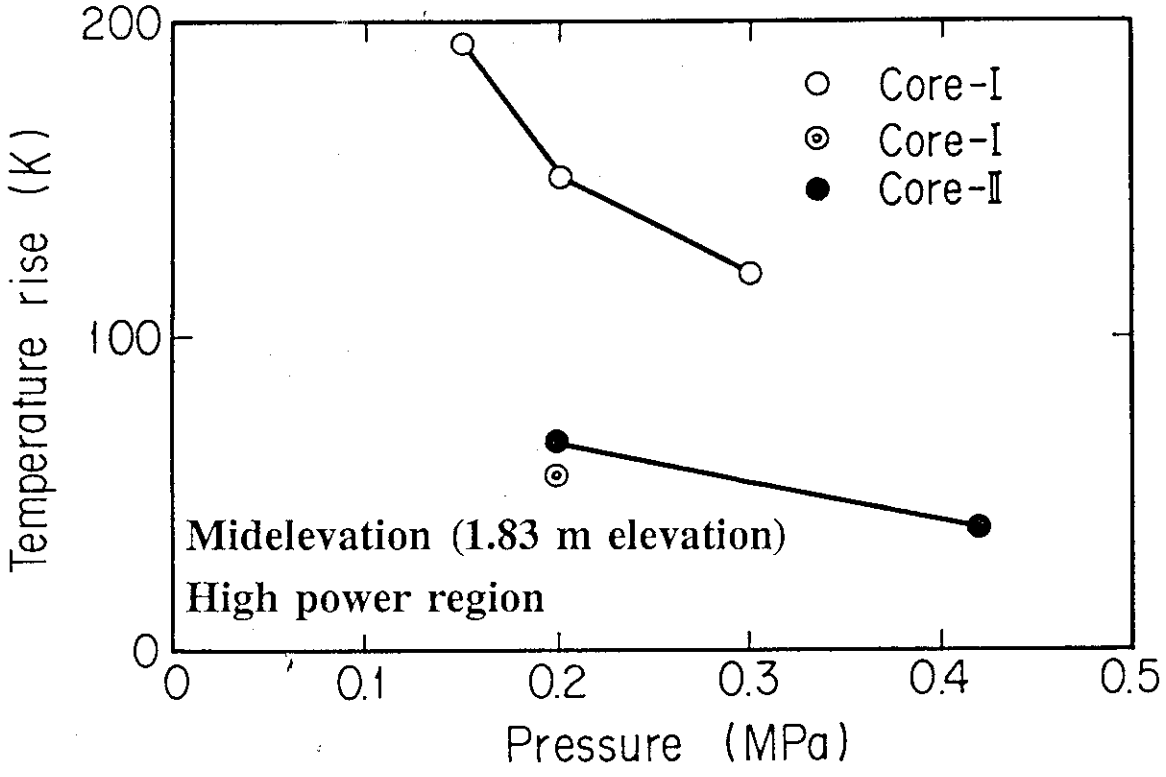

Fig. 4.16 Effect of pressure on temperature rise

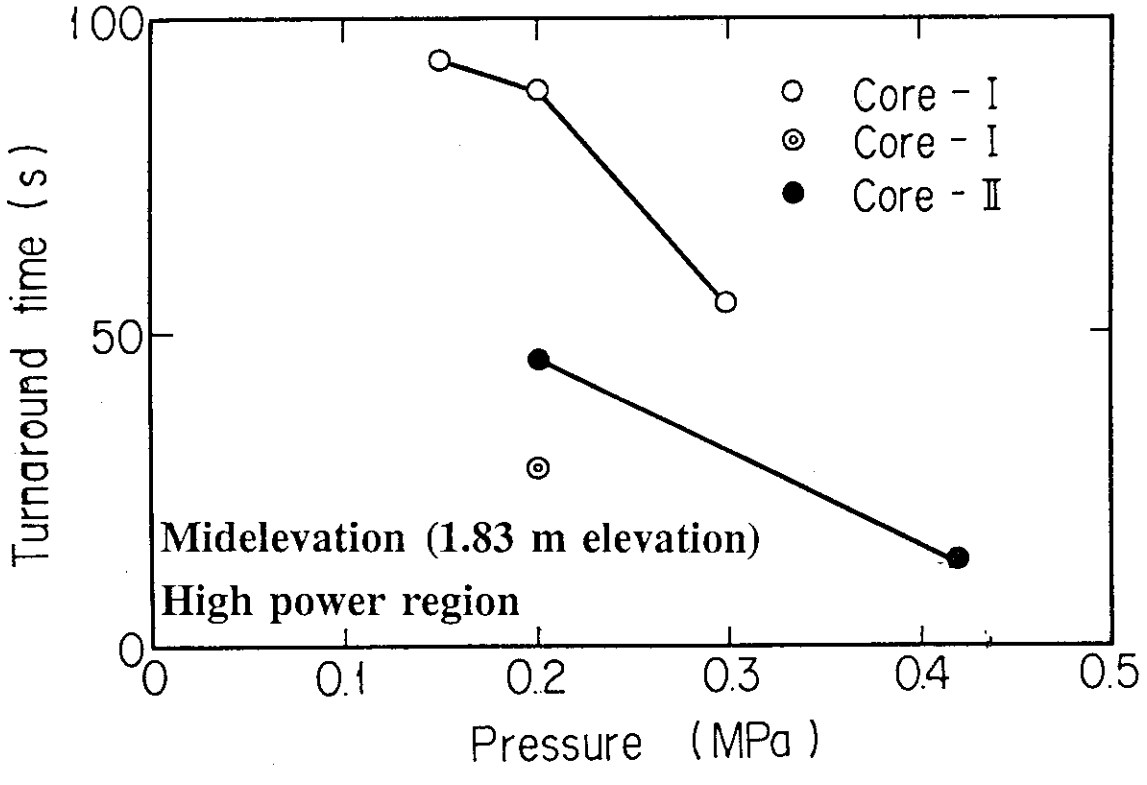

Fig. 4.17 Effect of pressure on turnaround time

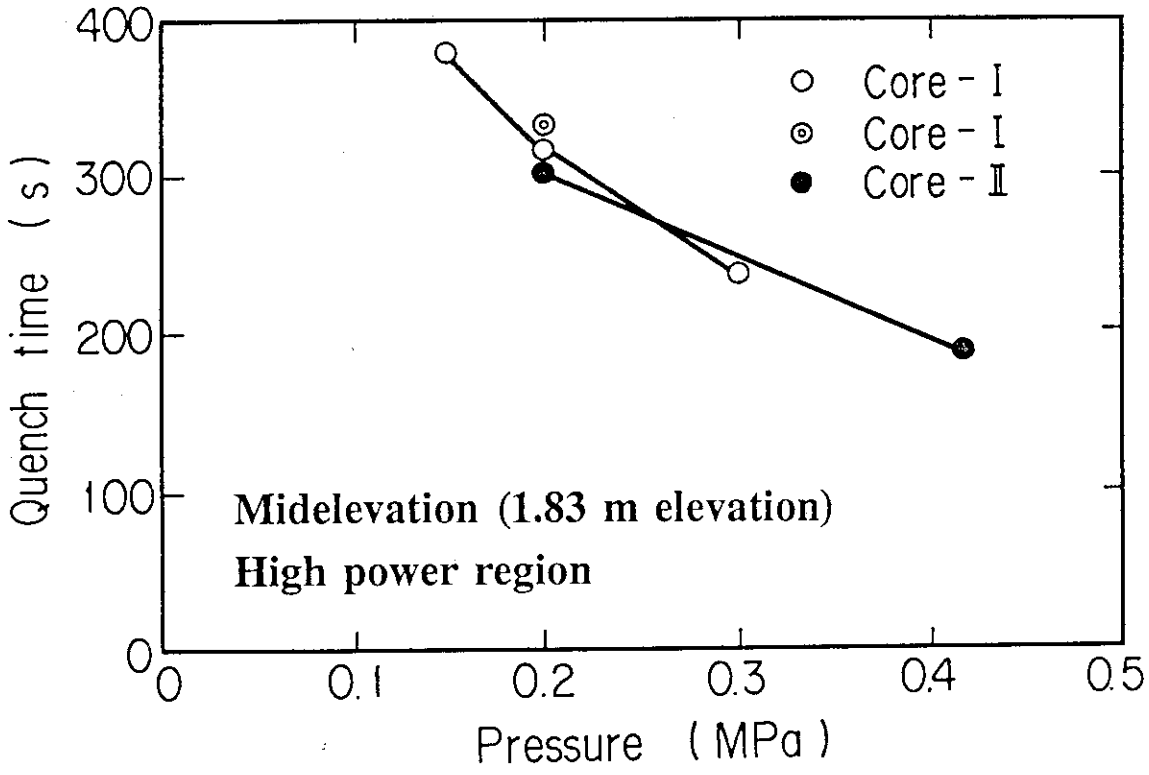

Fig. 4.18 Effect of pressure on quench time

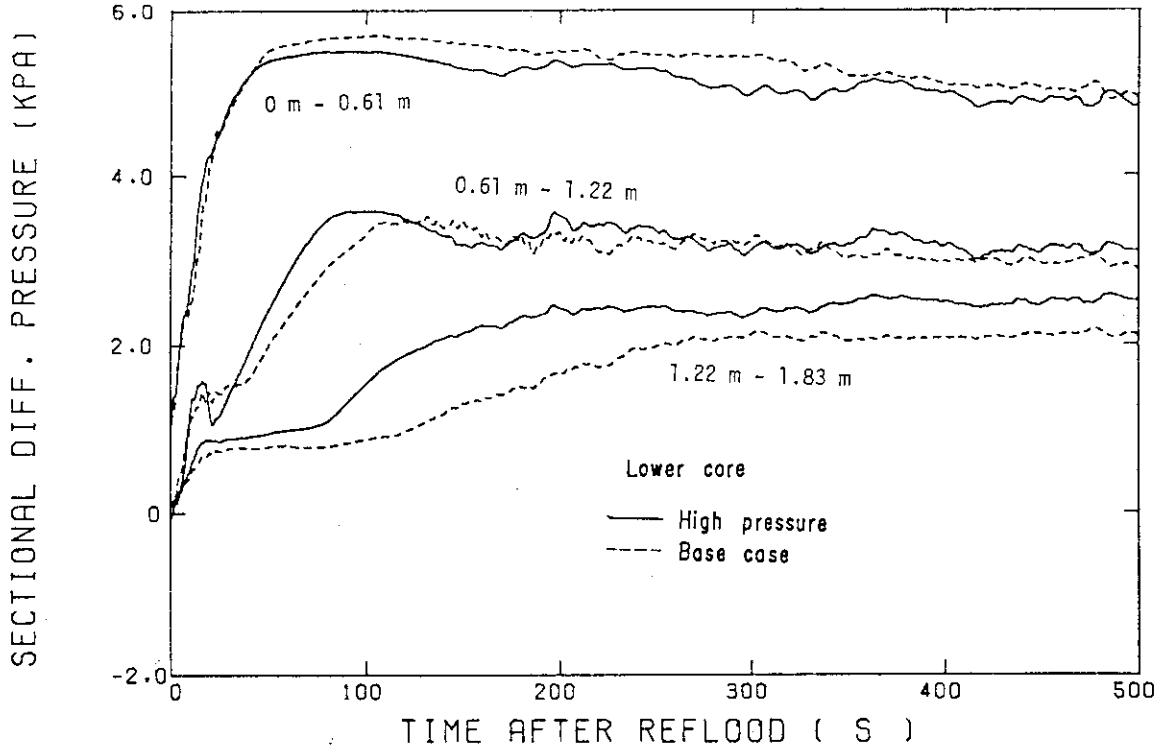

Fig. 4.19 Sectional differential pressure in lower core

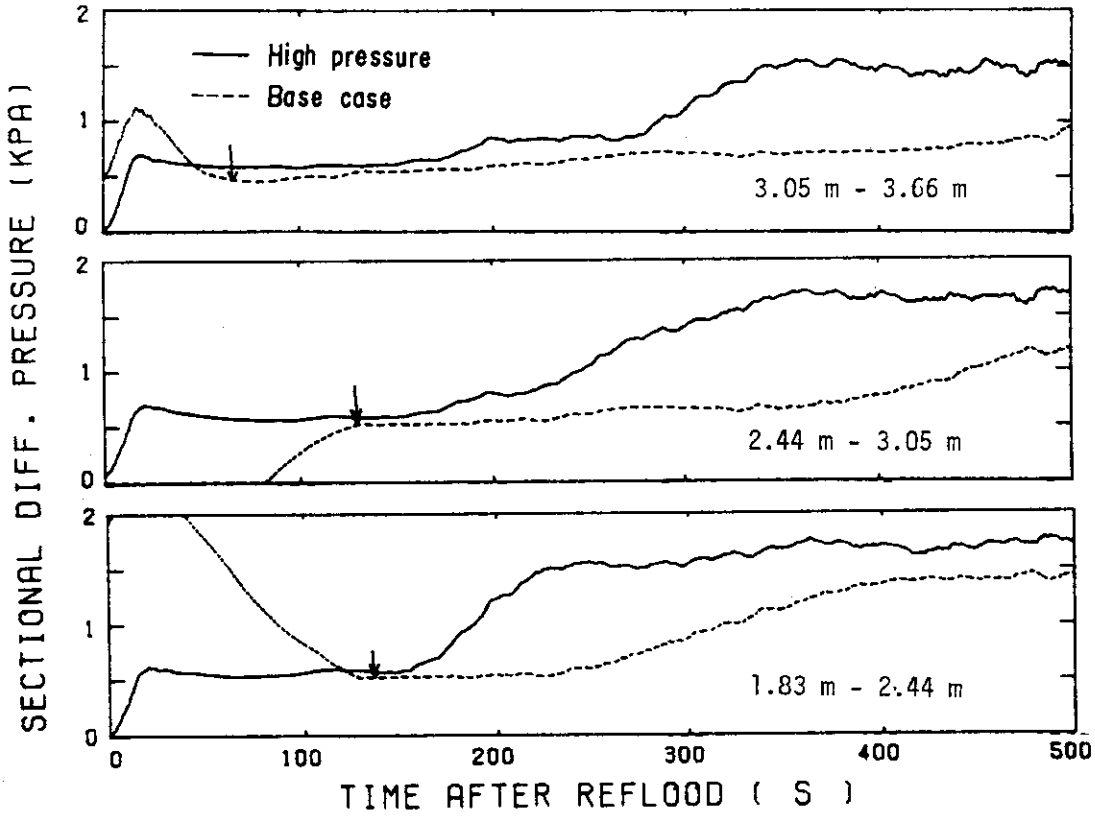

Fig. 4.20 Sectional differential pressure in upper core

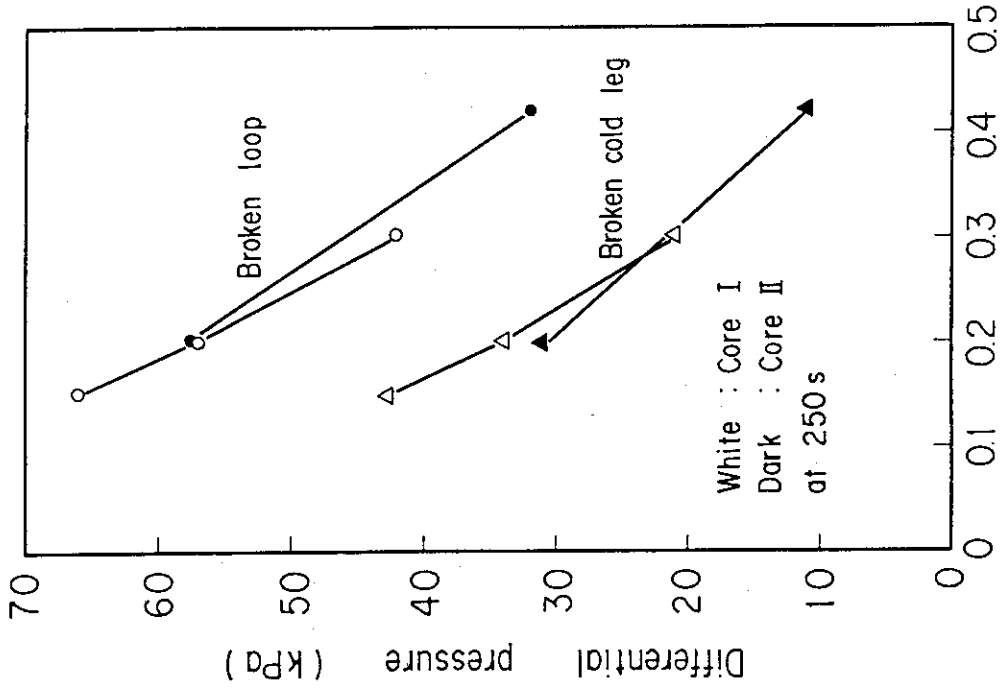

Fig. 4.21(b) Effect of pressure on broken loop differential pressure and broken cold leg differential pressure

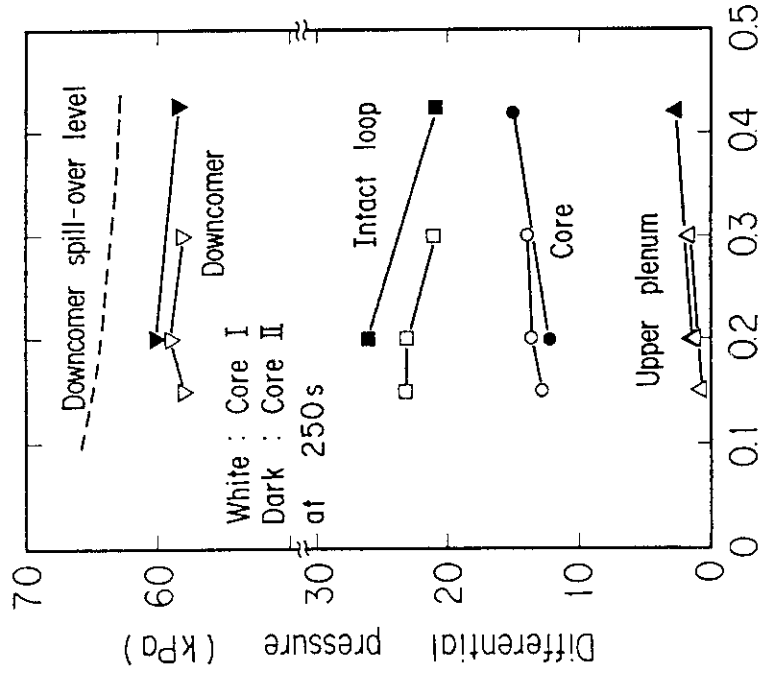

Fig. 4.21(a) Effect of pressure on core differential pressure, upper plenum differential pressure, intact loop differntial pressure and downcomer differential pressure

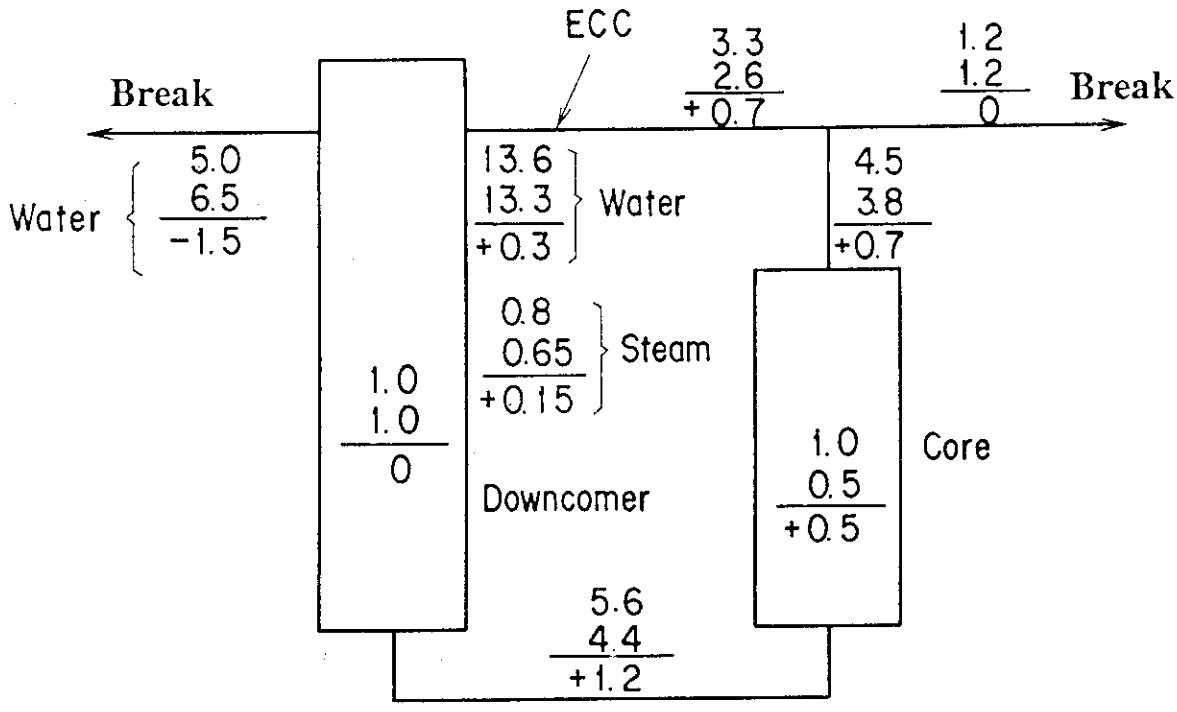

Fig. 4.22 Mass flow rate distribution in primary system in the high pressure test and the base case test

Appendix A Definition of Tag IDs

Figure List

1. Definition of Tag. ID for clad surface temperatures and heat fransfer coefficients

Notation : TEnnYlm (temperature)

HTEmmYlm (heat transfer coefficient)

nn : Bundle number (see Fig. A-1)

m : Elevation number

	Elevation (m)	Axial power factor
3	0.38	0.651
5	1.015	1.147
7	1.83	1.40
9	2.44	1.256
A	3.05	0.854

2. Definition of power zone and boundle number

See Fig. A-1

3. Definition of Tag. ID for void fraction

See Fig. A-2

4. Definition of Tag. ID for average linear power of heater rod in each power unit zone

See Fig. A-3

5. Definition of Tag. ID for differential pressure through downcomer, upper plenum, core and lower plenum

See Fig. A-4

6. Definition of Tag. ID for differential pressure through intact and broken loop and broken cold leg nozzle

See Fig. A-5

7. Definition of Tag. ID for fluid temperature in inlet and outlet plenum and secondary side of steam generator

See Fig. A-6

8. Definition of Tag. ID for ECC water injection rate, ECC water temperature and vented steam flow rate

See Fig. A-7

9. Definition of initial temperature, turnaround temperature quench temperature, temperature rise, turnaround time and quench time. (See Fig. A-8)

T_i : Initial temperature (Clad surface temperature at reflood initiation)

T_t : Turnaround temperature (Maximum clad surface temperature in each temperature history)

ΔT_r : Temperature rise ($= T_t - T_i$)

T_q : Quench temperature (Clad surface temperature at quenching)

10. Definition of quenching

See Fig. A-8

Quench time t_t is determined as

$$t_t = i \times \Delta t - (\text{reflood initiation time})$$

In above equation, i is determined by the following criteria.

(1) Clad surface temperature is high, compared with the saturation temperature.

$$T_i > T_{sat} + \Delta T_1$$

(2) Decreasing rate of clad surface temperature is large.

$$\frac{T_{i+1} - T_i}{\Delta t} < - C_{st}$$

(3) Clad surface temperature falls around the saturation temperature.

$$T_{i + k_1} \leq T_{sat} + \Delta T_1$$

(4) If the determined i is inadequate, the value i is manually re-determined.

Δt : Data sampling period (s)

T_i : Clad surface temperature (K)

T_{sat} : Saturation temperature at the pressure in upper plenum (K)

ΔT_1 : Temperature discrepancy (K)
Default value = 50.0

C_{st} : Decreasing rate of clad surface temperature (K/S)
Default value = 25.0

k_1 : Number of referred data (-)
Default value = 6

11. Definition of Tag. ID for core inlet mass flow rate, time-integral core inlet mass flow rate and carry-over rate fraction

(1) Core inlet mass flow rate : $\dot{m}_F$
Notation : MLCRI□ (□ = N, 1 or 11)

(2) Time-intefral core inlet mass flow rate : $\int \dot{m}_F dt$
Notation : IMLCRI□ (□ = N, 1 or 11)

(3) Carry-over rate fraction : $(\dot{m}_F - \dot{m}_{CR})/\dot{m}_F$
Natation : CRF□ (□ = N, 1 or 11)

where $\dot{m}_F$: Core inlet mass flow rate (See item 12)

$\dot{m}_{CR}$: Water accumulation rate in core

Suffix	$\dot{m}_F$ base on
N	Eq.(A.2)
1	Eq.(A.1) with K=15
11	Eq.(A.1) with K=20

12. Evaluation of core inlet mass flow rate

The reflood phenomena is a relatively slow transient and a steady state condition can be applied. In a steady state condition, based on the mass balance relations of the system, the core flooding mass flow rates $\dot{m}_F$s can be written as follows:

By using the data measured at the downstream of the core inlet, $\dot{m}_F$ is derived as,

$$\dot{m}_F = \dot{m}_C + \dot{m}_U + \dot{m}_B + \Sigma \dot{m}_I \quad , \qquad (A.1)$$

where $\dot{m}_C$ and $\dot{m}_U$ are the mass accumulation rates in the core and the upper plenum respectively. The $\dot{m}_B$ and $\dot{m}_I$ are the mass flow rates in the broken loop and the intact loop, respectively.

By using the data measured at the upstream of the core inlet, $\dot{m}_F$ is derived as,

$$\dot{m}_F = \Sigma \dot{m}_{DL} - \dot{m}_D - \dot{m}_O + \dot{m}_{ECC/LP} \quad , \tag{A.2}$$

where $\dot{m}_{DL}$ and $\dot{m}_O$ are the mass flow rates of the water flowing into and overflowing from the downcomer, $\dot{m}_{ECC/LP}$ and $\dot{m}_D$ are the mass flow rate of the ECC water injected into the lower plenum and the water accumulation rate in the dowmcomer respectively.

The $\dot{m}_I$s and $\dot{m}_B$ can be obtained from the pressure drops at the pump simulators with orifices by assuming the K-factor of the orifice is constant. The values of $\dot{m}_C$, $\dot{m}_D$ and $\dot{m}_U$ can be evaluated with the differential pressure ΔP_C, ΔP_D and ΔP_U, respectively, as follows:

$$\dot{m}_n = d(\Delta P_n S_n/g)/dt \quad (n : C, D, U) \quad , \tag{A.3}$$

where g is the gravitational acceleration and S_n is the cross sectional area. The value of $\dot{m}_O$ can be obtained from the liquid level X in the Containment tank 1 as,

$$\dot{m}_O = d(X\rho_\ell S_o)/dt \quad , \tag{A.4}$$

where ρ_ℓ is the liquid density and S_o is the cross sectional area of the containment tank 1.

The value of $\dot{m}_{DL}$, $\dot{m}_{DV}$ and h, which are liquid flow rate, steam flow rate and enthalpy of two phase mixture downstream each ECC port respectively, are obtained from the following mass and energy balance relations at each ECC port under the assumption of thermal equilibrium:

$$\dot{m}_{DV} + \dot{m}_{DL} = \dot{m}_{ECC} + \dot{m}_I \quad , \tag{A.5}$$

$$(\dot{m}_{DV} + \dot{m}_{DL})i = \dot{m}_{ECC}h_{ECC} + \dot{m}_I h_I \quad , \tag{A.6}$$

$$\text{if} \quad h_g \geq h \geq h_\ell \ , \ (\dot{m}_{DV} + \dot{m}_{DL})h = \dot{m}_{DV}h_g + \dot{m}_{DL}h_\ell$$

$$\text{if} \quad h \geq h_g \quad , \ \dot{m}_{DL} = 0 \quad , \tag{A.7}$$

$$\text{if} \quad h \geq h_\ell \quad , \ \dot{m}_{DV} = 0$$

where h is enthalpy of fluid and h_ℓ and h_g are enthalpies of liquid and steam at the saturation temperature, respectively.

The fluid temperatures can be measured with thermocouples immersed in the fluid and the enthalpies h_I and h_{ECC} can be estimated.

Mass balance calculations were performed with Eqs. (A.1) and (A.2). The K-factor of the orifice in the pump simulator was evaluated in the following two ways.

The K-factor of 20 was obtained with the steam and water single phase calibration tests using the flow meter and spool piece data. The K-factor of 15 was obtained with the Pitot tube measurement in a typical reflood condition assuming the flat velocity profile in the pipings. In the differentiation, higher frequency components of the data tends to be amplified more. Therefore, in the differentiation of the differential pressure data, the smoothing procedure was used to suppress the high frequency components of the data.

In the Acc injection period, the calculated $\dot{m}_F$s with Eqs. (A.1) and (A.2) are significantly different from each other. This discrepancy may be caused by inaccuracy of the mass flow rate injected into the system and by the unaccounting of the storage of water in the cold leg pipe. The former might be introduced from the slow time response of the flow meter (time constant 1 second) and the change of the gas volume in the injection line. In this period, especially before the steam generation from the core becomes noticeable, the mass flow rate, $\dot{m}_F$, calculated with Eq. (A.1) is probably reasonable, since the calculation uses the increasing rates of the masses in the core and the upper plenum and their accuracy is good enough for our estimation.

In the LPCI injection period, the calculated $\dot{m}_F$s are slightly different from each other. Judging from the time-integral values of both $\dot{m}_F$s, their average values are nearly proportional. The discrepancy was inferred to be caused by the disregard of the bypass of steam and liquid from the upper plenum without going through the hot legs in the calculation with Eq. (A.1). And additionally the discrepancy was caused by the disregard of the steam generation in the downcomer due to the hot wall of the pressure vessel in the calculation with Eq. (A.2). It was estimated that the disregard of the downcomer steam generation causes the error of 0.25 kg/s on predicted $\dot{m}_F$. The estimation was made by comparing the results of the tests with hot and cold downcomer conditions.

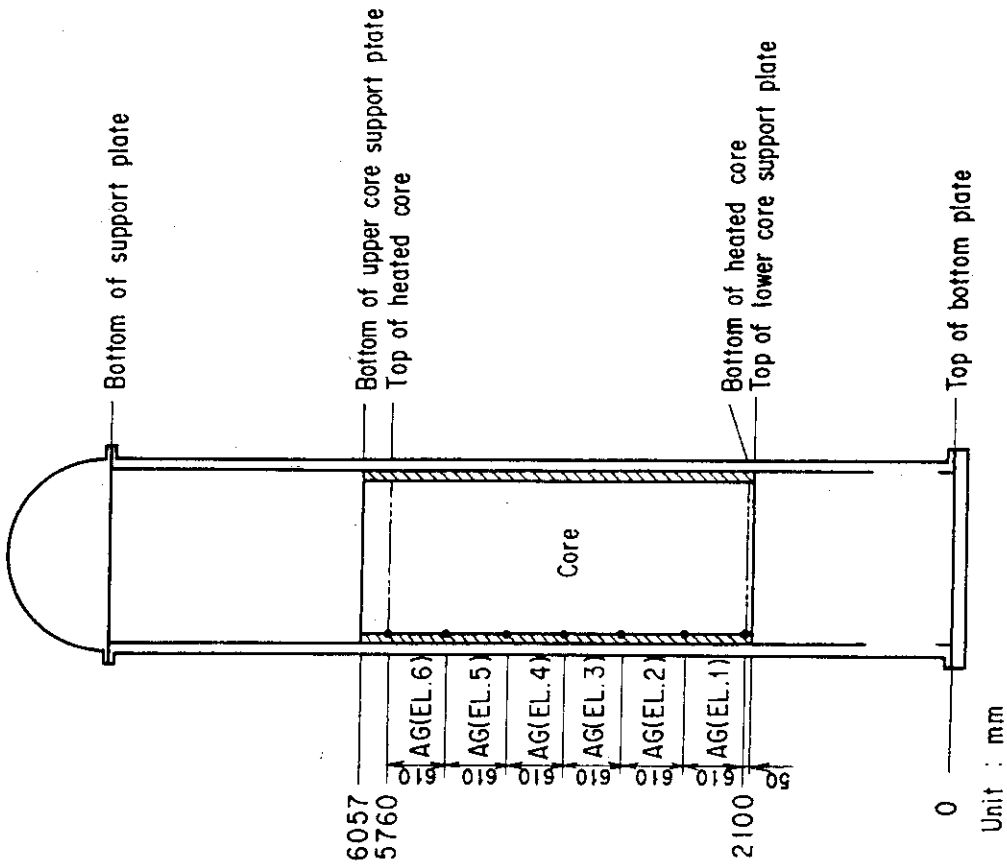

Fig. A-2 Definition of Tag. ID for void fraction (AG(EL.1) ∿ AG(EL.6))

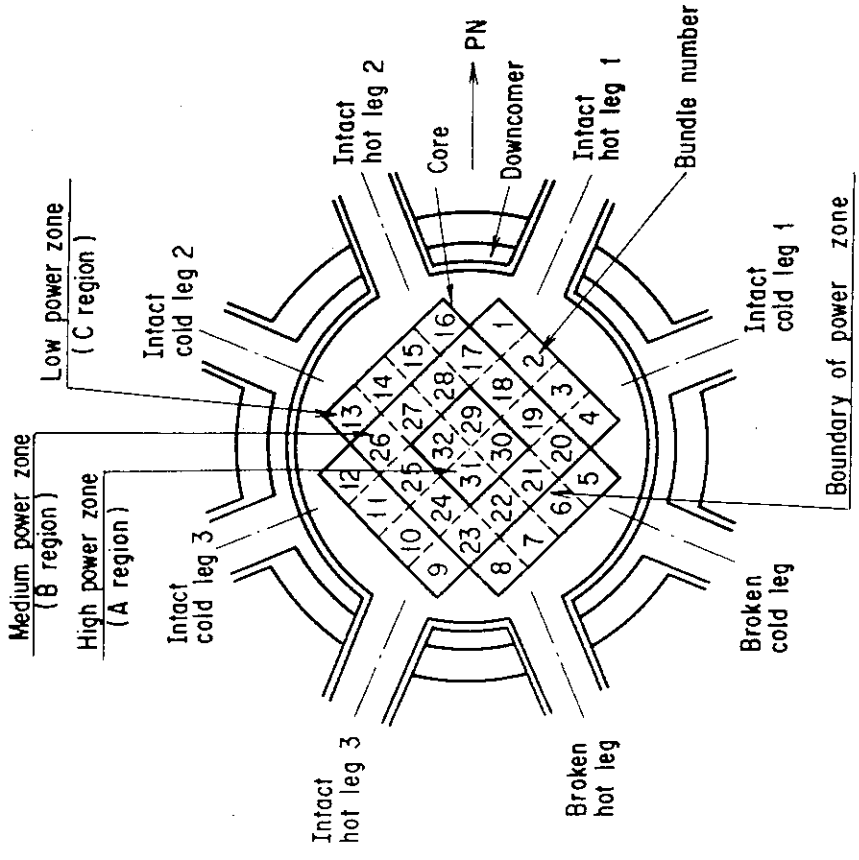

Fig. A-1 Definition of power zones and bundle numbers

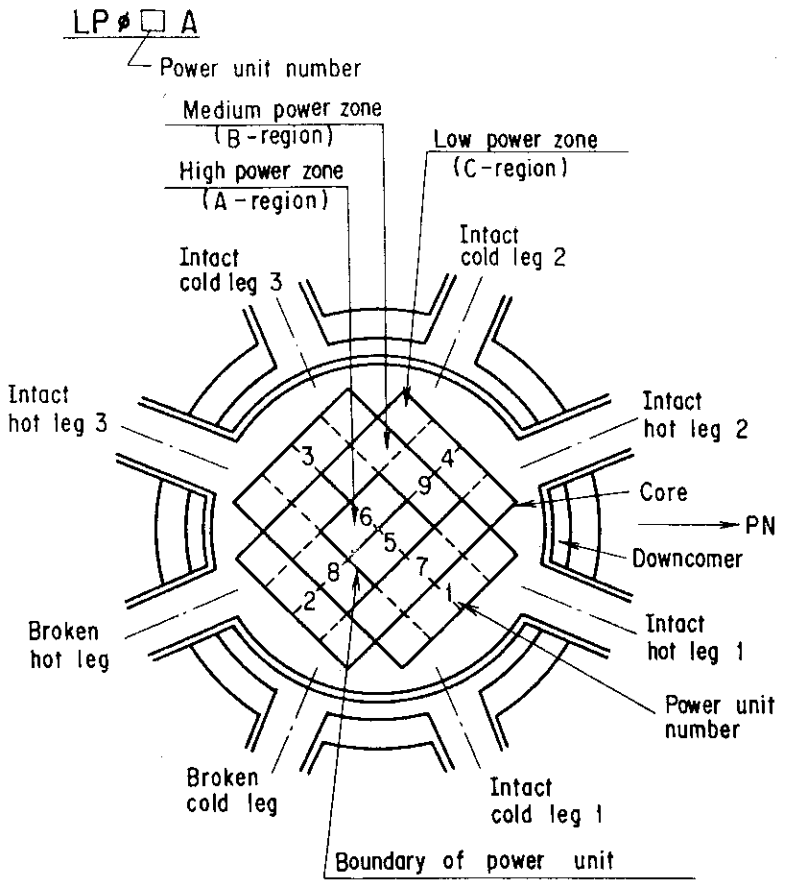

Fig. A-3 Definition of Tag. ID for average linear power of heater rod in each power unit zone (LP01A ∿ LP09A)

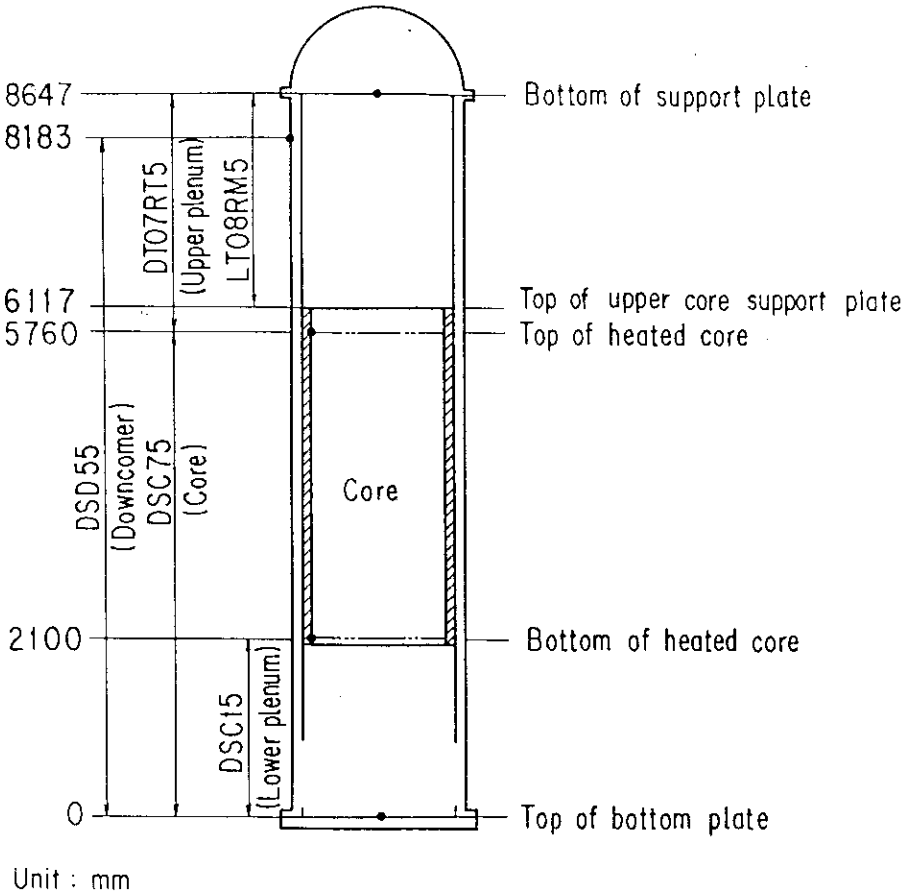

Fig. A-4 Definition of Tag. ID for differential pressure through downcomer, upper plenum, core, and lower plenum (DSD55, DT07RT5, LT08RM5, DSC75, DSC15)

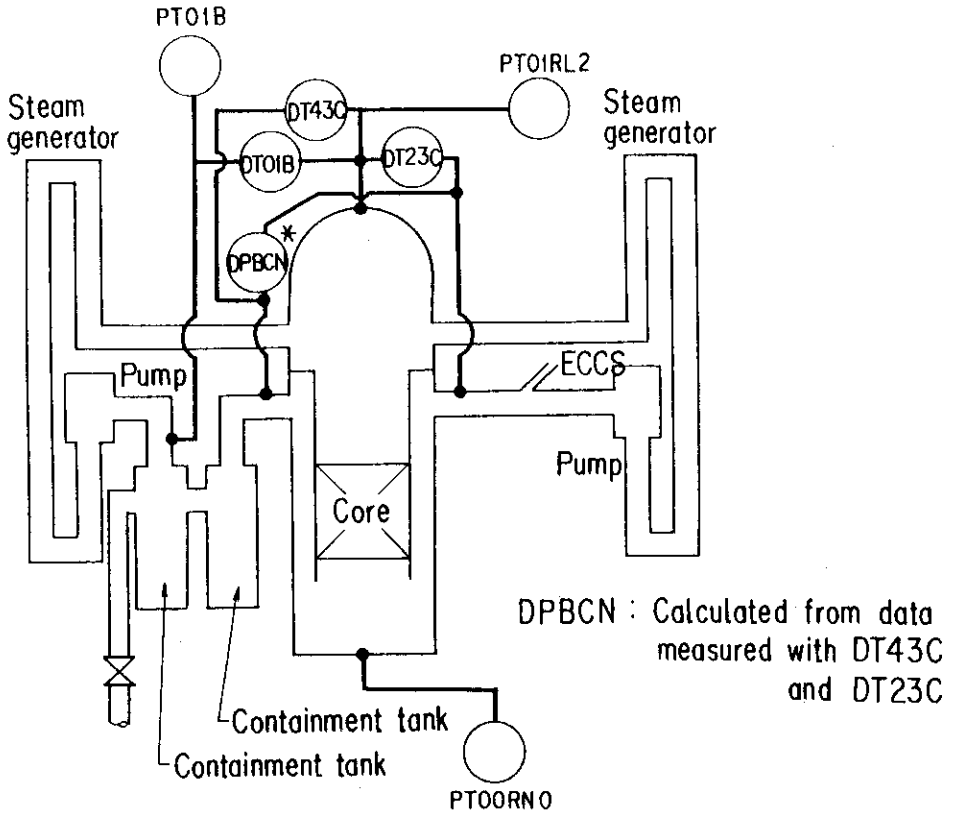

Fig. A-5 Definition of Tag. ID for pressures in upper and lower plena and containment tank 2 (PT01RL2, PT00RN0, PT01B) and for differential pressure through intact and broken loop and broken cold leg nozzle (DT23C, DT01B, DPBCN)

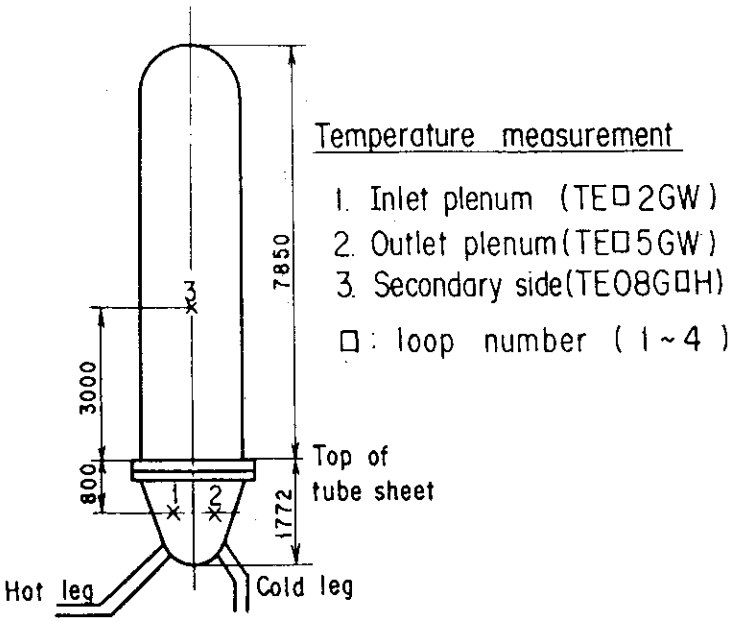

Fig. A-6 Definition of Tag. ID for fluid temperature in inlet and outlet plenum and secondary of steam generator (TE□2GW, TE□5GW, TE08G□H)

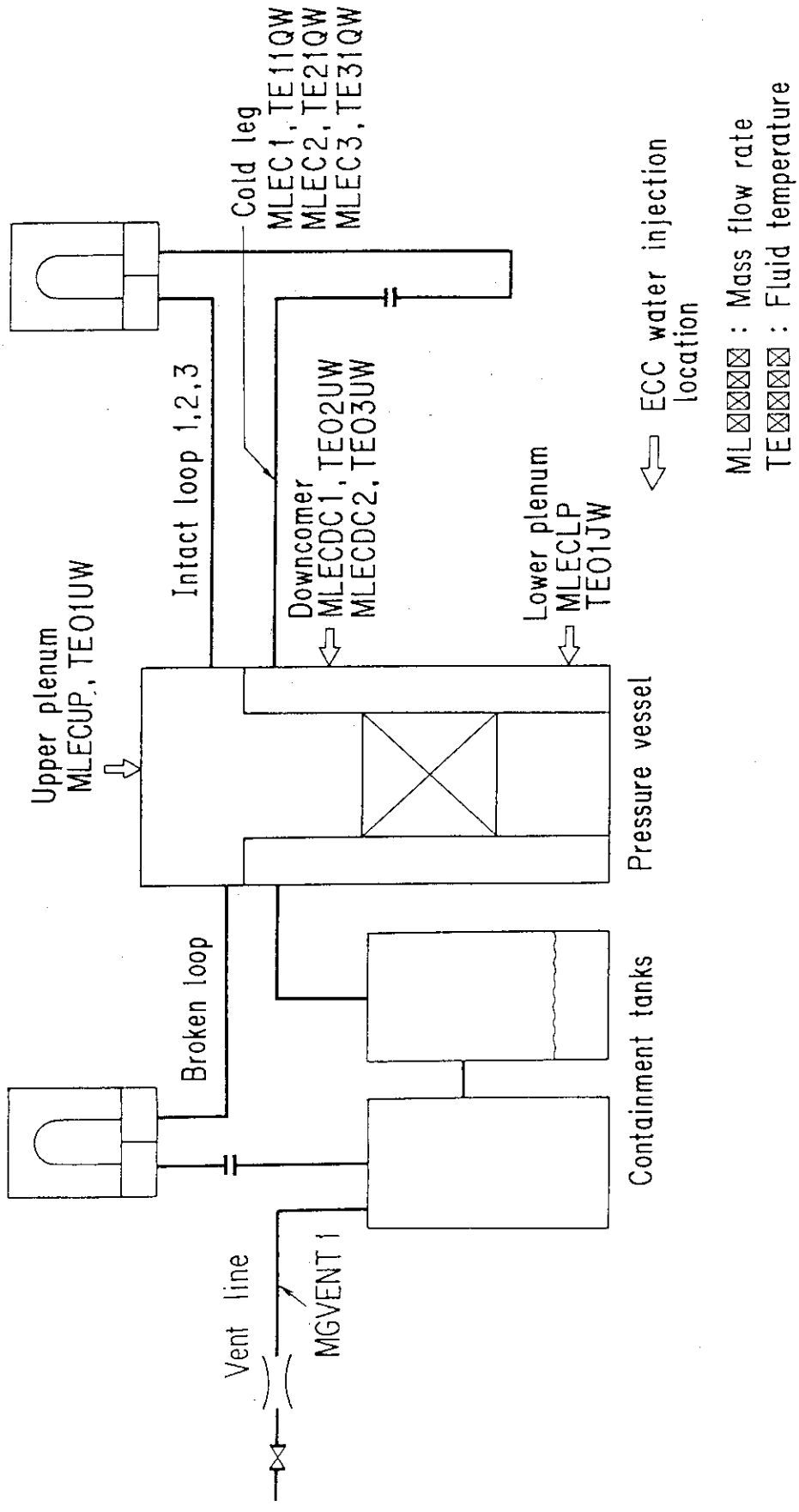

Fig. A-7 Definition of Tag. ID for ECC water injection rate, ECC water temperature and vented steam flow rate
(MLEC1, MLEC2, MLEC3, MLECLP, MLECUP, MLECDC1, MLECDC2, TE11QW, TE21QW, TE01JW, TE01UW, TE02UW, TE03UW, MGVENT1)

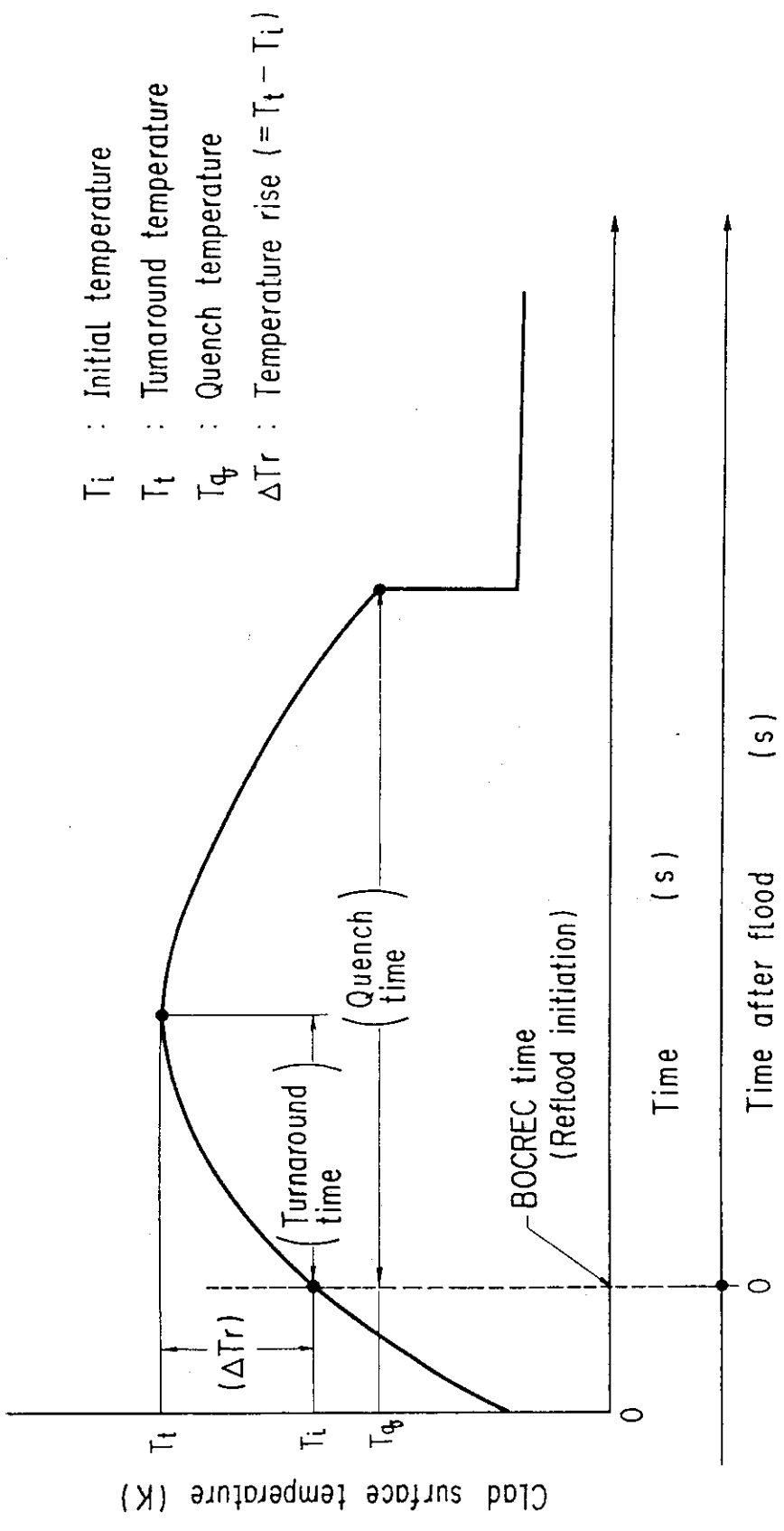

Fig. A-8 Definition of initial temperature, turnaround temperature, quench temperature, temperature rise, turnaround time and quench time

Appendix B Selected Data of CCTF Test C2-1 (Run 55)

Figure List

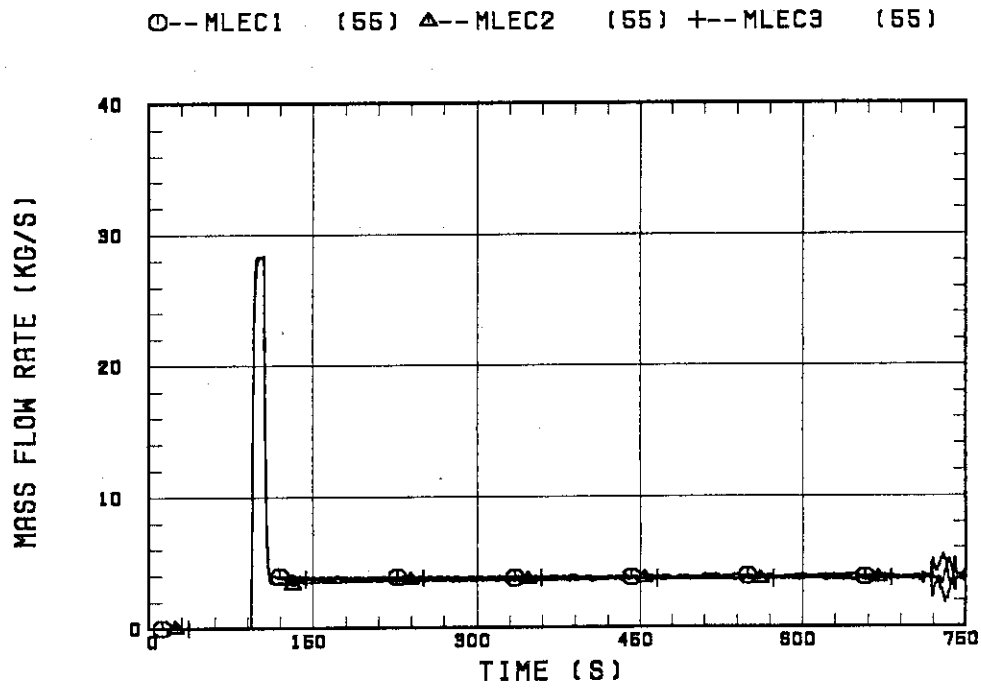

Fig. B-1 ECC water injection rates into the primary system

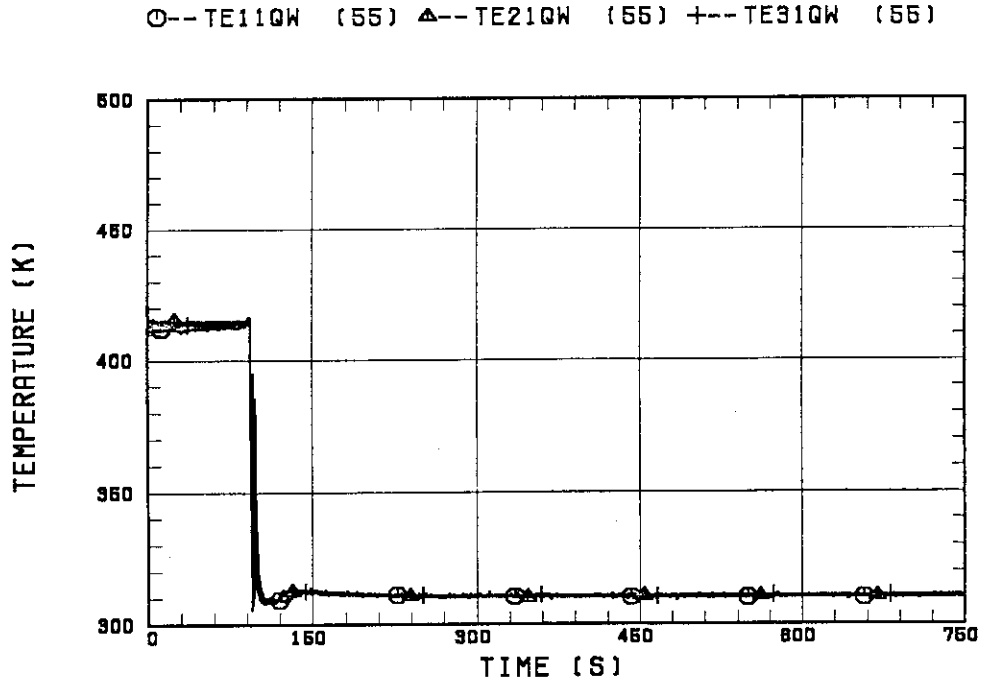

Fig. B-2 ECC water temperature

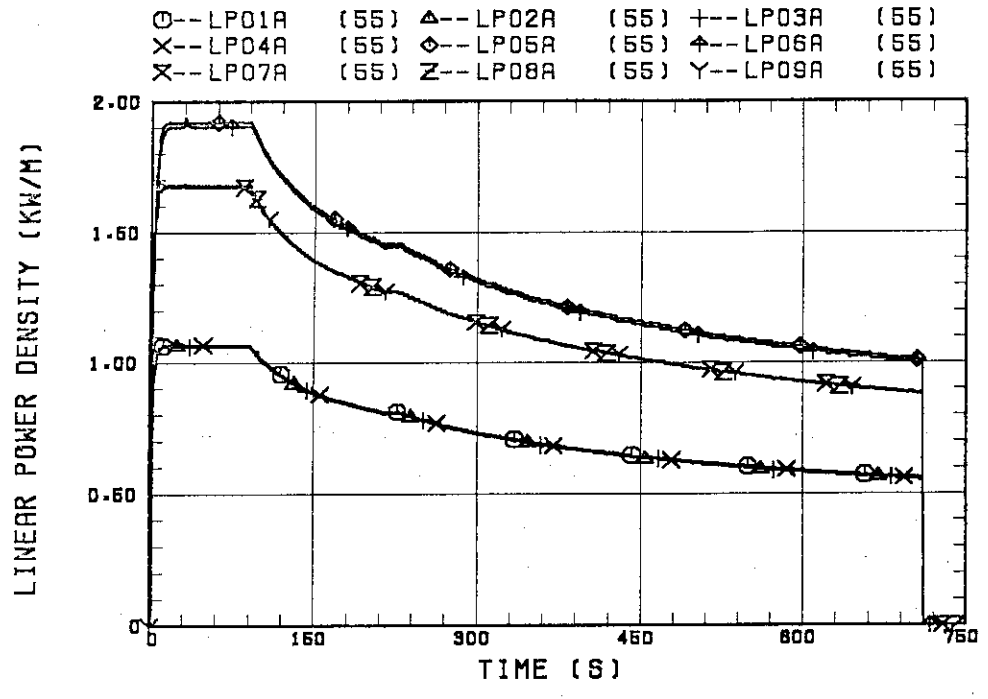

Fig. B-3 Average linear power of heater rod in each power unit zone

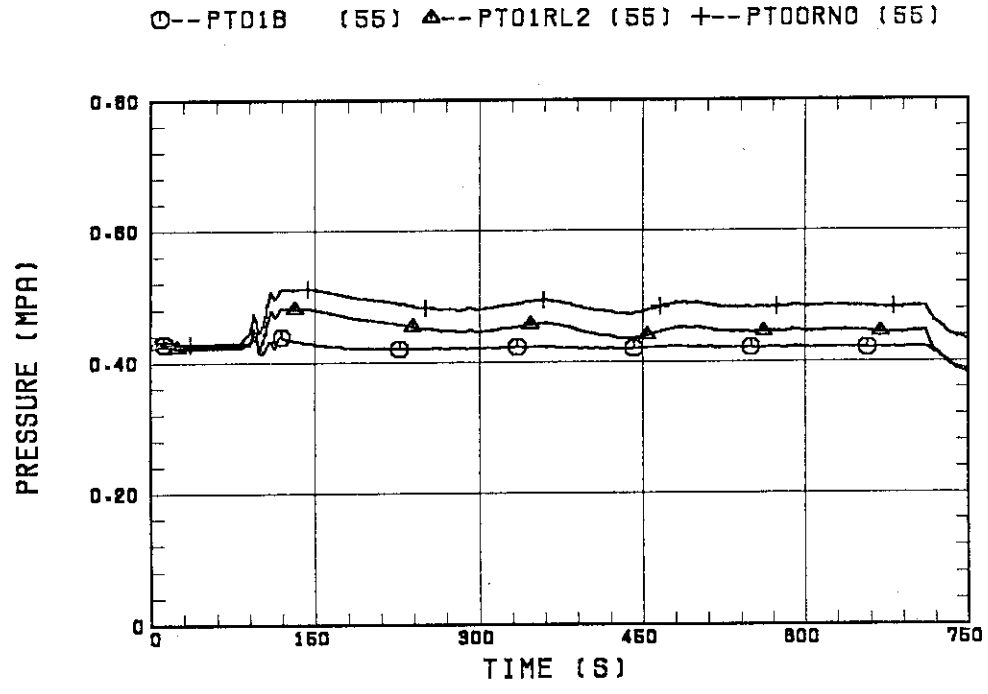

Fig. B-4 Pressure history in containment tank 2, upper plenum and lower plenum

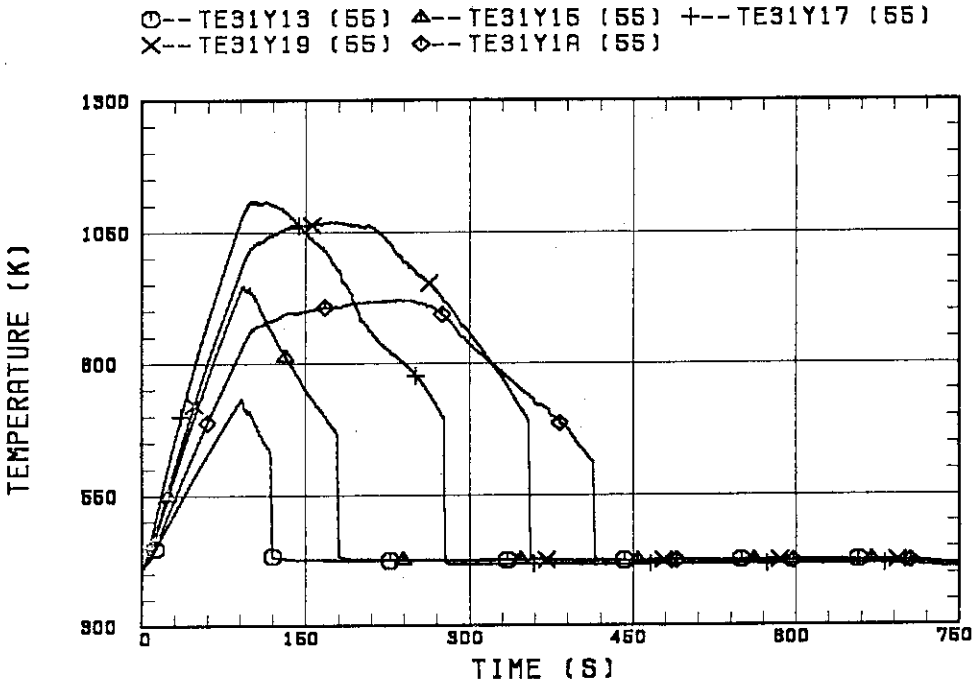

Fig. B-5 Clad surface temperature at various elevations along a heater rod in high power region (A region)

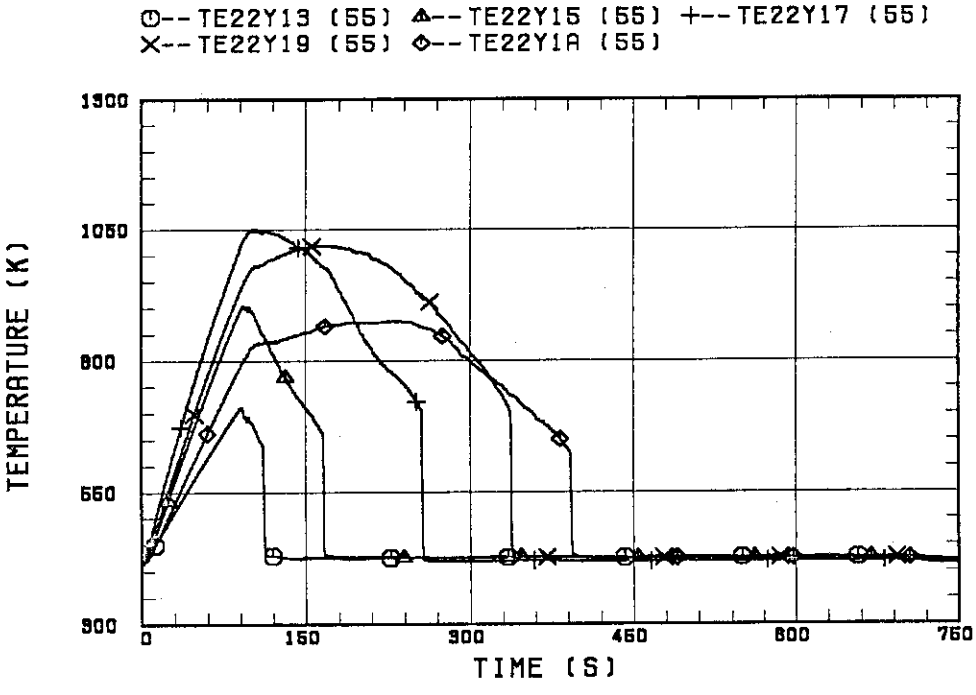

Fig. B-6 Clad surface temperature at various elevations along a heater rod in medium power region (B region)

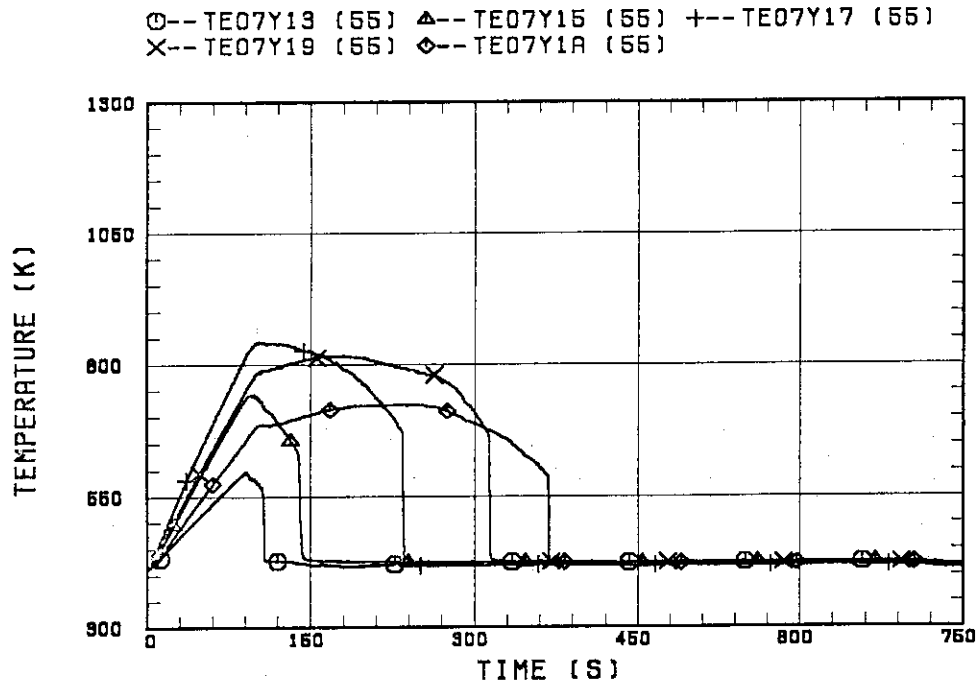

Fig. B-7 Clad surface temperature at various elevations along a heater rod in low power region (C region)

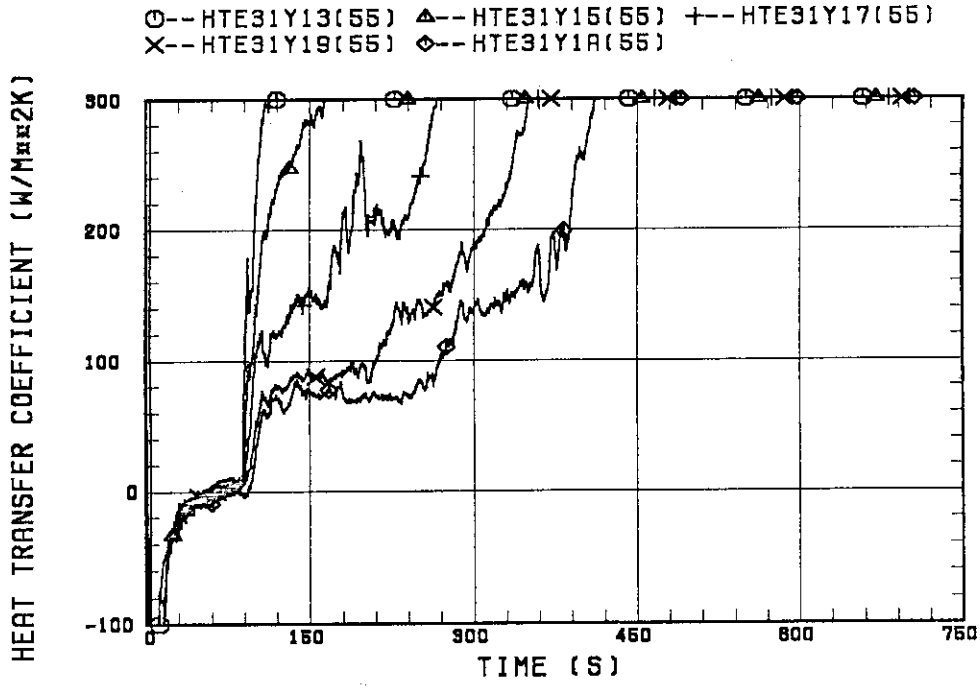

Fig. B-8 Heat transfer coefficient at various elevations along a heater rod in high power region (A region)

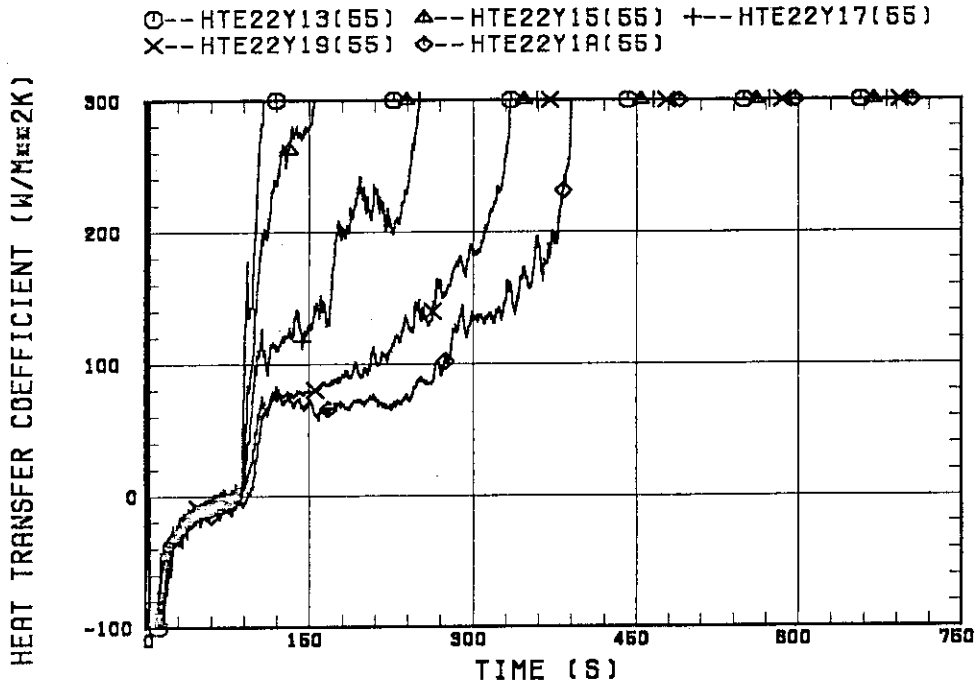

Fig. B-9 Heat transfer coefficient at various elevations along a heater rod in medium power region (B region)

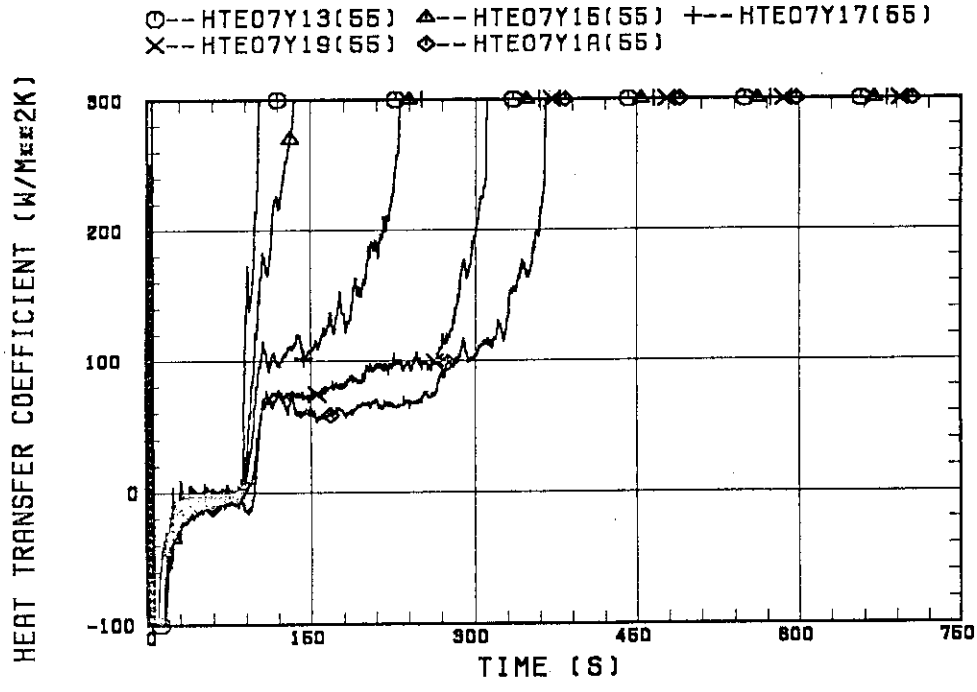

Fig. B-10 Heat transfer coefficient at various elevations along a heater rod in low power region (C region)

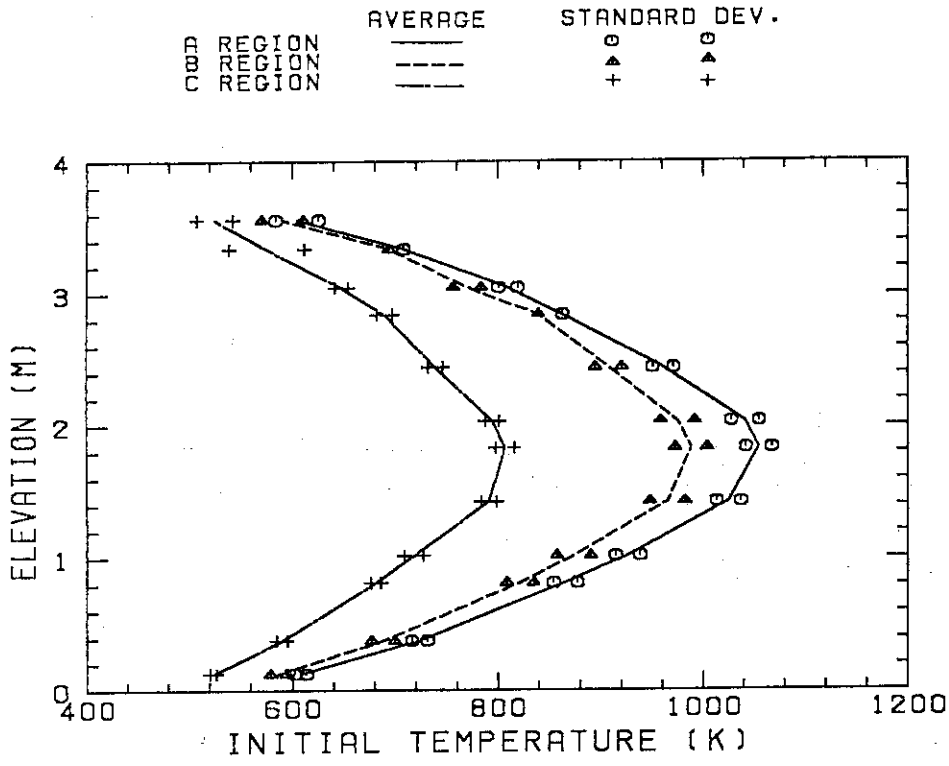

Fig. B-11 Initial clad surface temperature

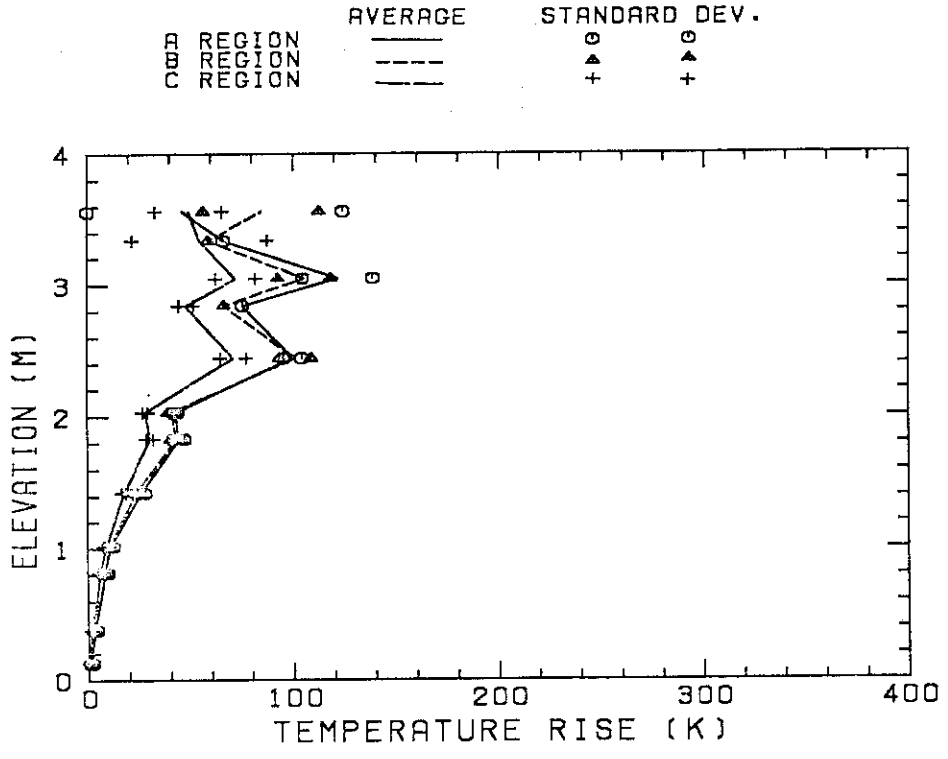

Fig. B-12 Temperature rise

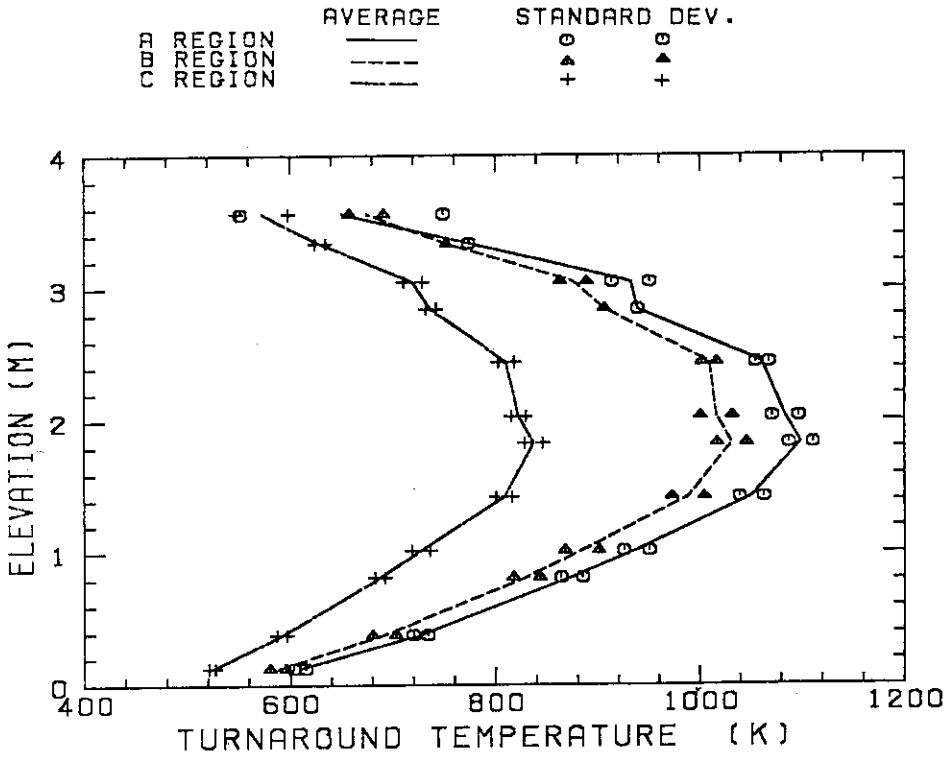

Fig. B-13 Turnaround temperature

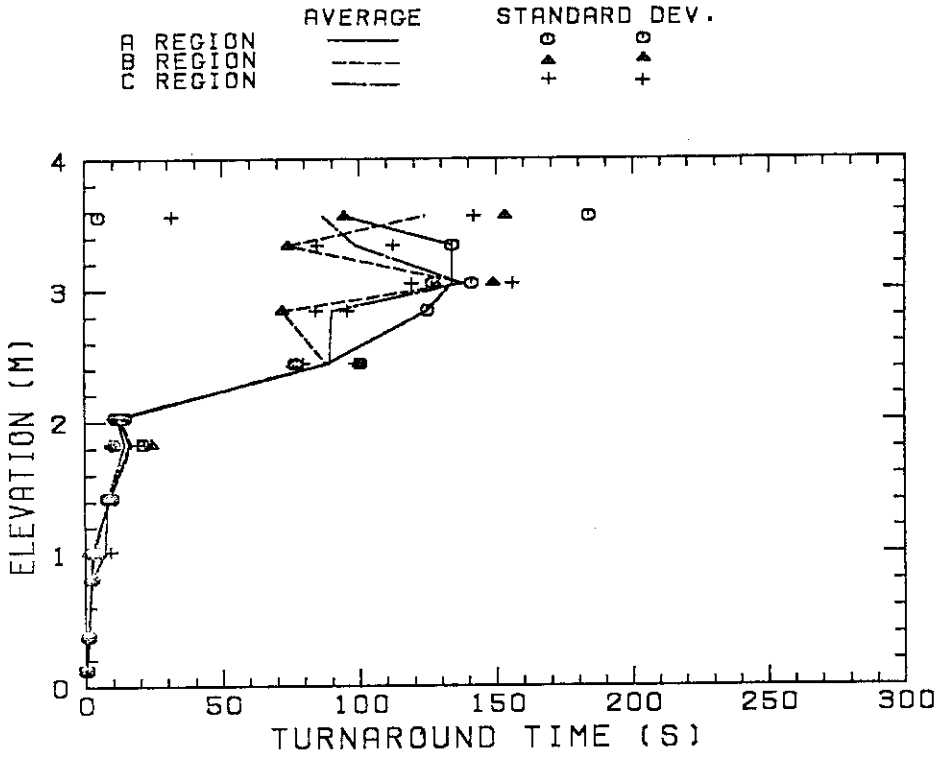

Fig. B-14 Turnaround time

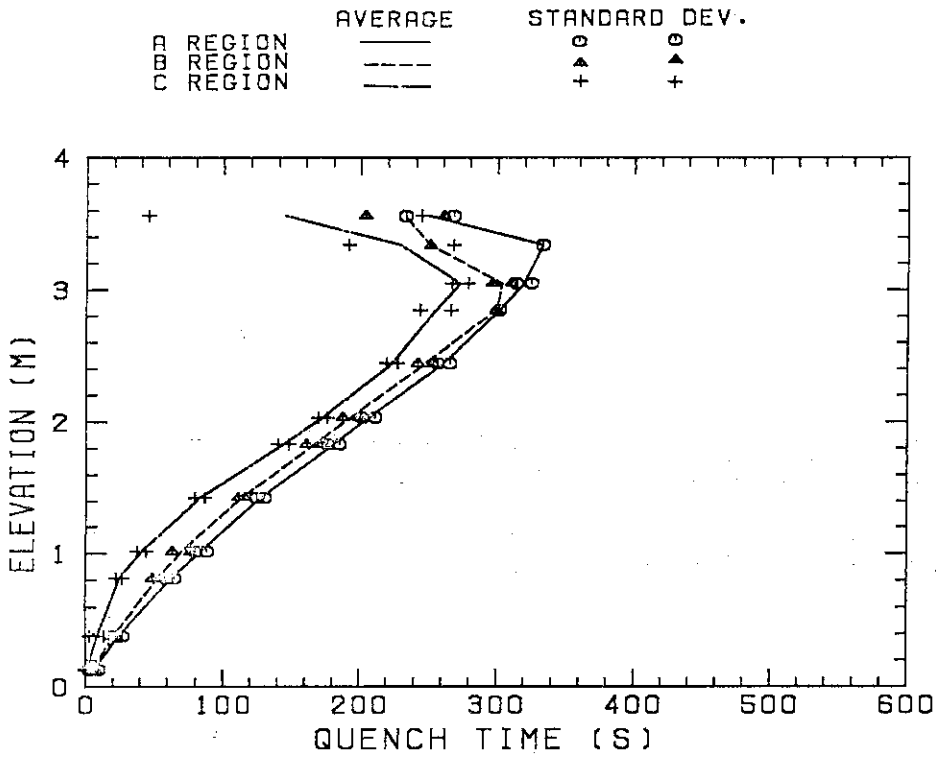

Fig. B-15 Quench temperature

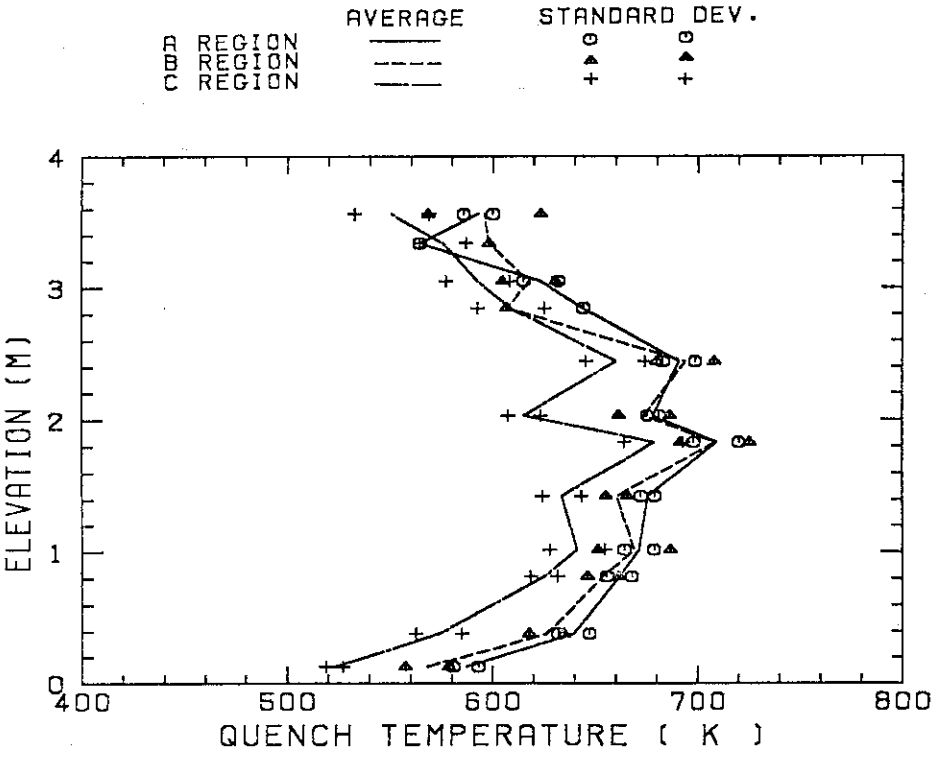

Fig. B-16 Quench time

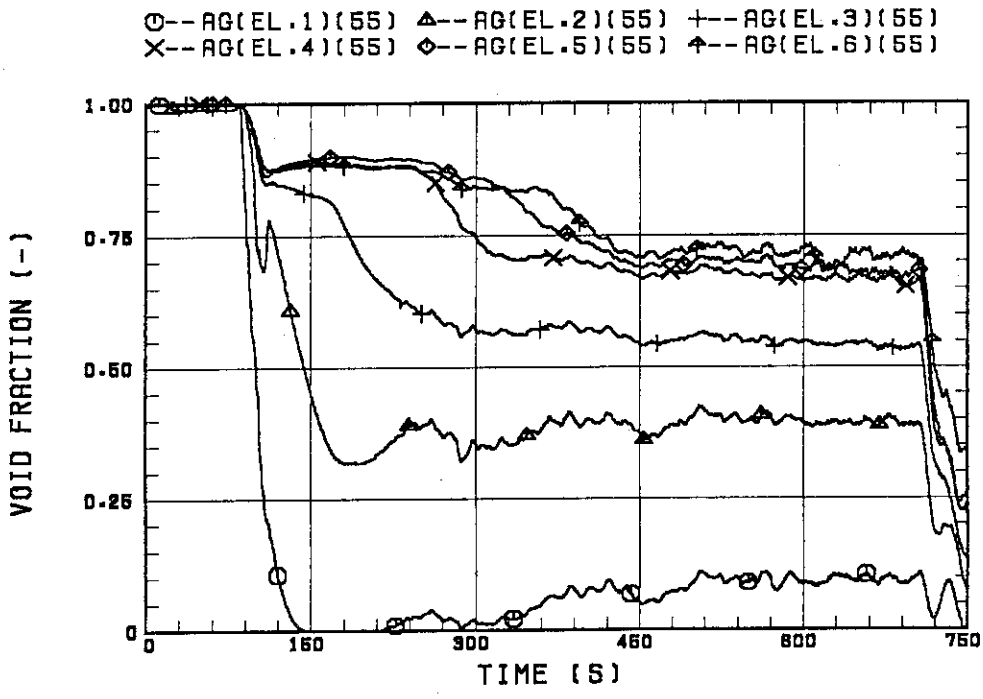

Fig. B-17 Void fraction in core

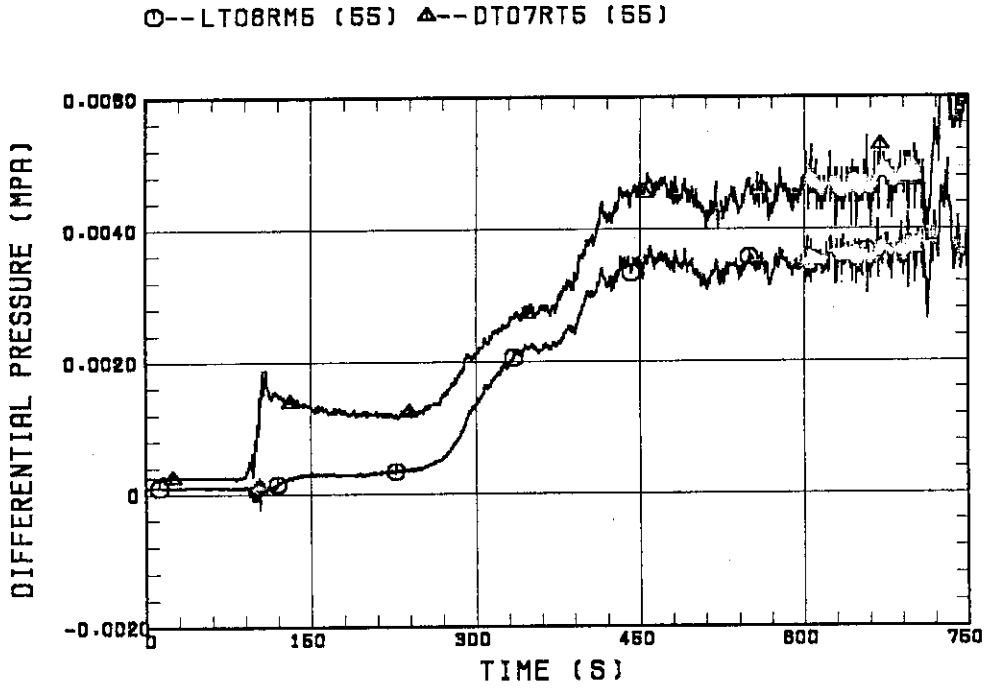

Fig. B-18 Differential pressure through upper plenum

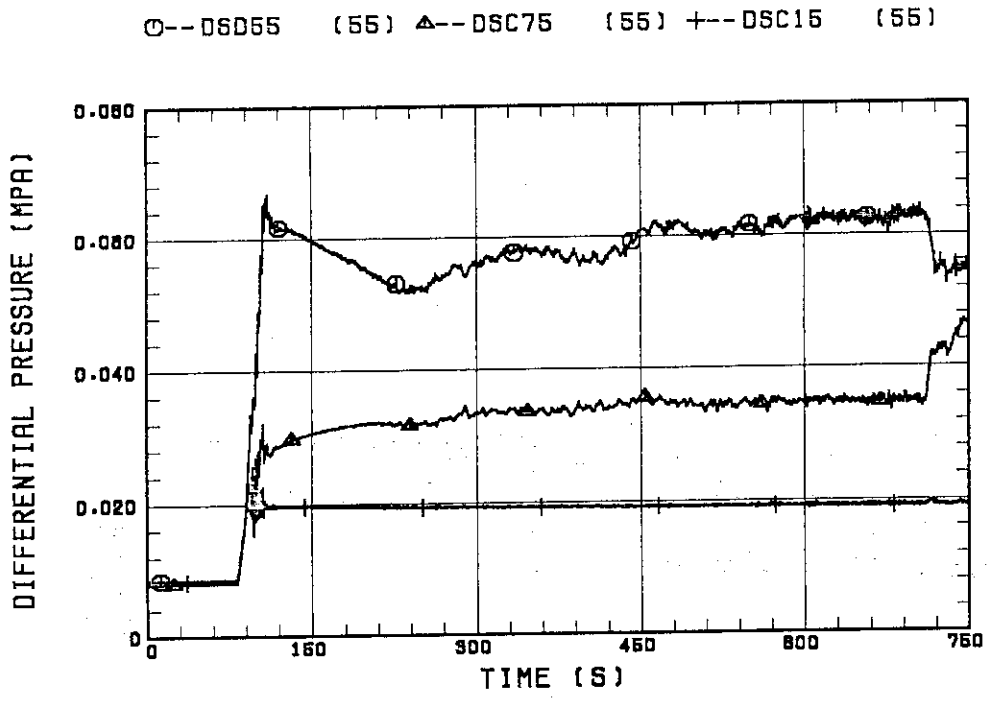

Fig. B-19 Differential pressure through downcomer, core, and lower plenum

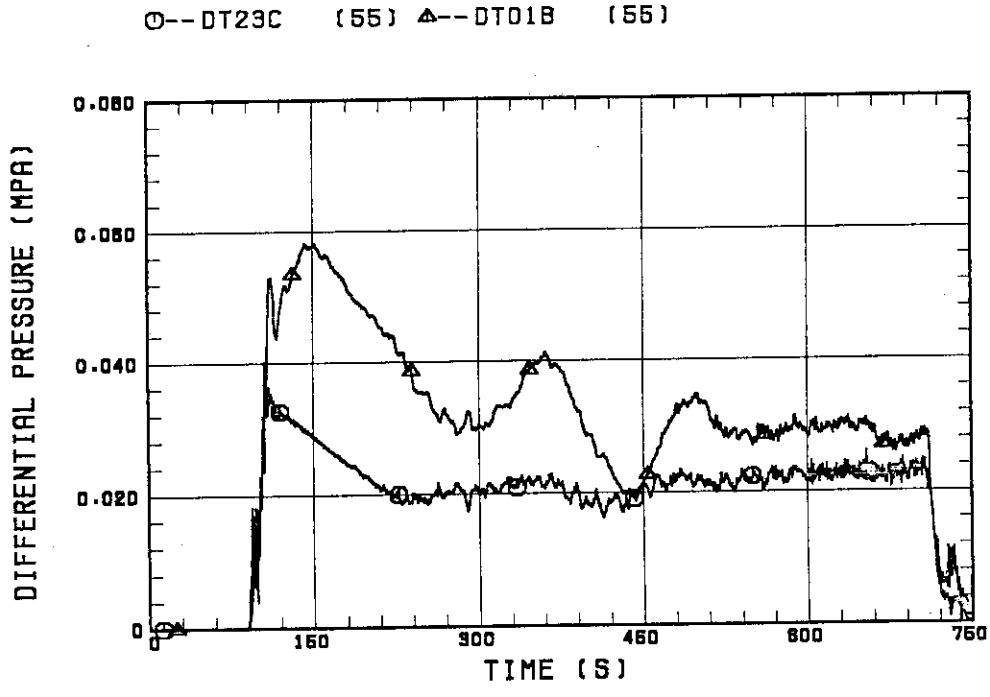

Fig. B-20 Differential pressure through intact and broken loops

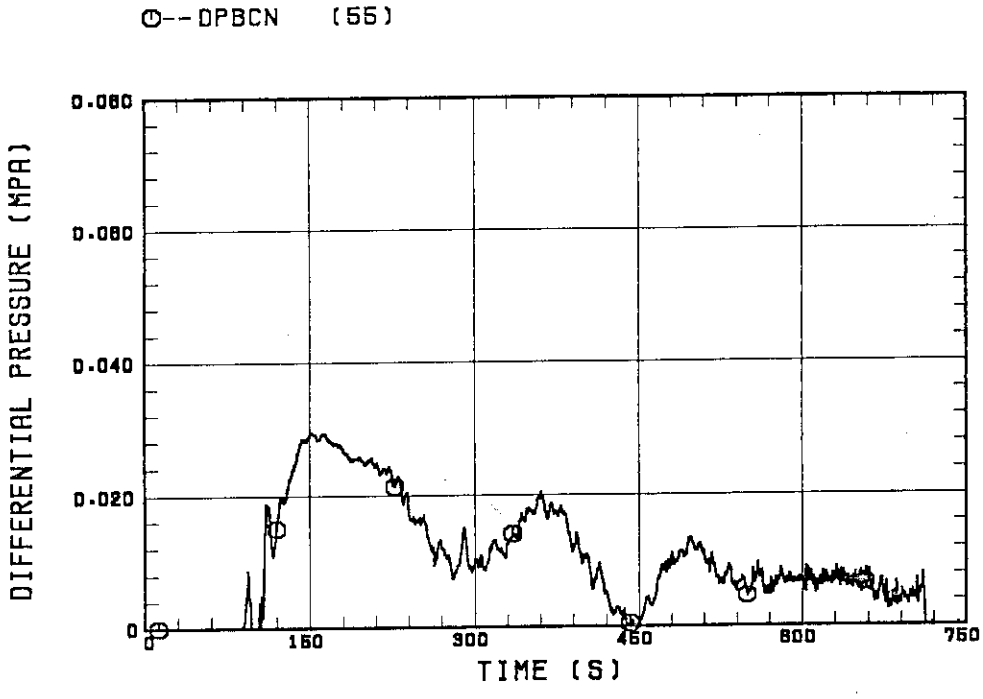

Fig. B-21 Differential pressure through broken cold leg nozzle

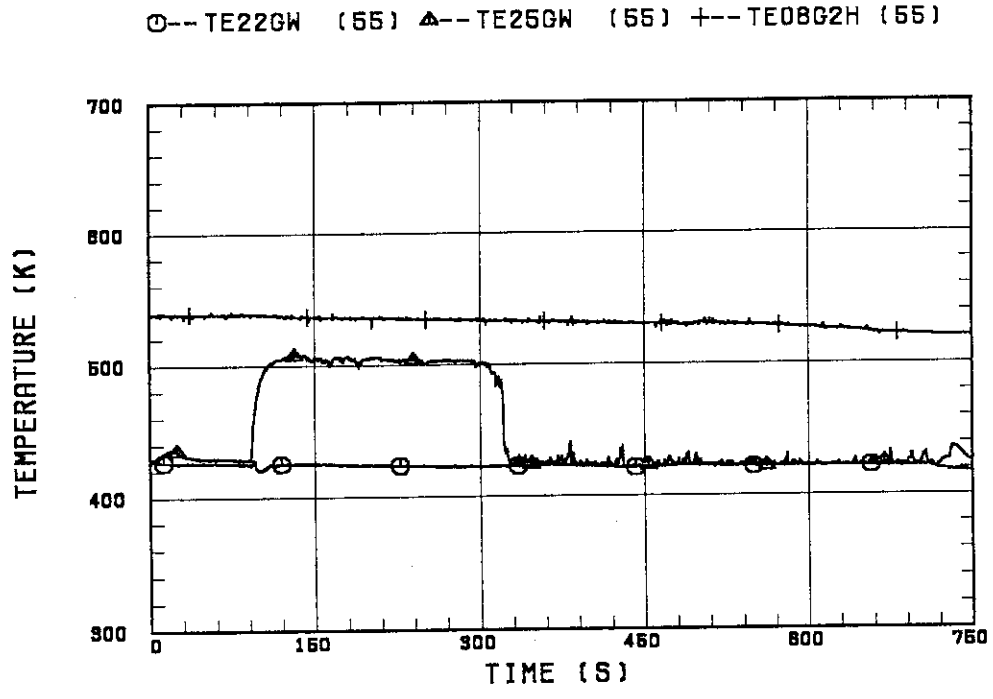

Fig. B-22 Fluid temperature in inlet plenum, outlet plenum, and secondary of steam generator 1

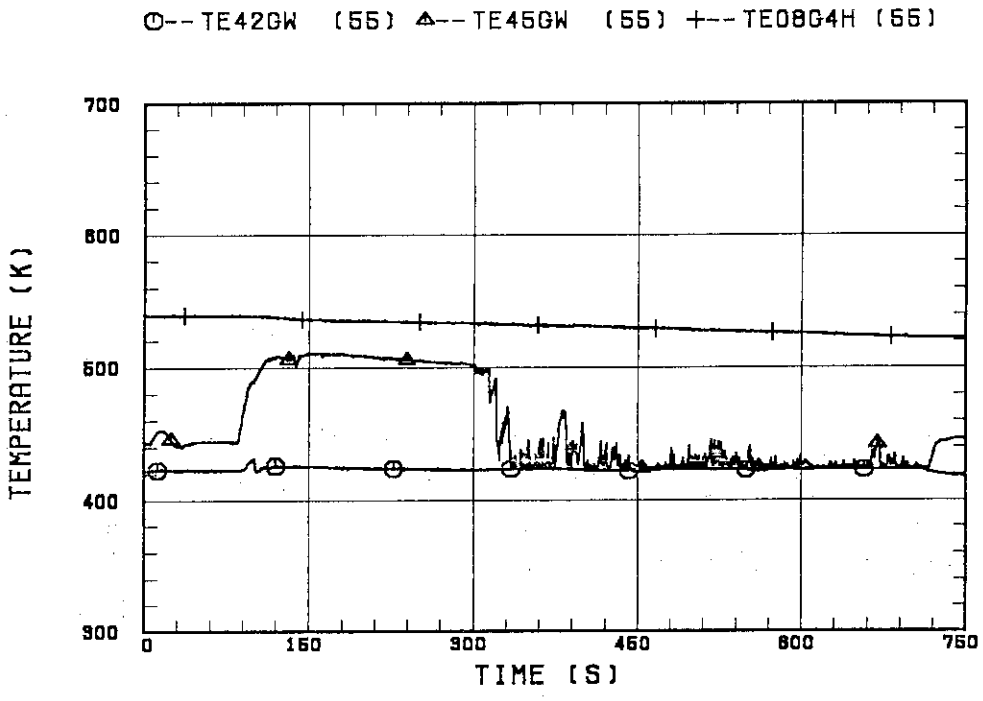

Fig. B-23 Fluid temperature in inlet plenum, outlet plenum, and secondary of steam generator 2

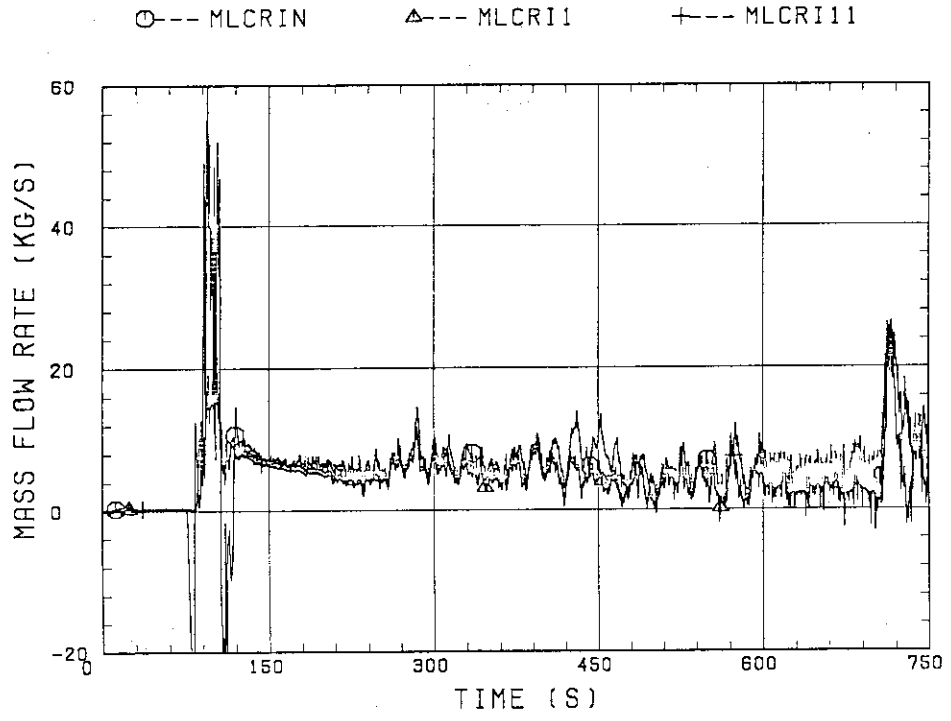

Fig. B-24 Core flooding mass flow rates evaluated with Eqs. (A.1) and (A.2)

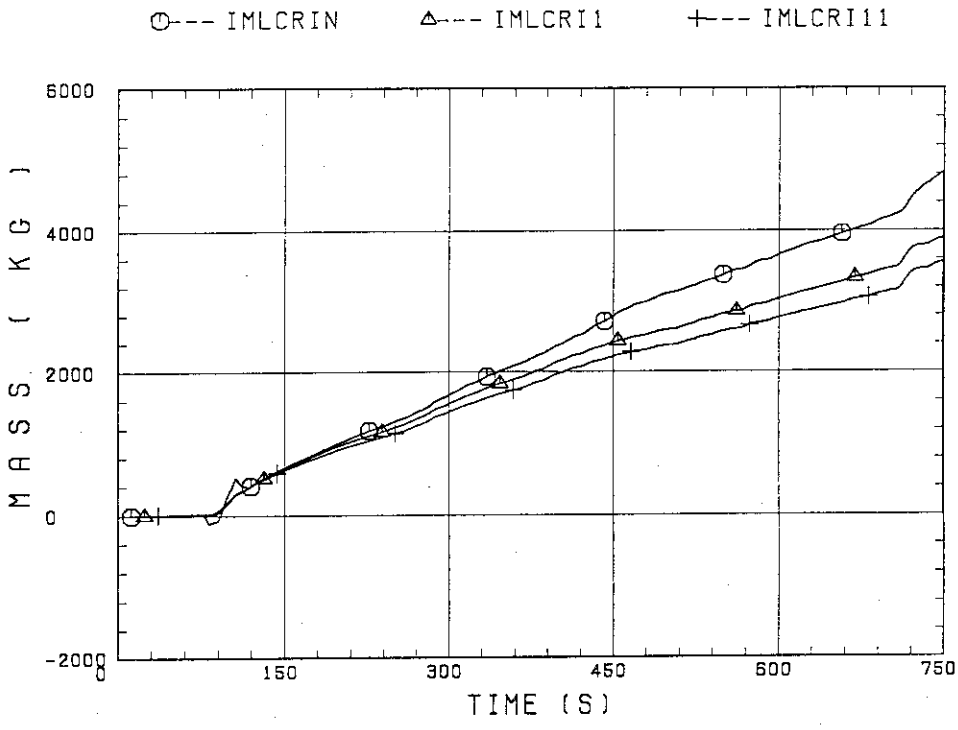

Fig. B-25 Time-integral mass flooded into core evaluated with Eqs. (A.1) and (A.2)

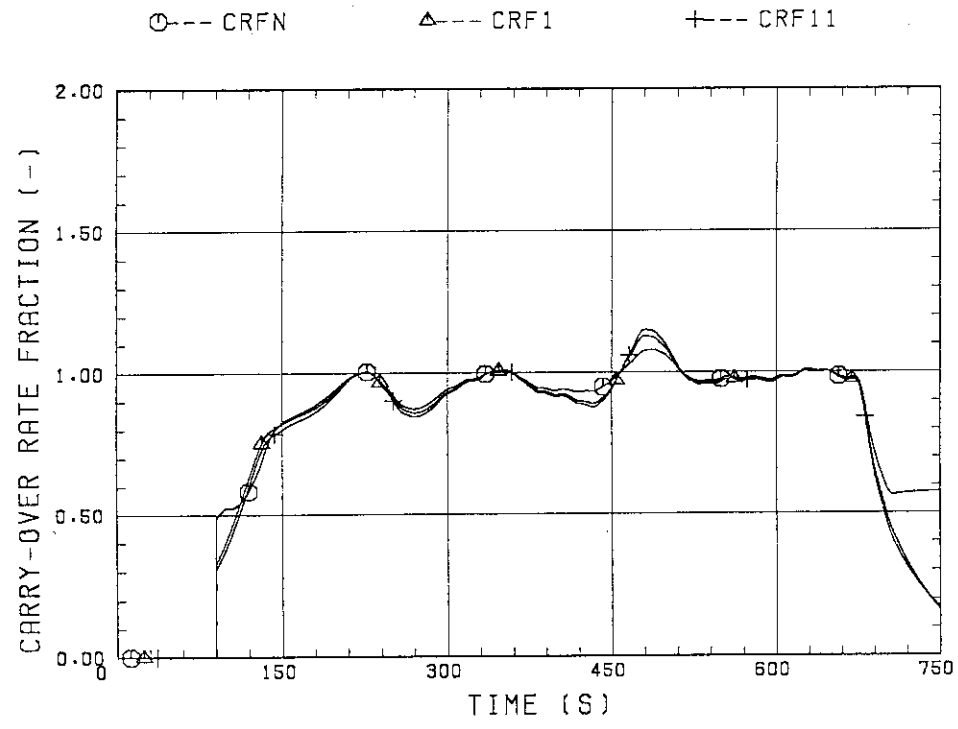

Fig. B-26 Carry-over rate fraction

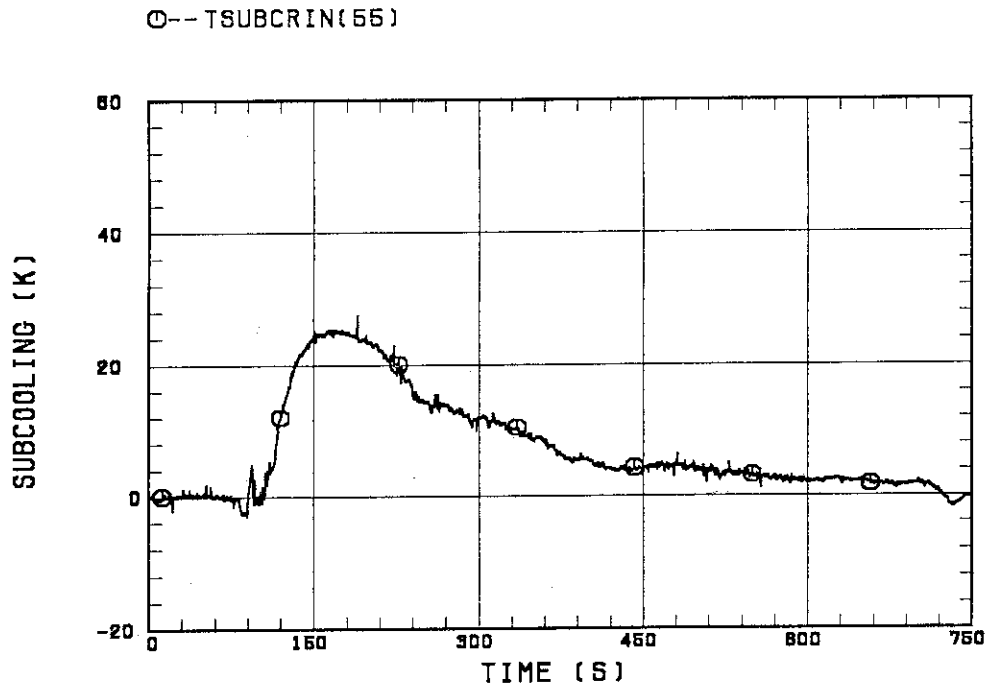

Fig. B-27 Core inlet subcooling

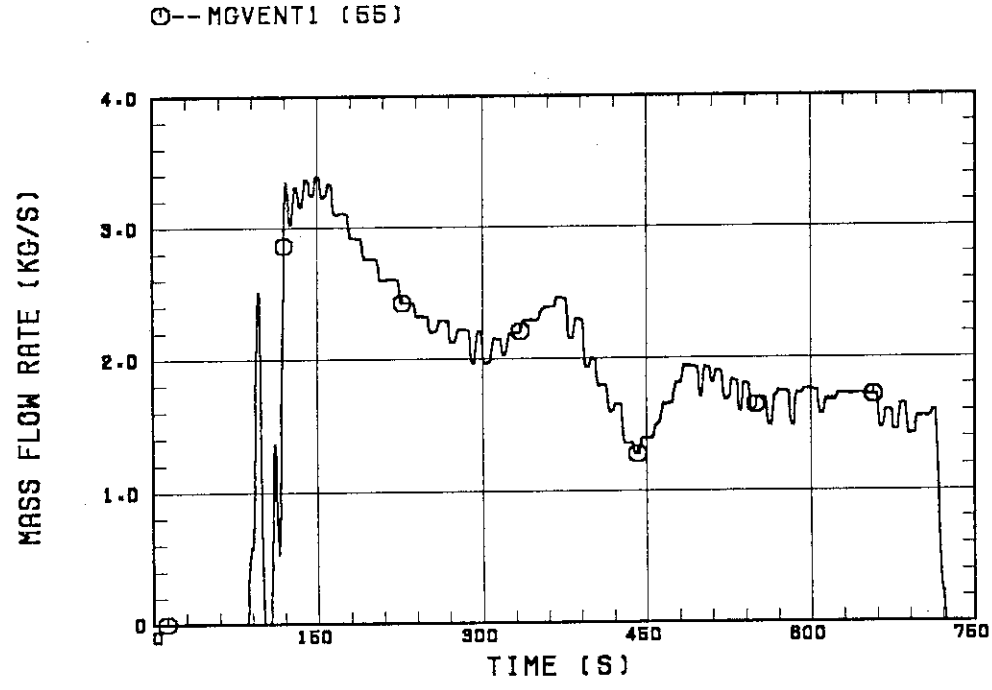

Fig. B-28 Exhausted mass flow rate from containment tank 2